INL/EXT-17-42666

Light Water Reactor Sustainability Program

Risk-Informed External Hazards Analysis for Seismic and Flooding Phenomena for a Generic PWR

Carlo Parisi, Steve Prescott, Zhegang Ma, Bob Spears, Ronaldo Szilard, Justin Coleman, Ben Kosbab

July 2017

DOE Office of Nuclear Energy

INL/EXT-17-42666

Light Water Reactor Sustainability Program

Risk-Informed External Hazards Analysis for Seismic and Flooding Phenomena for a Generic PWR

Carlo Parisi
Steve Prescott
Zhegang Ma
Bob Spears
Ronaldo Szilard
Justin Coleman
Ben Kosbab*

July 2017

Idaho National Laboratory
Idaho Falls, Idaho 83415
***SC Solutions**
Marietta, Georgia

http://www.inl.gov/lwrs

Prepared for the
U.S. Department of Energy
Office of Nuclear Energy
Under DOE Idaho Operations Office
Contract DE-AC07-05ID14517

EXECUTIVE SUMMARY

This report describes the activities performed during the FY2017 for the DOE Light Water Reactor Sustainability Risk-Informed Safety Margin Characterization (LWRS-RISMC), Industry Application #2, External Events (IA2). The scope of IA2 is to deliver a risk-informed external hazards safety analysis for a representative nuclear power plant. Following the advancements occurred during the previous Fiscal Years (toolkits identification, models development), FY2017 focused on:

- increasing the level of realism of the analysis;
- improving the tools and the coupling methodologies.

In particular the following objectives were achieved:

- development of a SAPHIRE code PRA models for 3-loops Westinghouse PWR;
- set-up of a methodology for performing static-dynamic PRA coupling between SAPHIRE and EMRALD codes;
- coupling RELAP5-3D/RAVEN for performing Best-Estimate Plus Uncertainty analysis and automatic limit surface search;
- execute sample calculations for demonstrating the capabilities of the toolkit in performing a risk-informed external hazards safety analyses.

The effect of building pounding during seismic events was added because of its potential safety significance within the nuclear industry. This is a consequence of increased seismic hazard and of possible seismic gaps reduction due to NPP aging. Dynamic simulation of interaction between turbine and auxiliary buildings, including non-linear-soil-structure interaction, was initiated.

Probability of failure and event trees of a generic 3-loops Westinghouse PWR were derived from a generic SAPHIRE model in order to inform the simulation. Seismically induced Loss of Offsite Power, Station Blackout, and fire suppression piping failure events were considered in this study. SAPHIRE allowed a pre-screening of all possible branches of the event tree and a selection of those with the largest CDF increase for analysis using dynamic PRA and physics simulation through implementation in the EMRALD code.

Four sequences were identified with a potential for significant change in CDF (two Loss of Offsite Power and two Station Blackout). EMRALD performed dynamic PRA calculations of these sequences, integrating risk analysis with on-line deterministic safety analysis results (seismically-induced internal flooding calculations by NEUTRINO code and system analysis by RELAP5-3D code).

A more recent version of NEUTRINO flooding analyses was used, with a similar model to FY2016, with improvements in handling spray phenomena.

The coupled calculations of RELAP5-3D system thermal-hydraulic code and RAVEN risk-analysis code allow informing EMRALD dynamic PRA calculations with Best-Estimate plus Uncertainty (BEPU) analysis. RAVEN identified the most relevant uncertain parameters, performed the Monte Carlo perturbation of the RELAP5-3D input deck and processed all the output data. First and fourth order statistics were applied for having a 95/95 value of the peak cladding temperature for all the Station Blackout and Loss-of-Offsite Power events. Best-Estimate calculations were used for deriving limit surfaces as

function of relevant transient parameters (e.g., battery time vs. recovery time, seal leakage vs. steam generator depressurization time). This data was used by EMRALD for determining the final core status (core damage/core safe). BEPU calculations were also used for deriving a limit surface, which include uncertainty results.

The final coupling of seismic, flooding, system thermal-hydraulic, uncertainty quantification and risk-analysis shows a demonstration of advanced risk-informed external hazards analysis. Moreover, the modularity of the developed methodology allows its application also to other external hazards than just seismic (e.g., high winds, intense precipitation, coastal flooding).

Further improvements could be obtained in the future by carrying out all calculations (deterministic and probabilistic) on a single high-performance computing machine, leveraging the parallel calculation architecture. Thus, appropriate software modifications are identified and recommended.

CONTENTS

FIGURES

TABLES

ACRONYMS

3D	Three Dimensional
AC	Alternating Current
AFW	Auxiliary Feed-Water
A-SPRA	Advanced Seismic PRA
ATWS	Anticipated Transients Without Scram
BAF	Bottom of Active Fuel
BDBA	Beyond Design Basis Accident
BEPU	Best Estimate Plus Uncertainty
BOP	Balance of Plant
CD	Core Damage
CDF	Core Damage Frequency
CFR	Code of Federal Regulation
CSAU	Code Scaling, Applicability and Uncertainty Evaluation
DBA	Design Basis Accident
DC	Direct Current
DG	Diesel Generator
DOE	Department of Energy
DSA	Deterministic Safety Analysis
ECCS	Emergency Core Cooling System
EE	External Events
EEVE-A	External Events Project – Advanced
EEVE-B	External Events Project – Baseline
EDG	Emergency Diesel Generator
EPRI	Electric Power Research Institute
EQ	Earthquake
ESF	Engineered Safeguards Systems
EPS	Emergency Power System
FAB	Feed and Bleed
FOM	Figure Of Merit
FY	Fiscal Year
HPC	High Performance Computing
HPI	High Pressure Injection

HPIS	High Pressure Injection System
HX	Heat Exchange
IA2	Industry Application 2 (External Events)
IAEA	International Atomic Energy Agency
IGPWR	INL Generic PWR
IE	Initiating Event
INL	Idaho National Laboratory
LLOCA	Large Loss of Coolant Accident
LOCA	Loss of Coolant Accident
LOOP	Loss Of Offsite Power
LOSC	Loss of Seal Cooling
LPIS	Low Pressure Injection System
LS	Limit Surface
LWR	Light Water Reactor
LWRS	Light Water Reactor Sustainability
MCC	Main Circulation Circuit
MCP	Main Coolant Pump
MOOSE	Multi-Physics Object-Oriented Simulation Environment
MSIV	Main Steam Isolation Valve
MSLB	Main Steam Line Break
NC	Natural Circulation
NLSSI	Non-linear Soil-Structure Interaction
NPP	Nuclear Power Plant
NRC	Nuclear Regulatory Commission
NUREG	Nuclear Regulatory Report
OPR	Offsite Power Recovery
PCT	Peak Clad Temperature
PIRT	Phenomena Identification and Ranking Table
PORV	Pilot-Operated Relief Valve
PRA	Probabilistic Risk Assessment
PRZ	Pressurizer
PWR	Pressurized Water Reactor
RA	Risk Assessment
RAVEN	Risk Analysis and Virtual Control Environment
RCS	Reactor Cooling System

RCP	Reactor Coolant Pump
R&D	Research and Development
RELAP5-3D	Reactor Excursion and Leak Analysis Program 5 – 3D
RIMM	Risk-Informed Margin Management
RISMC	Risk Informed Safety Margin Characterization
ROM	Reduced Order Model
RPV	Reactor Pressure Vessel
RWST	Refueling Water Storage Tank
TAF	Top of Active Fuel
TDAFP	Turbine Driven Auxilliary Feedwater Pump
TD-AFW	Turbine Driven AFW
TH	Thermal-Hydraulics
SA	Severe Accident
SBO	Station Black-Out
SG	Steam Generator
SLOCA	Small Loss of Coolant Accident
SM	Surrogate Model
SPH	Smooth Particle Hydrodynamics
SPRA	Seismic PRA
SRV	Steam Relief Valve
SSCs	Structures, Systems, and Components
SSI	Soil-Structure Interaction
SV	Safety Valve
SVC	Support Vector Classifier
SVM	Support Vector Machine
SWGR	Switchgear Room
TH	Thermal-hydraulic
UP	Upper Plenum
UQ	Uncertainty Quantification
UPS	Uninterruptible Power Supply

1. INTRODUCTION

1.1 Rationale

This report provides information about the activities performed during FY2017 for the development of the DOE Light Water Reactor Sustainability Risk-Informed Safety Margin Characterization (LWRS-RISMC), Industry Application #2, External Events (IA2) (Szilard and al. 2015). IA2 focuses on deploying an innovative external hazards safety analysis methodology identifying and developing an effective toolkit and their relative computational models for a US LWR (Szilard, et al. 2016). INL selected for its demonstration analysis a generic 3-loops Westinghouse PWR (INL generic PWR, or IGPWR (Parisi, et al. 2016), (Smith and al., Risk-Informed Safety Margin Characterization (RISMC) Pathway Technical Program Plan 2015)).

The ultimate goal of the IA2 is to perform an advanced risk-informed external hazards safety analysis for LWRs. Combined use of Probabilistic Risk Analysis (PRA) and Deterministic Safety Analysis (DSA) is pursued, with the final target of achieving a 'Virtual Nuclear Power Plant Risk Quantification'. Justification of the activity and a general description of the Risk-Informed Margin Management (RIMM) approach applied hereafter can be found in (Szilard and al. 2015), (see Figure 1) and (Smith and al., Risk-Informed Safety Margin Characterization (RISMC) Pathway Technical Program Plan 2015).

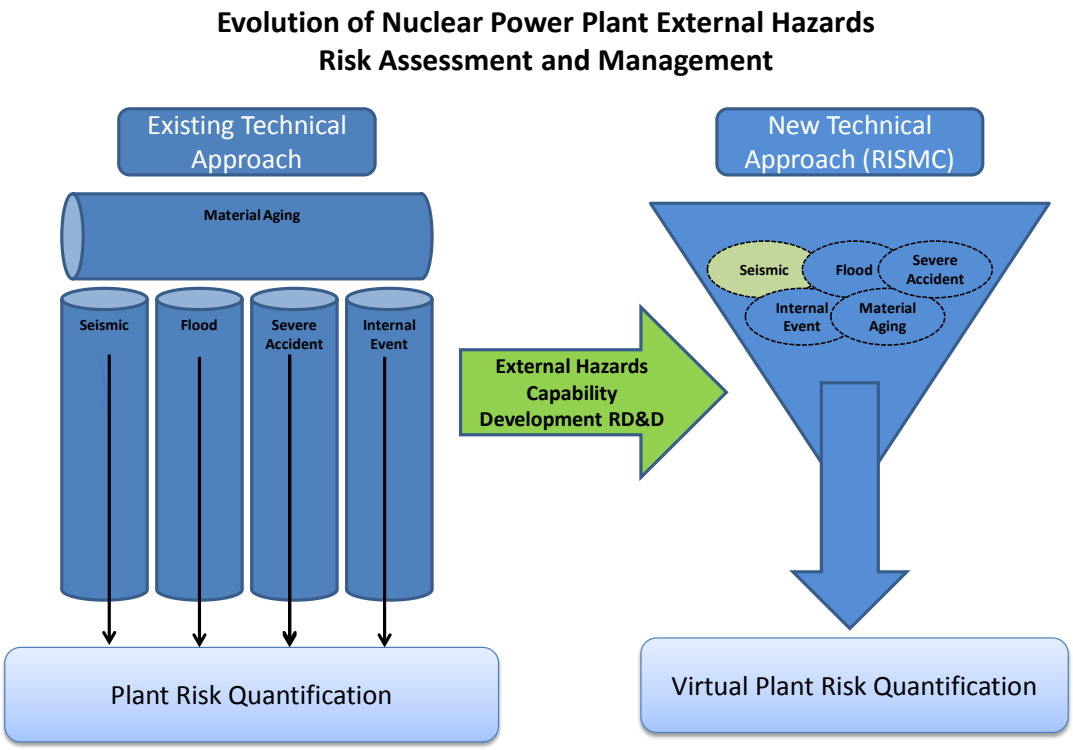

Figure 1. Current Risk Calculation Approach versus an Advanced RIMM approach.

1.2 External Hazards Analysis Workflow

In order to address such complex multi-physics and multi-scale analysis, a non-hazard specific workflow has been developed (see Figure 2 below) so that it could be applied to whatever external hazard safety analysis (earthquake, wind, tsunami, etc.). This workflow allows engineers to focus work on the correct areas by using existing models and data (Traditional Fault Trees and Event Trees) with new data and methods in stages to determine if continued analysis may be significantly beneficial.

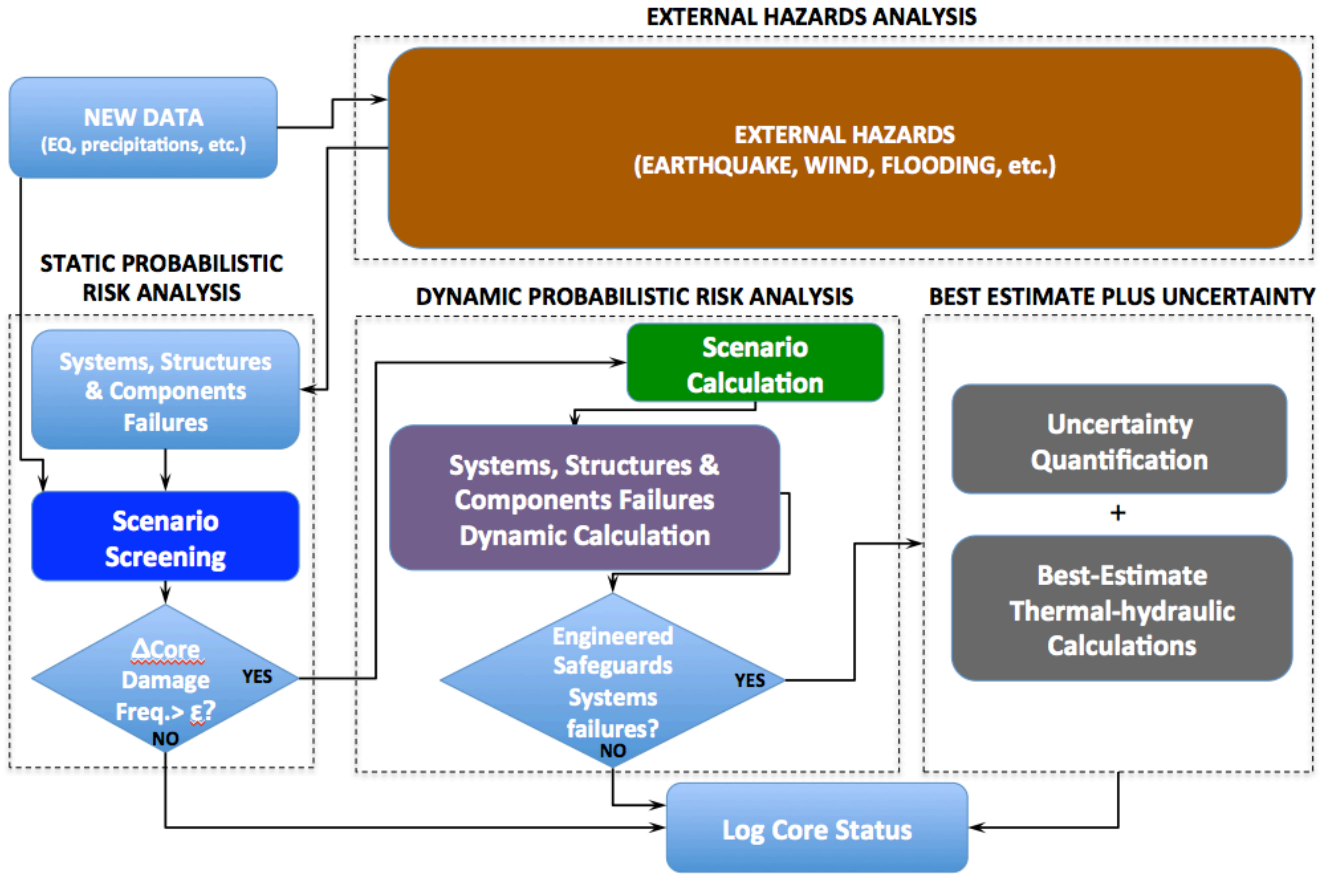

Figure 2. External Events Workflow.

The External Events (EE) generating hazards for the NPP are simulated in the top block. Deterministic software is to be used for determining the mechanical effects on the system, structure or components (SSC) of a NPP. The SSC failure modes and probabilities are used for informing the available static PRA.

When new data is available or hazard identified (e.g., new precipitation models, new earthquake (EQ) hazard curves, degraded piping, etc.), the new SSC failure modes and probabilities along with a conservative or maximum failure rates from any physics based models, are calculated and the static PRA tool is used to assess any positive increase in core damage frequency (CDF). If such increase is greater than a user-defined threshold, the significant failure sequences are then passed to the dynamic PRA tool for performing a more accurate risk evaluation.

The dynamic PRA re-simulate the selected scenarios performing dynamic calculations of the SSC failure modes (e.g., calculating the flooding patterns of a pipe break). If safety-significant components are affected by the selected SSC failure then Best-Estimate plus Uncertainty (BEPU) calculations are run for determining the core status (core damage/core safe). Every time the workflow is run, an update of the core status (i.e., the CDF

probability) is performed. The developed workflow is consistent with the safety analyses options listed by the IAEA in its Safety Guide (IAEA 2009) and it corresponds to the option 4 of the Table 1.

Table 1. Options for Safety Analyses.

Option	Computer Code	Availability of Systems	Initial and Boundary Conditions
1) CONSERVATIVE	Conservative	Conservative Assumptions	Conservative Input Data
2) COMBINED	Best Estimate	Conservative Assumptions	Conservative Input Data
3) BEST ESTIMATE	Best Estimate	Conservative Assumptions	Realistic + Uncertainty
4) RISK INFORMED	Best Estimate	Derived from PRA	Realistic + Uncertainty

For IA2, we considered seismic risk as the external hazard. The workflow was updated as shown in Figure 3. Most of the tools used for analysis are INL-developed tools. Information about them can be found in the next chapter.

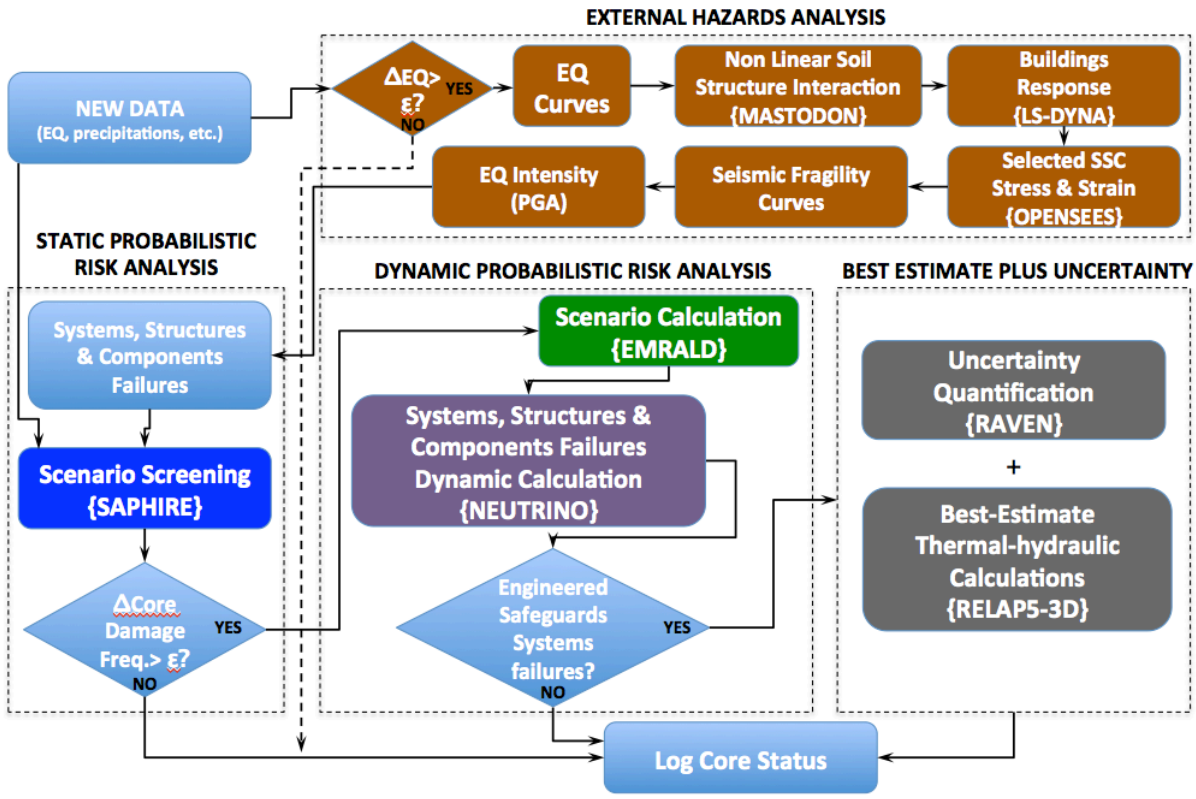

Figure 3. External Events Workflow and Toolkit.

The approach above shows that in order to perform a new EE hazard analysis, the change in the CDF evaluated by the static PRA has to be greater than a threshold indicated by the safety analyst. In that case, the steps that are to be followed are:

- External Hazards Analysis: Seismic analysis
    - Use updated EQ curves
    - Perform Non-Linear Soil Structure Interaction (NLSSI)
    - Calculate the Building Dynamic Response
    - Calculate the selected SSC stress & strain
    - Derive the new Seismic Fragility Curves for the SSC (failure probability vs. peak ground acceleration)
- Static PRA
    - update SSC failure probabilities
    - calculate if the updated SSC failure probabilities lead to a significant increase of CDF
    - if yes, perform dynamic PRA calculations for updating CDF with Best Estimate (BE) methods
- Dynamic PRA
    - run selected scenarios using dynamic PRA
    - perform dynamic calculations of selected SSC failure
    - if failures of safety relevant components are detected then perform BEPU of NPP dynamic
- BEPU
    - run NPP scenario using BE system thermal-hydraulic code plus Uncertainty
- Determine core status (failed/safe)
- Update the CDF metric

1.3 Structure of the Report

The report was organized in order to provide an easy access to the different parts of the calculation workflow described above. The structure of the report is the following one:

- in Chapter 2 we provide an brief description of the used toolkits and the references to each code documentation
- in Chapter 3 we provide the description of the computational models used for the analysis, in particular:
    - section 3.1 reports the External Hazard Analysis (seismic analysis)
    - section 3.2 reports the PRA part (both static and dynamic)
    - section 3.3 reports the dynamic SSC failure mode calculation (flooding)
    - section 3.4 and 3.5 reports the BEPU calculation of the system
- in Chapter 5 we provide the final results
- in Chapter 6 the summary and the path forward are given.

2. RISMC Toolkit Development for External Hazards

2.1 The External Events (EEVE) Toolkit

The multi-physics and multi-scale analyses are required for performing a risk-informed EE safety analysis. For this purpose, we identified two toolkits, the EEVE-A and EEVE-B (External EVEnts – Advanced/Baseline toolkits), see (Parisi, et al. 2016) for a detailed description. A schematic illustration of the proposed toolkits is given in Figure 4 below.

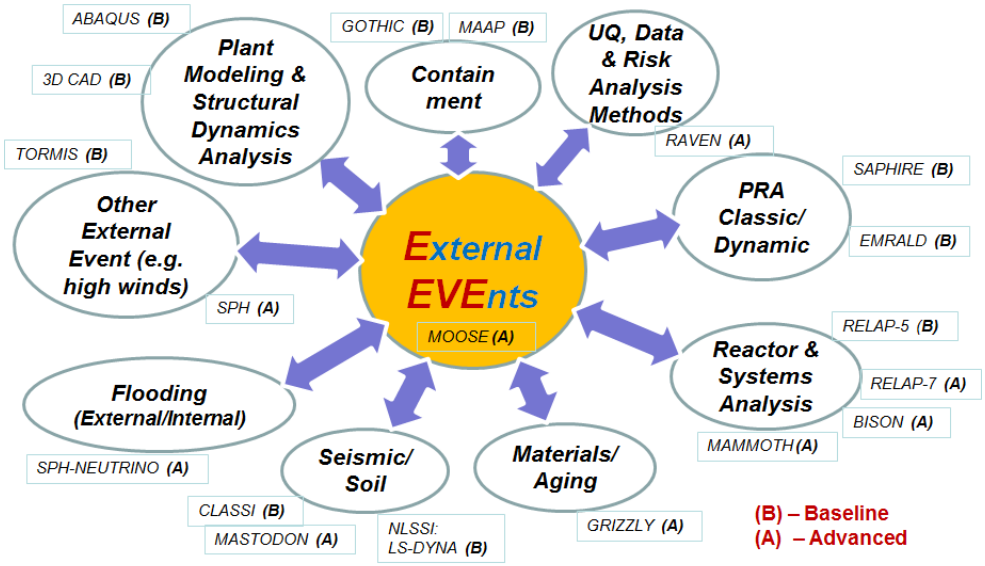

Figure 4. Schematic Illustration of EEVE-A and EEVE-B.

For FY2017 activities we set up a toolkit that includes part of the baseline and part of the advanced tools. The workflow of their coupling is shown in Figure 3 in Chapter 1. The list of the used tools and their respective task / block of the workflow is given in Table 2.

Table 2. Tools for the FY2017 EE Analysis.

Tools	Function	Block
LS-DYNA	EQ Analysis	External Event
OPENSEES	Piping Analysis	
SAPHIRE	PRA	Static PRA
EMRALD	Dynamic PRA	Dynamic PRA
NEUTRINO	3D Flooding Simulation	
RELAP5-3D	System TH	BEPU
RAVEN	Sensitivity/Uncertainty	

A short description of the tools used in reported below highlighting the improvement/modifications occurred during FY2017.

2.2 MASTODON & LS-DYNA

LS-DYNA is a commercially available finite element code that performs both implicit and explicit finite element analysis. LS-DYNA explicit is used for the NLSSI analysis (LS-DYNA 2013).

Multi-hazard Analysis for STOchastic time-DOmaiN phenomena (MASTODON) (Coleman, et al. 2017) is a finite element application that aims at analyzing the response of 3-D soil-structure systems to natural hazards such as earthquakes, and floods. MASTODON currently focuses on the simulation of seismic events and has the capability to perform extensive 'source-to-site' simulations including earthquake fault rupture, nonlinear wave propagation and NLSSI analysis. The unique capability of MASTODON is that as a MOOSE based application (Gaston, Hansen and Newman 2009) it seamlessly couples with other physics based applications such as GRIZZLY, RELAP-7, and BISON. This allows for modeling the response of a nuclear power plant to earthquake scenarios down to the pellet level. MASTODON will stochastically model virtual natural hazards and phenomena at virtual NPPs.

MASTODON is being developed as a dynamic probabilistic risk assessment framework that enables analysts to not only perform deterministic analyses, but also perform probabilistic or stochastic simulations for the purpose of risk assessment on a single platform. MASTODON performs calculations in effective stress space using a nonlinear hysteretic soil constitutive model (I-soil), and a u-p-U formulation to couple solid and fluid, as well as structural materials such as reinforced concrete. It is also equipped with interface models that simulate gapping, sliding and uplift at the interfaces of solid media such as the foundation-soil interface of structures. MASTODON also includes absorbing boundary models for the simulation of infinite or semi-infinite domains, fault rupture model for seismic source simulation, and the domain reduction method for the input of complex, three-dimensional wave fields.

2.3 NEUTRINO

NEUTRINO is a physics-based simulation tools that can be used to predict the behavior of water in a 3D environment (CentroidLab n.d.). NEUTRINO was used for this and previous work because of its advanced tools including particle emitters, ability to couple dynamically with other applications, and its advanced easy to use interface. The NEUTRINO software uses an IISPH solve engine which is faster than many similar tools, and still acceptably accurate. An advanced "Z Sorted Compact Hashing" method is used to accomplish quick nearest neighbor lookup when computing particle interactions (Sampath, Montanari and Akinci 2016).

Several new features in NEUTRINO have been added since the work done in FY2016, including a scientific visualization package to visually desired particle attributes and the ability to dynamically set or adjust any object property through the communication protocol. Initial work has also been done on incorporating the NEUTRINO solve engine to run inside of MOOSE.

2.4 EMRALD

EMRALD, is a dynamic PRA code (Prescott, Smith and Samptah 2014). When running an EMRALD model, users are able to determine the cascade of events over time that can lead to a specified outcome. It also allows for coupling with physics based simulation code for contributing to dynamic component failure and final PRA results.

EMRALD based on three-phased discrete event simulation (see Figure 5).

To initialize, all states in the model marked initial start states are added to the Current and New State List.

1. While there are States in the New State list, For each State:
   - Add the Events to the Time Queue or Conditional List.
   - Execute any Immediate Actions.

2. If any Conditional Event's criteria is met:
   - Execute that Event's action/s.
   - Go to Step1.
3. Jump to the next chronological event.
   - Process that event's action/s.
   - Go to Step1.

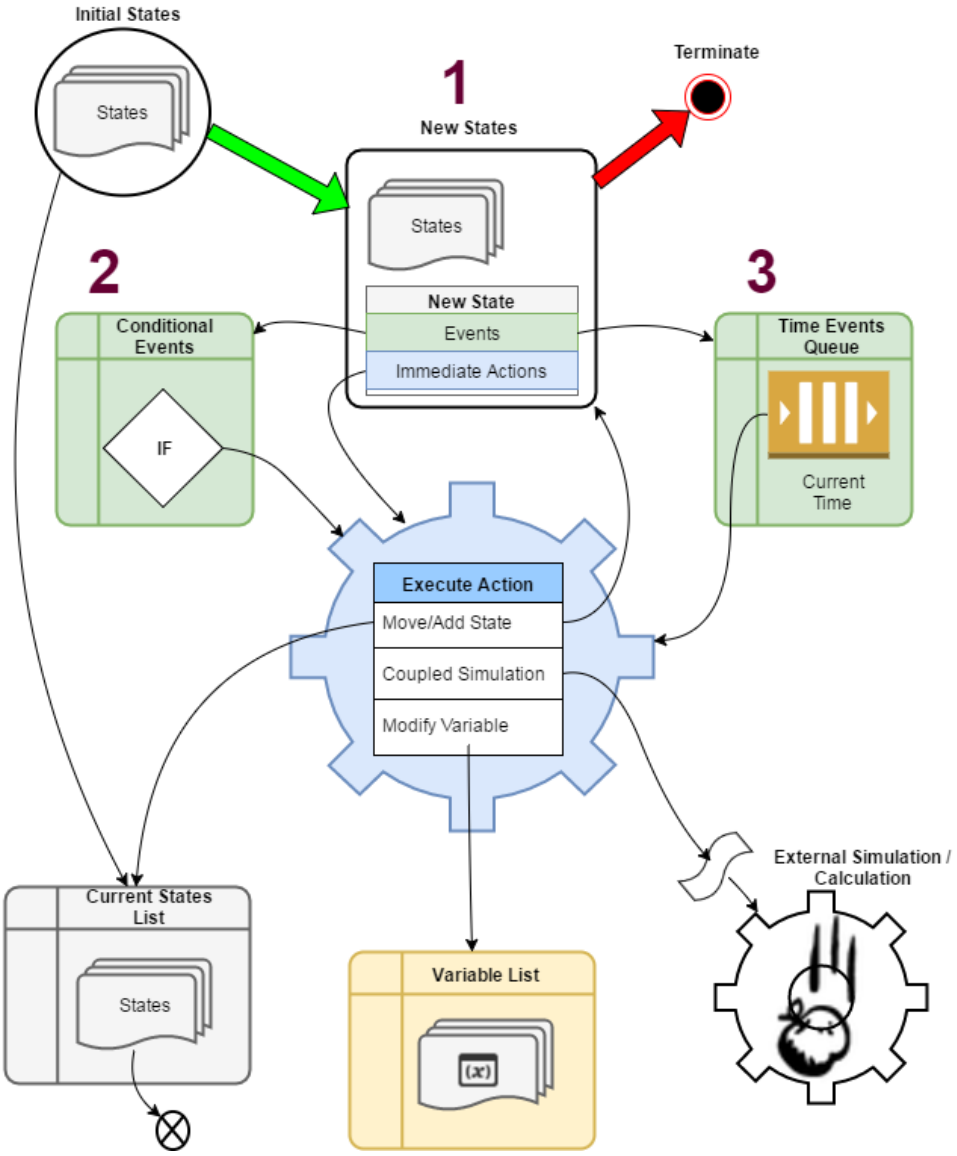

Figure 5. EMRALD Execution Based on Three Phase Discrete Event Simulation.

See section 4 of (US NRC, Risk Assessment of Operational Events Handbook Volume 2 - External Events 2008) for more details on EMRALD capabilities, modeling, or calling other analysis methods.

Initial work has also been done on implementing core EMRALD capabilities as a MOOSE animal called Red-Tail which will allow other MOOSE applications to be driven or adjusted by a state based model.

2.5 RELAP5-3D

RELAP5-3D code (The RELAP5-3D(c) Code Development Team 2015) is the INL-developed BE system thermal-hydraulic (TH) code of the RELAP5 family. It is capable of performing transient simulations of LWR systems during normal and accidental conditions (LOCAs, both large and smalls, ATWS, loss of feedwater, main steam line break, etc.).

The code solves a nonhomogeneous and nonequilibrium model for the two-phase flow using a fast, partially implicit numerical scheme. RELAP5-3D differs from the other RELAP5 versions thanks to a multi-dimensional TH and 3D neutron kinetic modeling capability. The code development and validation is based on an extensive set of experimental data and its applicability to BEPU technology has been demonstrated (Schultz 2015).

In the IA2, the code is applied for performing calculations for Loss of Offsite (LOOP) transient and Station Blackout (SBO) accident. The simulations are run inside the code applicability range, i.e. until the code predicts the onset of the fuel damage (peak cladding temperature, PCT = 2200 F). The applicability range of RELAP5-3D is shown in Figure 6.

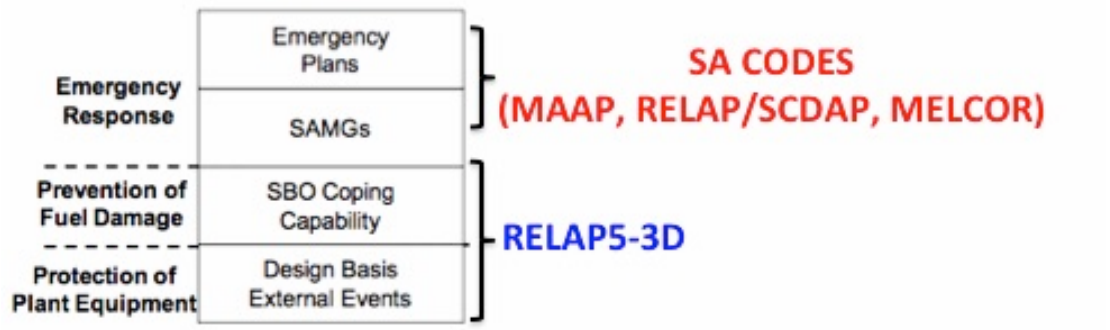

Figure 6. RELAP5-3D Role in LOOP and SBO Calculations.

References to the applicability of RELAP5 codes in simulating the above scenarios can be found in the open literature, e.g. in (Prosek and Cizelj 2013), (Matev 2006).

2.6 RAVEN

Sensitivity/uncertainty analysis is performed by coupling RELAP5-3D system TH code to the RAVEN code (Alfonsi, et al. 2017). RAVEN code is a generic software framework to perform parametric and probabilistic analysis based on the response of complex system codes. RAVEN is coupled to RELAP5-3D via an Application Programming Interface (API), which allows the analyst to perform input space sampling using Monte Carlo, Grid or Latin Hyper Cube sampling schemes.

RAVEN has the capability to run on High Performance Computing machines (HPC), which allows the execution of hundreds of parallel serial runs. RAVEN strength lies also in its system feature discovery capabilities such as: constructing limit surfaces, separating regions of the input space leading to system failure, and using dynamic supervised learning techniques.

3. External Hazards Advanced PRA Demonstration

In the following sections, the key components of the demonstration of the External Hazards analysis are presented. We started analyzing seismic buildings, modeling not only the structural behavior of the each building but also their mutual interactions. The static and dynamic PRA models presented in section 3.2 are informed by the seismic models results and, after screening runs, they explore the selected domains of interest (in this case selected Loss-of-Offsite Power (LOOP) and Station Blackout (SBO) sequences). Section 3.3 shows the three-dimensional flooding analysis, which is performed for assessing the failure probabilities and failure modes of some components of the engineered safeguards systems. Section 3.4 and 3.5 presents the Best-Estimate plus Uncertainty calculations of the selected sequences.

3.1 Seismic Models

Physics based simulation tools can be used to predict 3D NLSSI behavior. For this demonstration, LS-DYNA was used because of its nonlinear soil modeling capabilities and its ability to efficiently solve large finite element problems.

Figure 7 to Figure 13 show the finite element model used to perform the NLSSI analysis. The full model (shown in Figure 7) consists of 208 mass elements, 10,485 beam elements, 38,125 shell elements, and 1,505,532 solid elements. The structure in the model represents the Auxiliary Building and Turbine Building for the Palisades Nuclear Plant. Figure 8 shows a model of the Auxiliary Building, Turbine Building, and Containment Structure developed by SC Solutions, Marietta, GA.

A portion of this structure (shown in Figures Figure 9 and Figure 10) is used for the structural model in this evaluation. The structural model (shown in Figure 8) was developed for modal analysis and has definitions within it that prevent it from running directly in the explicit solver. Most of the definition issues that had to be addressed related to where beam elements were defined with a density of zero (and a very high modulus of elasticity to approximate a rigid beam). For the explicit solver, these were simply changed to constrained nodal rigid bodies. Additional constrained nodal rigid bodies were defined for very short stiff beams in an attempt to improve the time step used in the model run.

The soil (shown in Figure 12) consists of 37 nonlinear layers with unique material properties. There is an added 38th soil layer at the bottom of the soil that is elastic and used to bring the seismic waves into the model. The soil layer geometry and material properties are from (Spears and Coleman 2015). The units used in the reference are feet (or inches), kips, and seconds. Consequently, the finite element model was generated and run with feet, kips, and seconds units. The output acceleration time histories are given in g's. This report is documented in SI units.

The structure has significant embedment under the Turbine Building and there is underground structure under the Auxiliary Building also. To accommodate this, below ground structure is rigidly constrained to nearby soil nodes. Additionally, at the soil surface, constrained interpolation is defined to cause the soil nodes to be tied to the lower surface of the structure. Considering the significant embedment, the soil being tied to the structure is considered reasonable. Further study can be performed with the soil and structure having frictional contact but the primary impact consideration in this demonstration is between the Auxiliary Building and Turbine Building. Figure 11 identifies these buildings and the boundary where impact can occur. To capture potential impact, the shell elements aligned vertically along the boundary of the Auxiliary Building are put in contact with the adjacent Turbine Building nodes.

For the soil (shown in Figure 12), the bottom of the elastic soil layer (bottom layer) has non-reflective boundary conditions and the top of the elastic soil layer has an applied seismic load time history. On the horizontal boundary of all of the soil, constraints are added to mimic an infinite horizontal continuum. The constraints are used to constrain each set of boundary nodes at a given elevation so that they translate the same in all directions. The top surface of the soil is free.

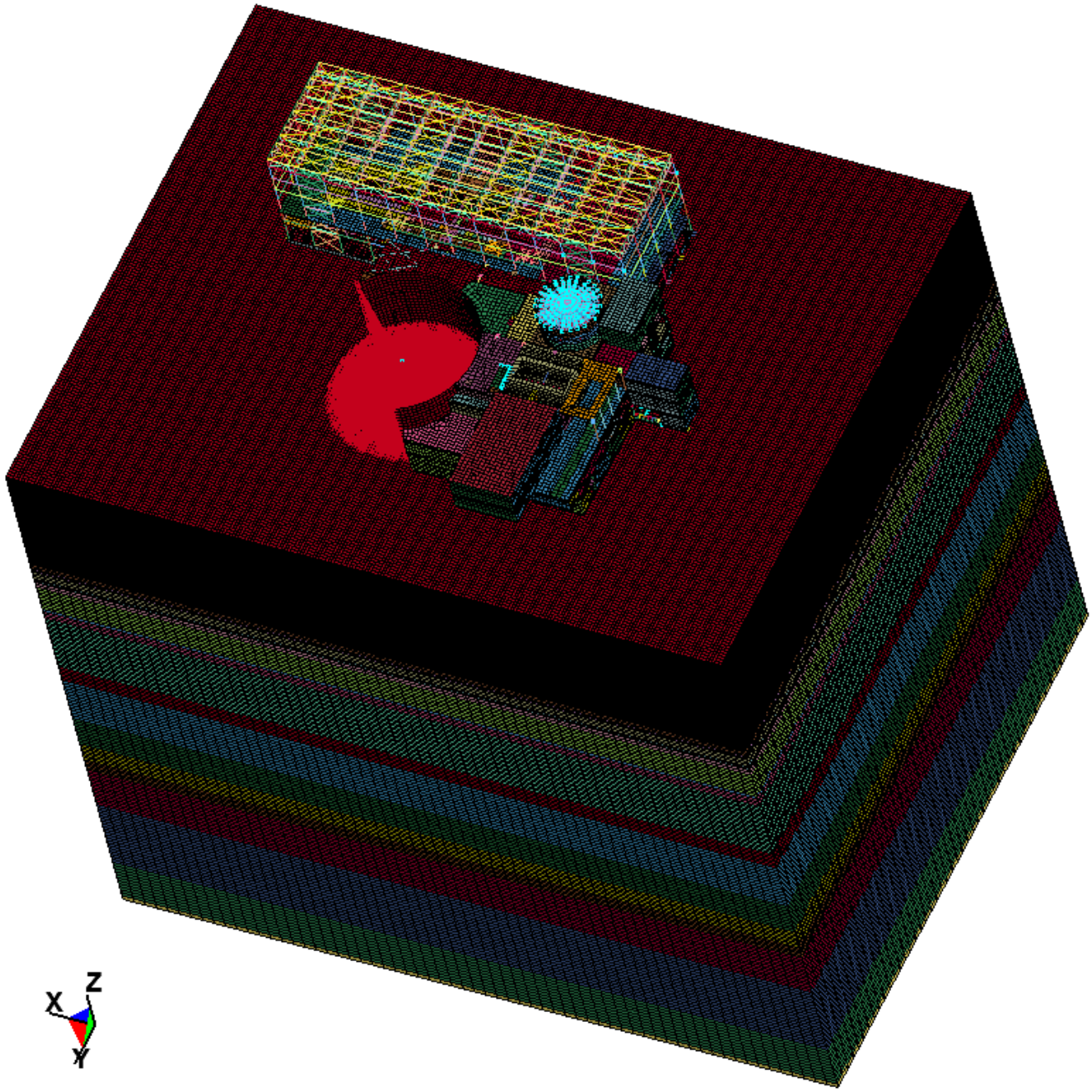

Figure 7. NLSSI Finite Element Model.

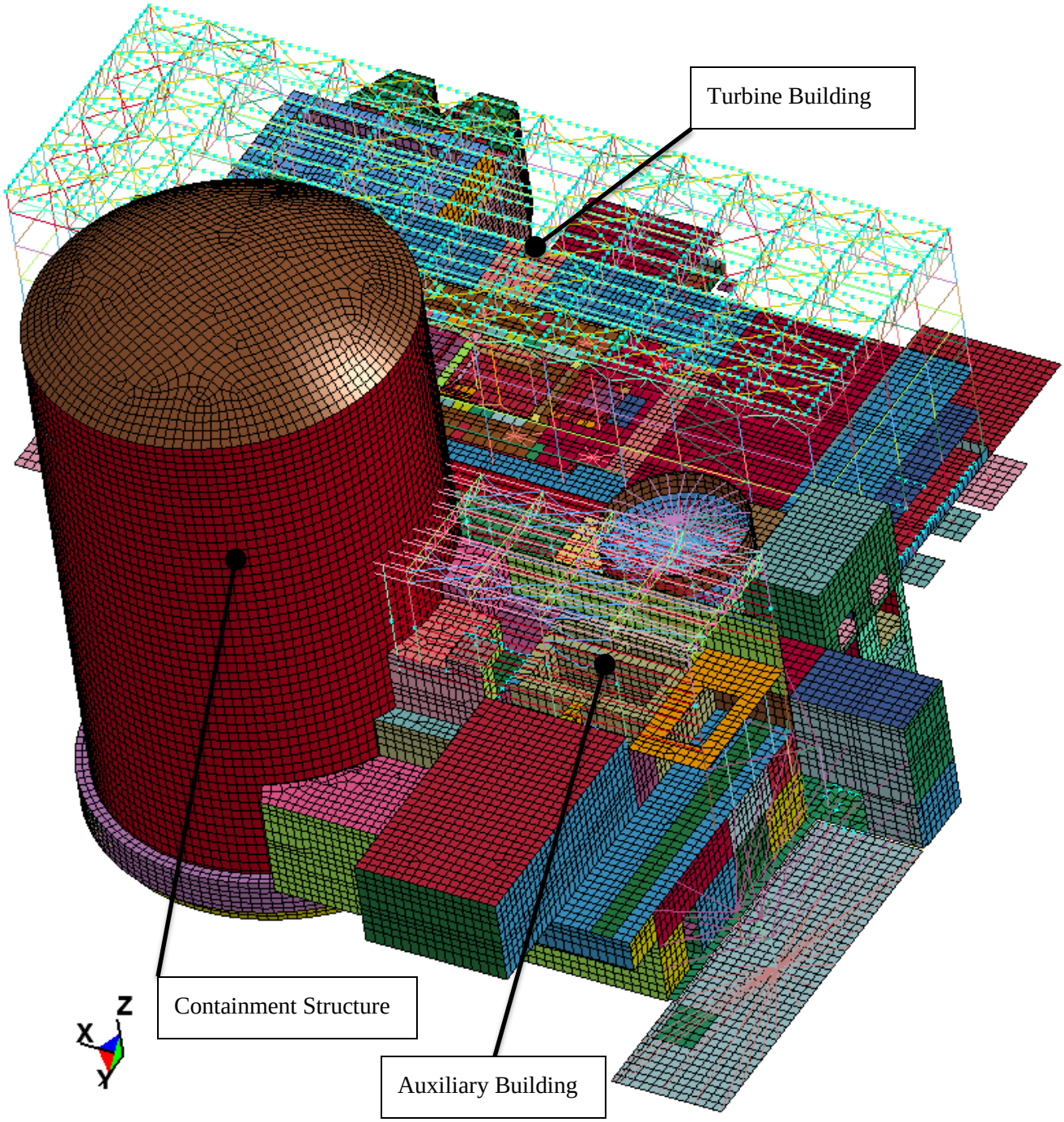

Figure 8. Auxiliary Building, Turbine Building, and Containment Structure Developed by SC Solutions.

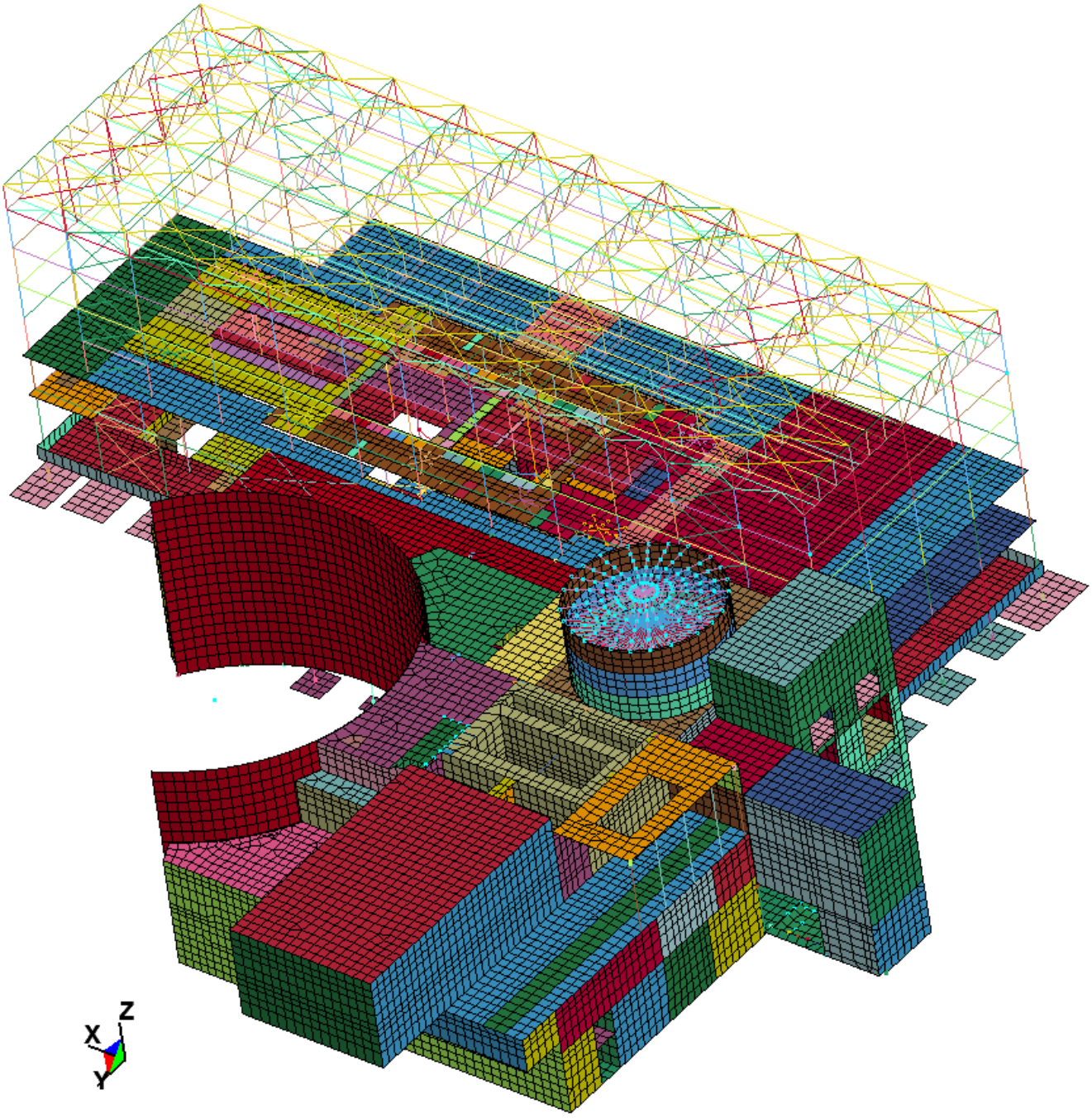

Figure 9. Portion of the Auxiliary Building and Turbine Building Used in the NLSSI.

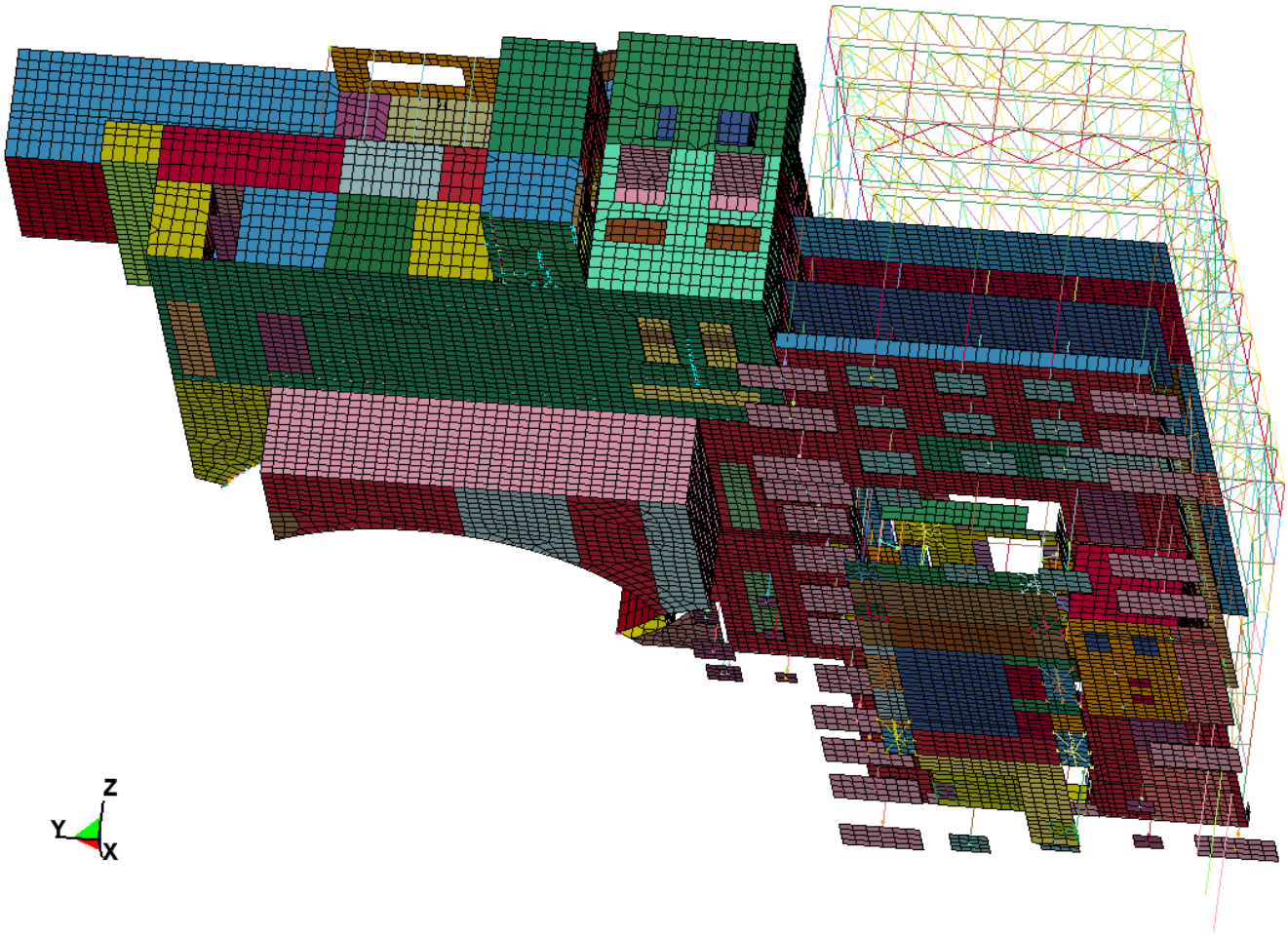

Figure 10. Portion of the Auxiliary Building and Turbine Building Used in the NLSSI (Viewed from Below).

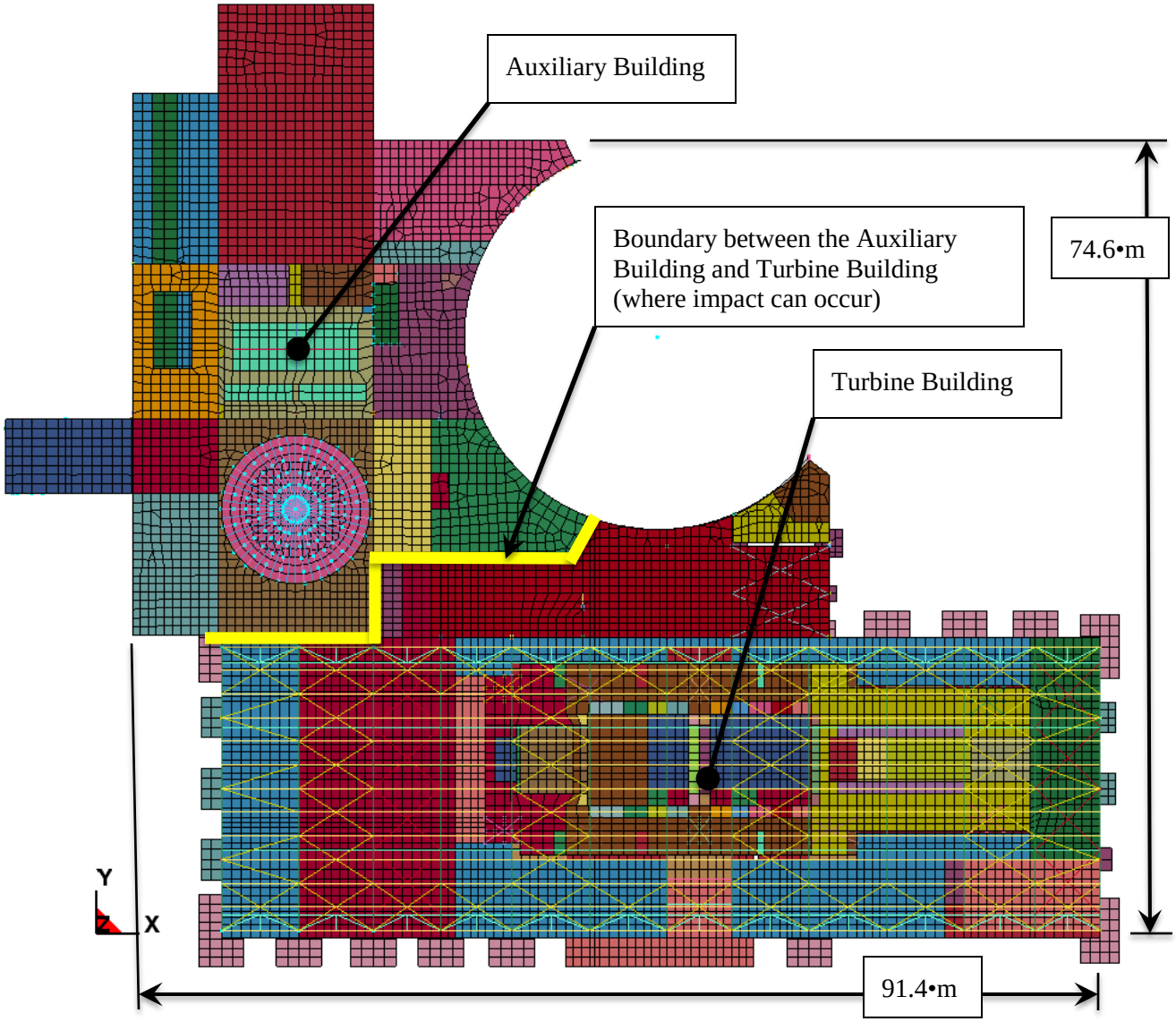

Figure 11. Boundary Where Impact between Structures Can Occur.

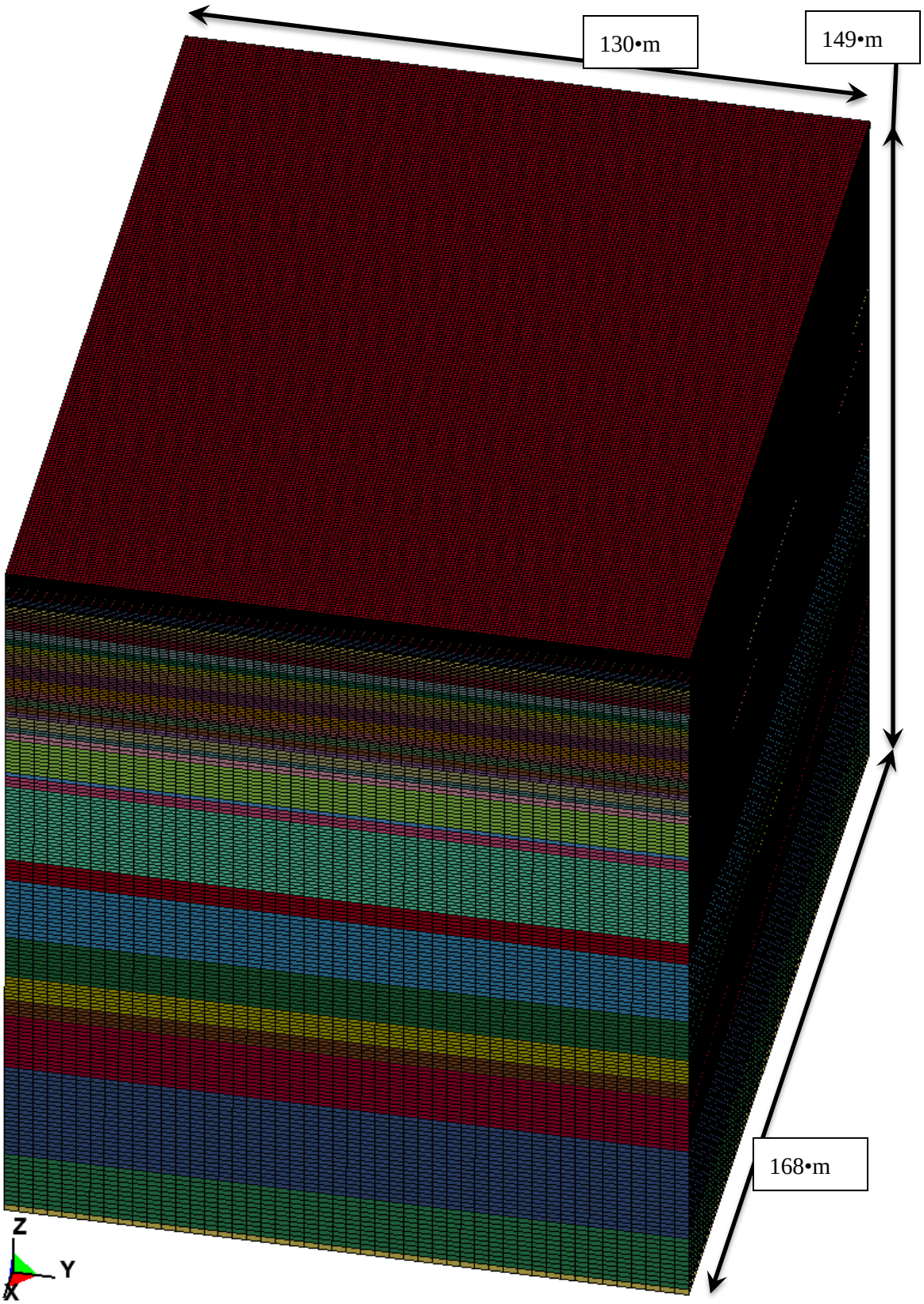

Figure 12. NLSSI Finite Element Soil Mesh.

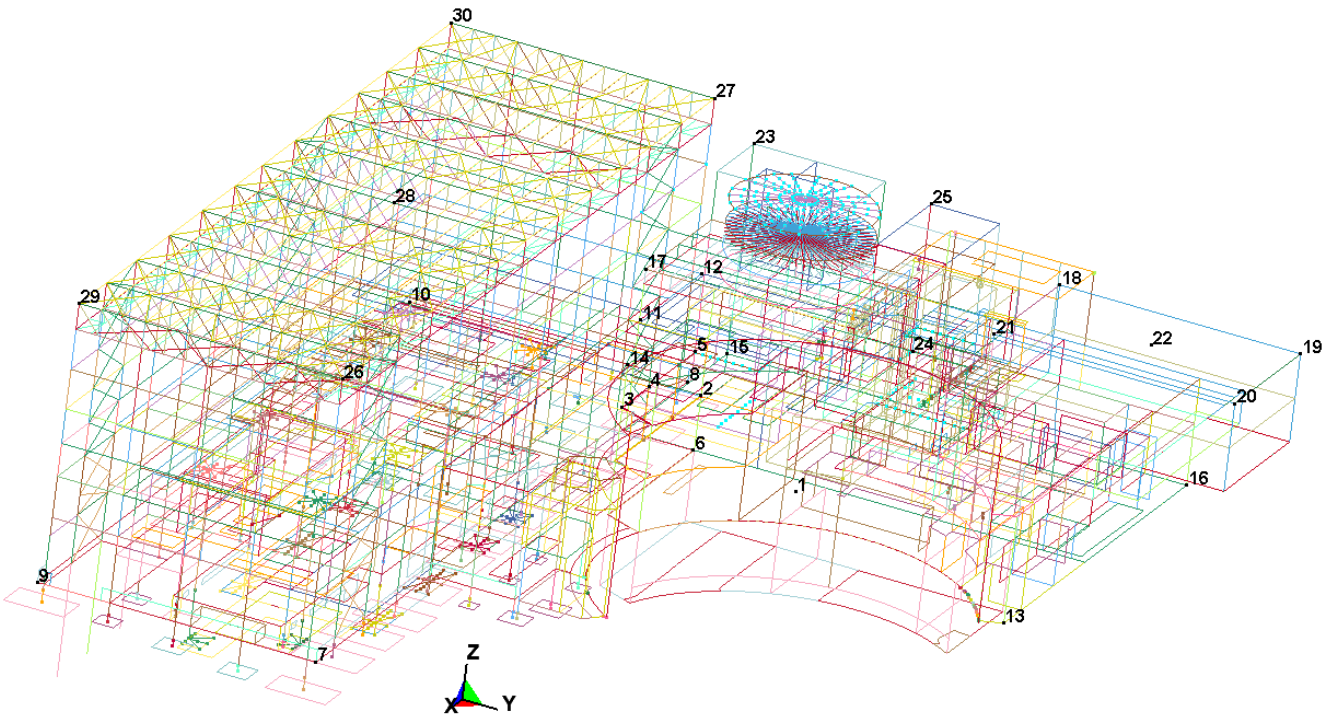

Figure 13. Acceleration Output Nodal Locations.

As shown in Figure 11, the structure footprint is about 91.4 m by 74.6 m. The height of the Turbine Building is about 28.2 m and the maximum modeled depth is about 11.3 m. The structure consists of masses, solids, shells, and beams mostly with material properties of concrete and steel. To accommodate all of the unique elements in the mesh, 468 parts are defined.

The soil mesh (shown in Figure 12) is 168 m by 130 m by 149 m. The soil element sizes are set to pass vertically propagating, planer shear and normal seismic waves up to 50 Hz with at least 10 elements per wavelength. Horizontally, the soil elements are sized to pass up to 15 Hz reflected waves with at least 10 elements per wavelength. A likely source of horizontal wave propagation is structural rocking and that does not produce significant high frequency content (unless it becomes severe enough to produce impact which can excite all frequencies).

All of the soil elements are rectangular parallelepiped in shape. Consequently, when there is a significant stiffness change between soil layers, the soil layer meshes don't align. To attach these soil layers, tied contact is used. Rayleigh damping is applied to the soil and structure. The Rayleigh damping in the soil is minimal and is just defined to ensure that some damping occurs even at very low strains. (The material properties defined in (Spears and Coleman 2015) are adjusted to accommodate the Rayleigh damping.) This damping is set so that there is 1% damping at 0.6 Hz and 1/2% at 100 Hz. The structural damping is set to best approximate 4% damping for the frequencies where the structure responds. This damping is set so that there is exactly 4% damping at 2.6 Hz and 11 Hz.

The model run output is acceleration in all three translational directions at 30 nodes (as shown in Figure 13). The model run input is the seismic, rock outcrop time histories shown in Figure 14. These time histories are taken from (Spears and Coleman 2015). To produce load time histories applied to the top of the elastic soil layer, the acceleration time histories are integrated to velocity time histories and then scaled with the stiffness and density properties of the elastic soil layer.

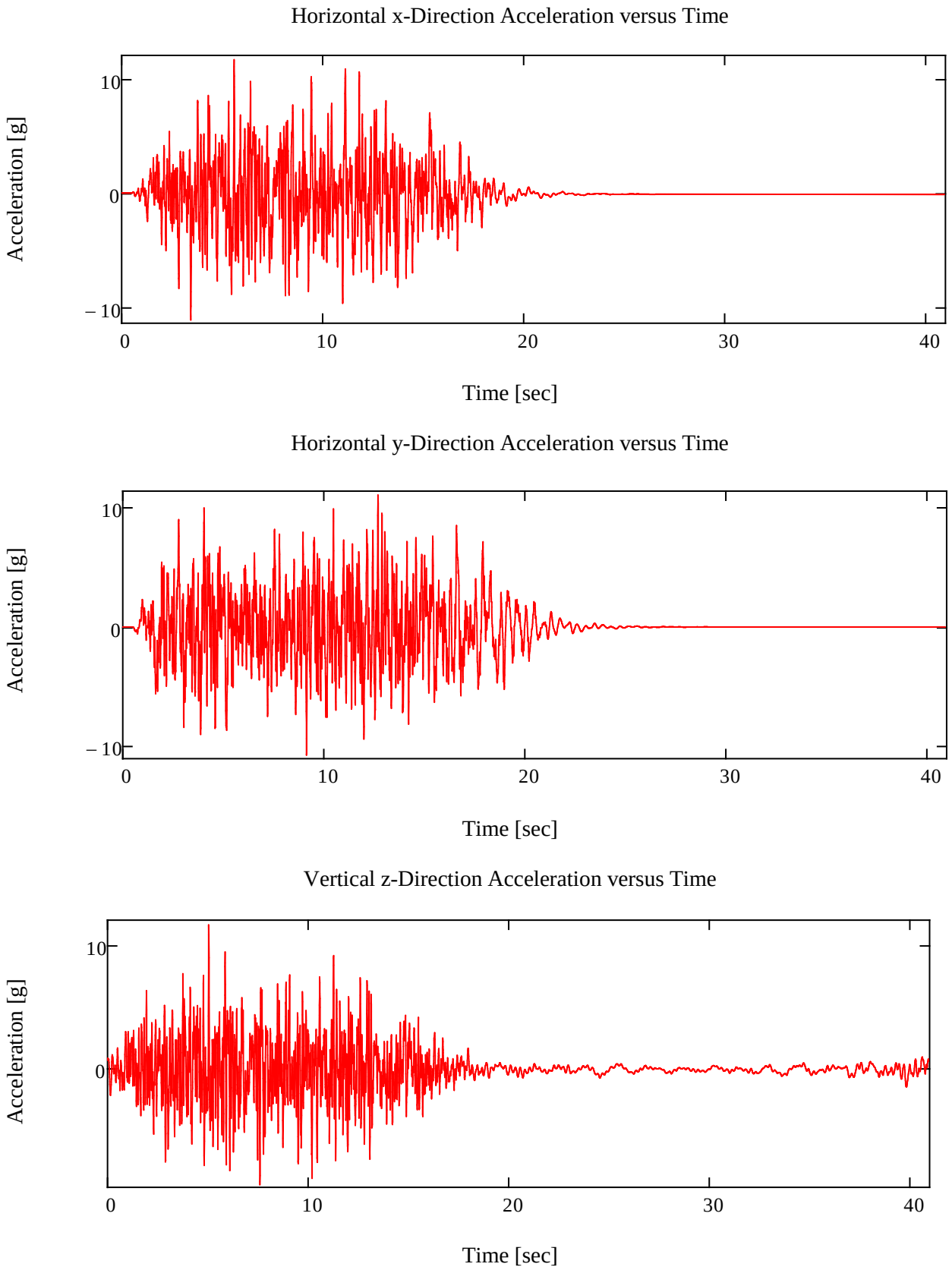

Figure 14. Horizontal and Vertical Seismic Time Histories.

3.2 PRA Models

The static and dynamic PRA models work together, leveraging existing static models to optimize work needed when developing any necessary dynamic model. Additionally static models are used as a base case or a check for the dynamic model to verify results before external contributions is included.

3.2.1 Static PRA Model

A generic internal events PRA model developed using SAPHIRE code (Smith and Wood, Systems Analysis Programs for Hands-on Integrated Reliability Evaluations (SAPHIRE) 2011) for a typical pressurized water reactor (PWR) plant was obtained and revised for the IA2 activities. This section presents the following works that have been performed for the PRA model: (1) revise the generic internal events PRA model to add seismic event model; (2) select PRA sequences to be analyzed in dynamic analysis and thermal hydraulic analysis; (3) simplify the PRA model and convert to EMRALD model; (4) quantify the SAPHIRE PRA model to compare the results with those from the integrated dynamic analyses.

3.2.1.1 Seismic Hazard Initiating Events

The available generic SAPHIRE PRA model includes only internal events. To be used in this project, the internal events PRA model was expanded to include seismic events. Volume 2 of Risk Assessment of Operational Events Handbook (US NRC, Risk Assessment of Operational Events Handbook Volume 2 - External Events 2008), which is also known as RASP Handbook, provides methods and guidance for the risk analysis of initiating events conditions associated with external events including seismic. The handbook was used as the main source to develop the seismic event model (including the generic SSC seismic-induced fragilities) for this project.

SEISMIC HAZARD INITIATING EVENTS

The following example seismic hazard vector (Table 3) taken from the RASP Handbook was used in this project to derive the seismic initiating event frequencies as a function of seismic acceleration g level. The vector provides the cumulative mean frequency of exceedance per year for the associated g value. For example, the frequency of a seismic event of magnitude 0.05g or higher is given as 3.04E-4/year.

Table 3. Seismic Hazard Vector.

Ground Acceleration (g)	Cumulative Exceedance Frequency (per year)
0.05	3.040E-04
0.08	1.777E-04
0.15	6.422E-05
0.25	2.748E-05
0.3	1.979E-05
0.4	1.141E-05
0.5	7.212E-06
0.65	4.043E-06
0.8	2.474E-06
1	1.409E-06

The above seismic acceleration range is partitioned into three categories, or bins, to define three discrete seismic event scenarios with increasing intensity: Bin-1 from 0.05g to 0.3g, Bin-2 from 0.3g to 0.5g, and Bin-3 above 0.5g. The three seismic bins are chosen based on previous study. The first bin is driven by seismically induced LOOP events and the third bin is driven by the seismic failure of major structures, leading to direct core damage. The second bin captures other important events such as small loss of coolant accident (SLOCA) and large loss of coolant accident (LLOCA). Table 4 shows the three seismic initiating events (IEs), the descriptions, the frequencies, the associated seismic bins, and the representative bin accelerations derived from the seismic hazard vector. The representative bin accelerations would be used later to determine the SSC seismic fragilities.

Table 4. Seismic Initiating Event Frequencies and Bin Accelerations.

Seismic IE	Seismic IE Description	Seismic IE Frequency (per year)	Seismic Bin	Bin Acceleration (g)
IE-EQK-BIN-1	SEISMIC INITIATOR (0.05 - 0.3 g)	2.842E-04	BIN-1	0.122
IE-EQK-BIN-2	SEISMIC INITIATOR (0.3 - 0.5 g)	1.258E-05	BIN-2	0.387
IE-EQK-BIN-3	SEISMIC INITIATOR (> 0.5 g)	7.212E-06	BIN-3	0.707

SEISMIC EVENT TREE MODELS

Three seismic event trees EQK-BIN-1, EQK-BIN-2, and EQK-BIN-3 are developed for the three seismic bins as shown below. The end state of a seismic sequence could be OK (no significant consequence), transfer to INT-LOOP event tree (seismic induced loss offsite power), transfer to INT-SLOCA event tree (seismic induced small loss-of-coolant), transfer to INT-LLOCA event tree (seismic induced large loss-of-coolant), and CD (core damage). This project focuses on the seismic induced loss offsite power sequences, which are transferred to internal-event LOOP event tree.

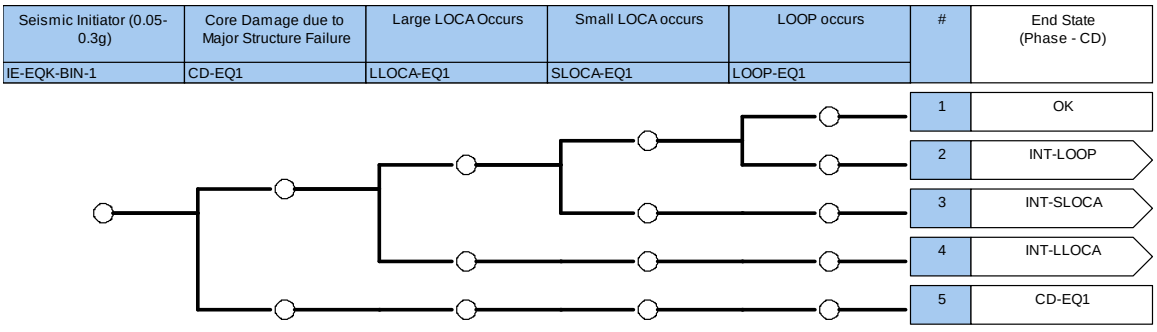

Figure 15. Seismic BIN-1 Event Tree.

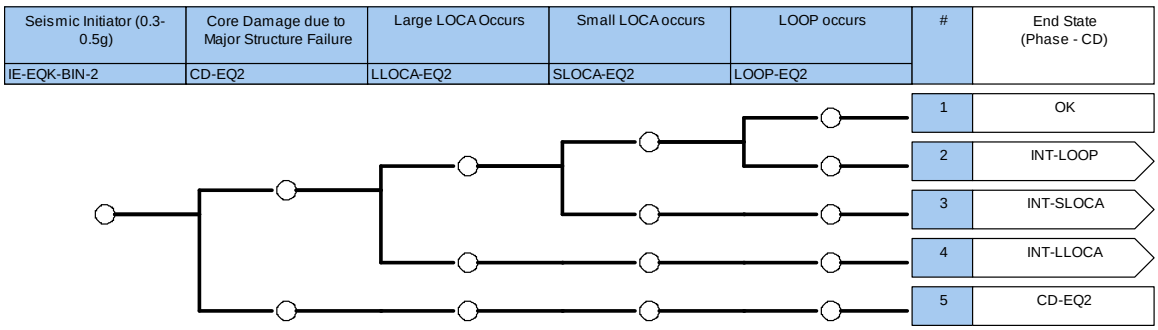

Figure 16. Seismic BIN-2 Event Tree.

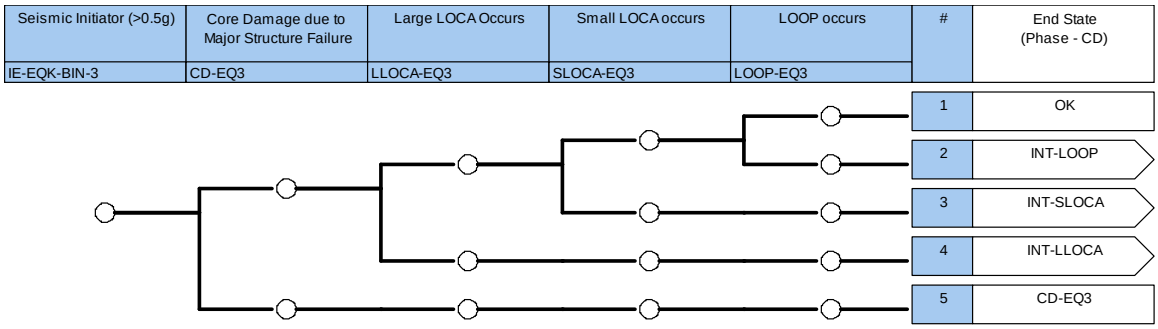

Figure 17. Seismic BIN-3 Event Tree.

SEISMIC FAULT TREE MODELS

Developing seismic fault tree models include two parts: (1) developing new fault trees for seismic event tree top events CD-EQ1, CD-EQ2, CD-EQ3, LLOCA-EQ1, etc.; and (2) revising existing front line and support system fault trees to incorporate seismic caused system and component failures. Each of the new seismic fault trees contain a single probability that represents the likelihood of the event occurs given the seismic bin event. Figure 18 shows the new seismic fault trees LOOP-EQ1, LOOP-EQ2, and LOOP-EQ3.

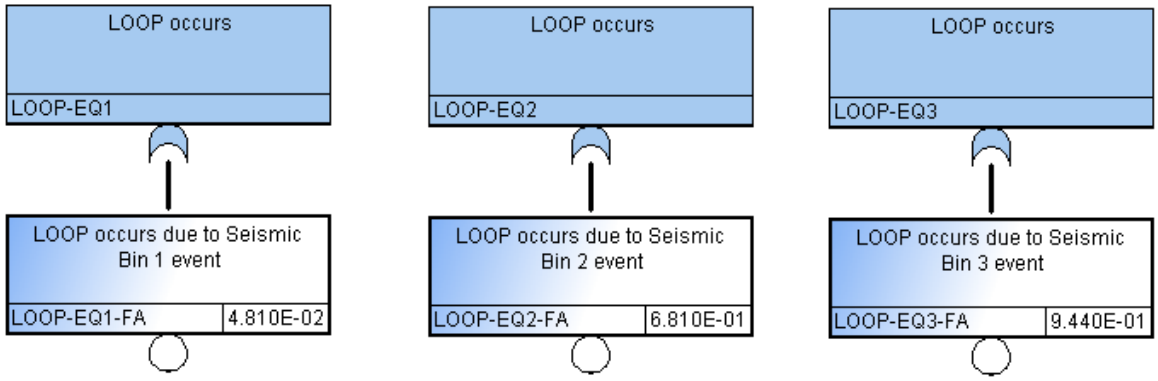

Figure 18. Seismic Fault Trees LOOP-EQ1, LOOP-EQ2, and LOOP-EQ3.

For existing front line and support system fault trees, seismic caused system and component failures are added to represent the contribution of seismic events to the system. As an example, Figure 19 shows the revised auxiliary feedwater (AFW) pump C fault tree AFW-TDP. Seismic subtree AFW-EQ is added to the fault tree to represent the contribution of seismic events to AFW failure. Figure 20 displays the seismic subtree AFW-EQ. The seismic subtrees are activated only when the seismic bin event is to be quantified and the associated flag event (EQ-BIN-1-OCCURS, EQ-BIN-2-OCCURS, or EQ-BIN-3-OCCURS) is set to TRUE. The seismic caused SSC failure basic events (such as EQ-AFW1-FA, EQ-AFW2-FA, and EQ-AFW3-FA) related to the seismic bin are thereby introduced and accounted in the model quantification.

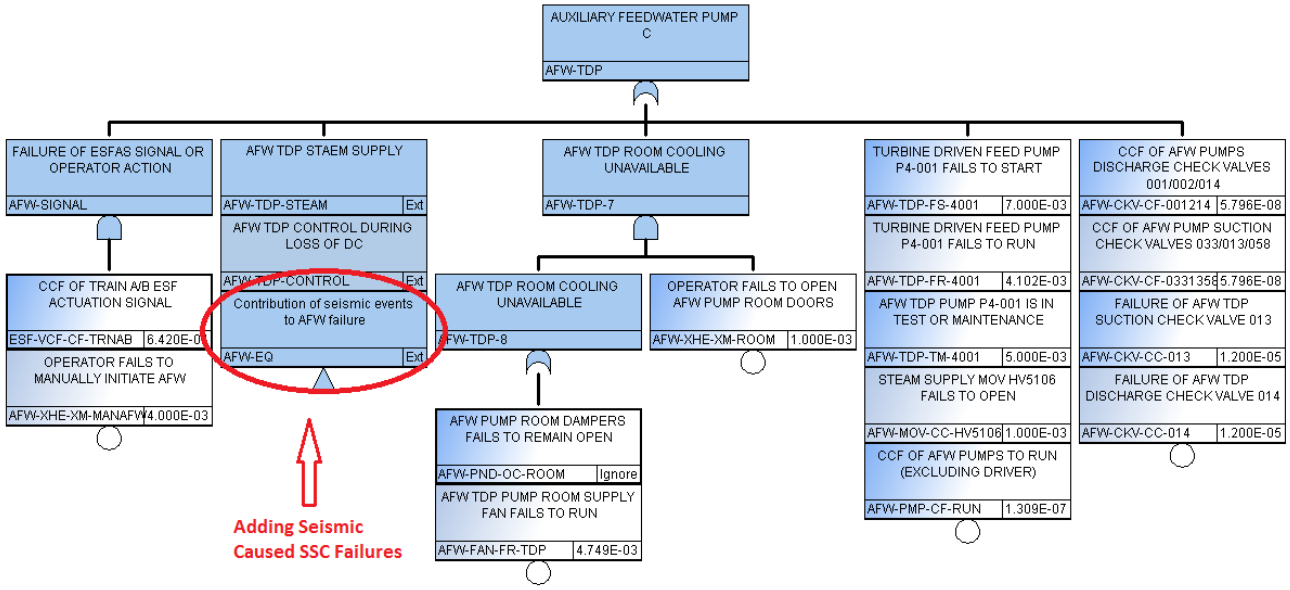

Figure 19. Revised Fault Tree AFW-TDP with Seismic Sub-Tree AFW-EQ.

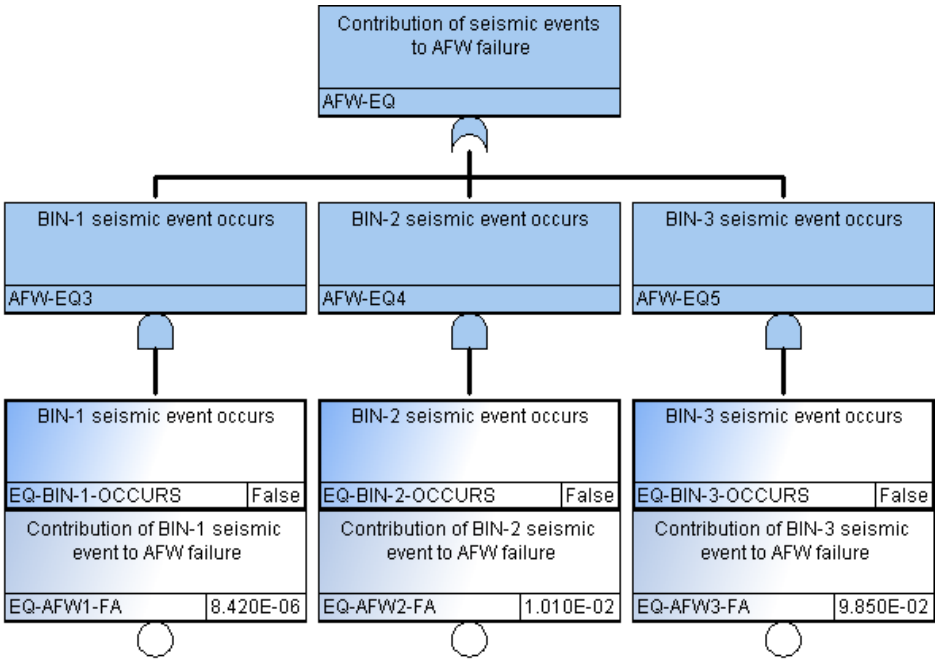

Figure 20. Seismic Sub-Tree AFW-EQ.

SSC SEISMIC FAILURE PROBABILITIES

SSC seismic failure probabilities used in this SAPHIRE model are calculated based on the SSC seismic fragilities which are obtained either from Appendix 4B of the RASP Handbook or from typical PWR plant external events PRA model. SSC seismic fragility information is represented by the median capacity of the component a_m, and uncertainty parameters βr and βu. Specifically, the mean seismic failure probability $P_{EQ}(a)$ at a bin acceleration level of a can be calculated with the following equation:

$$P_{EQ}(a) = \emptyset[ln(a/a_m)/(\beta_r^2 + \beta_u^2)^{1/2}]$$

where Φ is the standard normal cumulative distribution function.

Table 5 presents a summary of the SSC seismic fragilities and failure probabilities used in the SAPHIRE model. The data source of the seismic fragilities as well as the associated seismic basic events are also provided in the table.

Table 5. SSC Seismic Fragilities and Failure Probabilities.

Item	SSC Description	Data Source	Seismic Bin	Median Capacity (g)	βr	βu	SSC Failure probability	Comment
1	Reactor Pressure Vessel & Supports	RASP Handbook	BIN-1	2	0.3	0.35	6.50E-10	to CD-EQ
			BIN-2	2	0.3	0.35	1.83E-04	
			BIN-3	2	0.3	0.35	1.20E-02	
2	Steam Generators & Supports	RASP Handbook	BIN-1	2.5	0.3	0.4	7.70E-10	to CD-EQ
			BIN-2	2.5	0.3	0.4	9.53E-05	
			BIN-3	2.5	0.3	0.4	5.77E-03	
3	Reactor Coolant System Piping	RASP Handbook	BIN-1	3.8	0.35	0.5	8.79E-09	to CD-EQ
			BIN-2	3.8	0.3	0.35	3.61E-07	
			BIN-3	3.8	0.3	0.35	1.32E-04	
4	Buildings (control room ceiling grid turbine and auxiliary buildings)	RASP Handbook	BIN-1	1.1	0.3	0.35	9.19E-07	to CD-EQ
			BIN-2	1.1	0.3	0.35	1.17E-02	
			BIN-3	1.1	0.3	0.35	1.69E-01	
5	CD	sum of 1,2,3,4	BIN-1				9.29E-07	CD-EQ1
			BIN-2				1.20E-02	CD-EQ2
			BIN-3				1.87E-01	CD-EQ3
6	Reactor Coolant Pumps & Supports	RASP Handbook	BIN-1	2.5	0.3	0.4	7.70E-10	to LLOCA
			BIN-2	2.5	0.3	0.4	9.53E-05	
			BIN-3	2.5	0.3	0.4	5.77E-03	
7	Pressurizer & Supports	RASP Handbook	BIN-1	2.5	0.3	0.4	7.70E-10	to LLOCA
			BIN-2	2.5	0.3	0.4	9.53E-05	
			BIN-3	2.5	0.3	0.4	5.77E-03	
8	MLOCA	RASP Handbook	BIN-1				1.00E-07	to LLOCA
			BIN-2				4.00E-03	
			BIN-3				4.00E-02	
9	LLOCA	sum of 6,7,8	BIN-1				1.02E-07	LLOCA-EQ1
			BIN-2				4.19E-03	LLOCA-EQ2
			BIN-3				5.10E-02	LLOCA-EQ3

Item	SSC Description	Data Source	Seismic Bin	Median Capacity (g)	βr	βu	SSC Failure probability	Comment
10	SLOCA	RASP Handbook	BIN-1				1.50E-05	SLOCA-EQ1
			BIN-2				4.50E-02	SLOCA-EQ2
			BIN-3				2.50E-01	SLOCA-EQ3
11	Switchyard (Loss of Offsite Power)	RASP Handbook	BIN-1	0.3	0.3	0.45	4.81E-02	LOOP-EQ1
			BIN-2	0.3	0.3	0.45	6.81E-01	LOOP-EQ2
			BIN-3	0.3	0.3	0.45	9.44E-01	LOOP-EQ3
12	RPS	Typical Plant	BIN-1	1.5	0.3	0.5	8.42E-06	EQ-RPS1-FA
			BIN-2	1.5	0.3	0.5	1.01E-02	EQ-RPS2-FA
			BIN-3	1.5	0.3	0.5	9.85E-02	EQ-RPS3-FA
13	EDGs	Typical Plant	BIN-1	1.3	0.3	0.4	1.11E-06	EQ-EDG1-FA
			BIN-2	1.3	0.3	0.4	7.69E-03	EQ-EDG2-FA
			BIN-3	1.3	0.3	0.4	1.12E-01	EQ-EDG3-FA
14	AFW Storage Tank	Typical Plant	BIN-1	1.1	0.22	0.36	9.33E-08	EQ-CST1-FA
			BIN-2	1.1	0.22	0.36	6.64E-03	EQ-CST2-FA
			BIN-3	1.1	0.22	0.36	1.47E-01	EQ-CST3-FA
15	CCW	Typical Plant	BIN-1	1.03	0.28	0.28	3.57E-08	EQ-CCW1-FA
			BIN-2	1.03	0.28	0.28	6.72E-03	EQ-CCW2-FA
			BIN-3	1.03	0.28	0.28	1.71E-01	EQ-CCW3-FA
16	RWST	Typical Plant	BIN-1	1.29	0.22	0.36	1.14E-08	EQ-RWST1-FA
			BIN-2	1.29	0.22	0.36	2.16E-03	EQ-RWST2-FA
			BIN-3	1.29	0.22	0.36	7.70E-02	EQ-RWST3-FA
17	Intake structure	Typical Plant	BIN-1	1.5	0.3	0.5	8.42E-06	EQ-ISTR1-FA
			BIN-2	1.5	0.3	0.5	1.01E-02	EQ-ISTR2-FA
			BIN-3	1.5	0.3	0.5	9.85E-02	EQ-ISTR3-FA
18	Batteries	Typical Plant	BIN-1	1.06	0.27	0.35	5.02E-07	EQ-DC1-FA
			BIN-2	1.06	0.27	0.35	1.13E-02	EQ-DC2-FA
			BIN-3	1.06	0.27	0.35	1.80E-01	EQ-DC3-FA
19	Charging/HPI Pumps	Typical Plant	BIN-1	1.5	0.3	0.5	8.42E-06	EQ-CVS1-FA
			BIN-2	1.5	0.3	0.5	1.01E-02	EQ-CVS2-FA
			BIN-3	1.5	0.3	0.5	9.85E-02	EQ-CVS3-FA
20	RHR	Typical Plant	BIN-1	1.5	0.3	0.5	8.42E-06	EQ-RHR1-FA
			BIN-2	1.5	0.3	0.5	1.01E-02	EQ-RHR2-FA
			BIN-3	1.5	0.3	0.5	9.85E-02	EQ-RHR3-FA
21	SW Pumps	Typical Plant	BIN-1	1.5	0.3	0.5	8.42E-06	EQ-SWS1-FA
			BIN-2	1.5	0.3	0.5	1.01E-02	EQ-SWS2-FA
			BIN-3	1.5	0.3	0.5	9.85E-02	EQ-SWS3-FA
22	EPS	Typical Plant	BIN-1	1.3	0.3	0.4	1.11E-06	EQ-EPS1-FA
			BIN-2	1.3	0.3	0.4	7.69E-03	EQ-EPS2-FA

Item	SSC Description	Data Source	Seismic Bin	Median Capacity (g)	βr	βu	SSC Failure probability	Comment
			BIN-3	1.3	0.3	0.4	1.12E-01	EQ-EPS3-FA

3.2.1.2 LOOP/SBO Sequences for Simulation

There are hundreds of seismic accident sequences in the above SAPHIRE model. After discussions with the dynamic simulation and thermal hydraulic analysts, four of them are selected to be converted to the dynamic EMRALD model for simulations. The selected sequences have relatively higher frequencies and include important mitigating systems such as AFW and safety injection systems that are analyzed in the TH simulations. These sequences can also demonstrate the impact from the seismic induced flooding scenarios. The four selected seismic sequences are EQK 2-02-05, 2-15, 2-16-03-10, and 2-16-45. Each sequence can be initiated by any of the three seismic bins (BIN-1, BIN-2, and BIN-3). Using BIN-2 as an example, the sequences start with the seismic event tree EQK-BIN-2-IA2. Refer to Figure 21, Sequence 2 of the event tree has no direct core damage (which is represented as */CD-EQ2*), no seismic induced large LOCA (*/LLOCA-EQ2*), no seismic induced small LOCA (*/SLOCA-EQ2*), and seismic induced LOOP (*LOOP-EQ2*). The sequence is then transferred to the LOOP event tree, INT-LOOP-IA2.

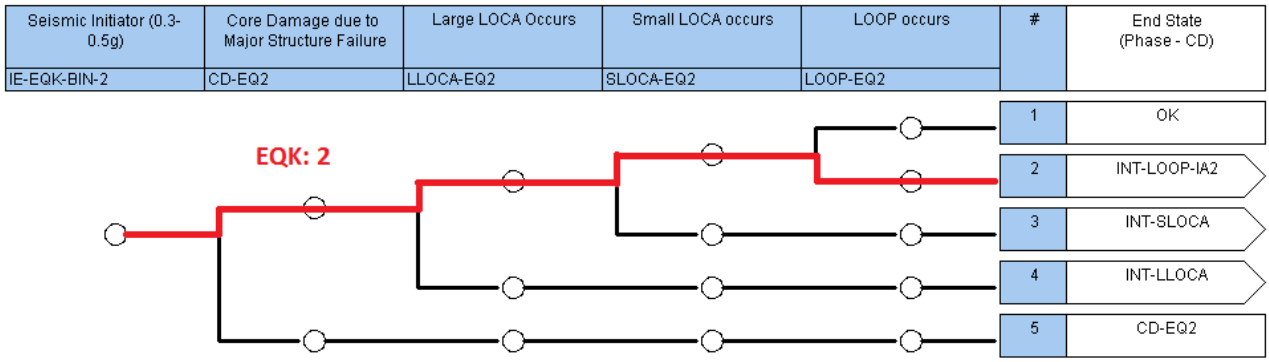

Figure 21. Seismic Event Tree EQK-BIN-2-IA2, Sequence 2.

Refer to Figure 22, Sequences 02 and 15 of the LOOP event tree, INT-LOOP-IA2, are LOOP sequences with successful starting and running of one of two emergency diesel generators (*/EPS*). In Sequence 02, AFW successfully starts and runs to provide water to steam generators (*/AFW*), primary system PORVs are closed (*/PORV*), however, RCP seal cooling could not be maintained (*LOSC*), the sequence is transferred to event tree INT-LOOP-1-IA2. In Sequence 15, AFW system fails to provide water to steam generator (*AFW*), the feed and bleed also fails (*FAB*), core damage occurs (EQK sequence 2-15). Sequence 16 of the LOOP event tree, INT-LOOP-IA2, is the SBO sequence with emergency diesel generators fail to supply Class 1E AC buses (*EPS)*. The sequence is transferred to the SBO event tree, INT-SBO-IA2.

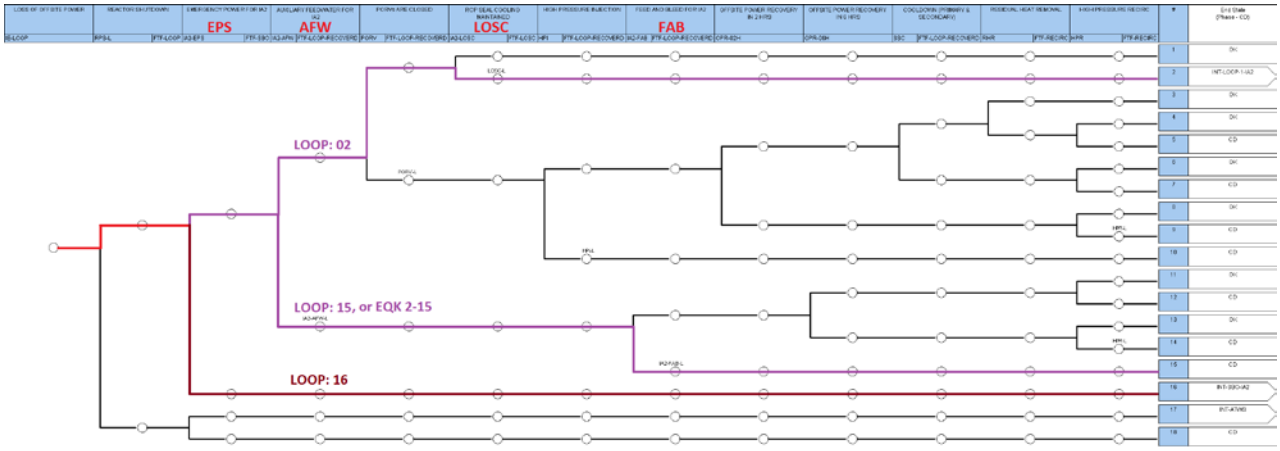

Figure 22. LOOP Event Tree INT-LOOP-IA2, Sequences 02, 15 (EQK Sequence 2-15), and 16.

In Sequence 05 of event tree INT-LOOP-1-IA2 (Figure 23), secondary rapid depressurization is successful (*/RSD-L*), RCP seal leakage rate is 182 gpm per pump with intact RCP seal stage 1 but binding/popping of RCP seal stage 2 (*/BP1 * BP2*), with no offsite power recovery within 2 hours (*OPR-02H*) and failure of high pressure injection (*HPI-L*), core damage occurs. Combining with previous sequences in seismic and LOOP event trees, the sequence can be represented as EQK sequence 2-02-05.

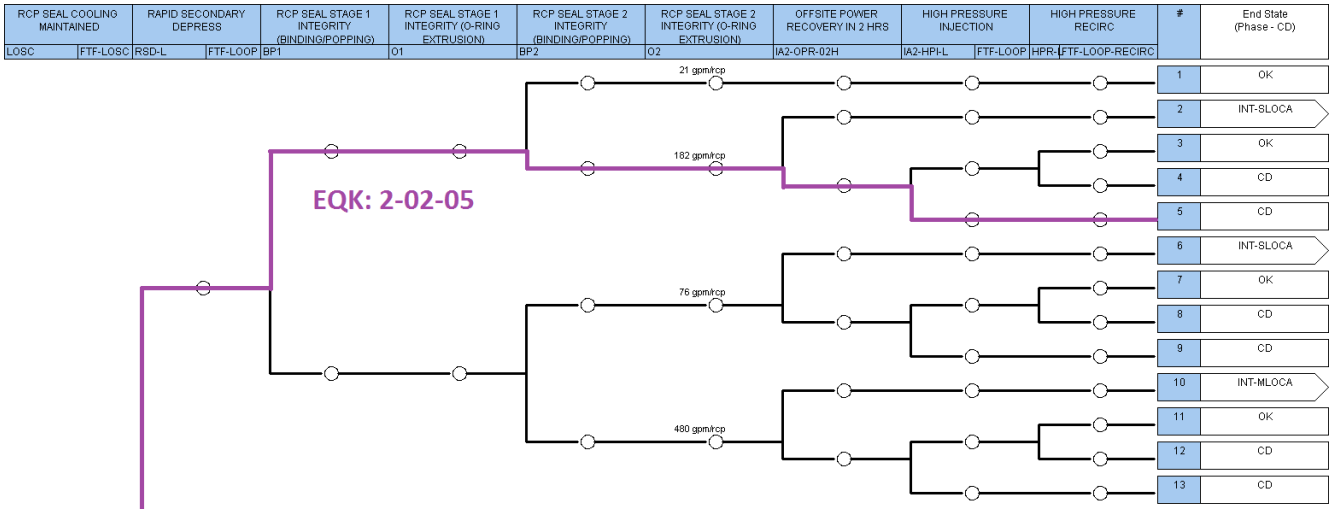

Figure 23. Event Tree INT-LOOP-1-IA2, Sequence 05 (or EQK Sequence 2-02-5).

Refer to Figure 24, Sequence 03 of the SBO event tree, INT-SBO-IA2, represents scenario that turbine-driven AFW pump (TDAFP) is able to provide water to steam generators (/AFW-B), primary system PORVs are closed (*/PORV*), secondary rapid depressurization success (*/RSD*), RCP seal leakage rate is 21 gpm per pump with both RCP seal stages 1 and 2 intact (*/BP1 * /BP2*), neither offsite power nor diesel generators are recovered within 4 hours (*OPR-04H * DGR-04H*). The sequence is then transferred to event tree INT-SBO-4-IA2.

In Sequence 45 of the SBO event tree, TDAFP fails to provide water to steam generators (*AFW-B*). With no recovery of offsite power or diesel generators within 1 hour (*OPR-01H * DEG-01H*), core damage occurs. Combining with previous sequences in seismic and LOOP event trees, this SBO sequence can be represented as EQK sequence 2-16-45.

In event tree INT-SBO-4-IA2 (Figure 25), with no AC power recovery, the plant could rely on long term manual control of AFW (*AFW-MAN*) and depressurization of steam generators (*SG-DEP-LT*) to remove residual heat. When both of them fail, core damage cannot be avoided. Combining with previous sequences in seismic, LOOP, and SBO event trees, this SBO sequence can be represented as EQK sequence 2-16-03-10.

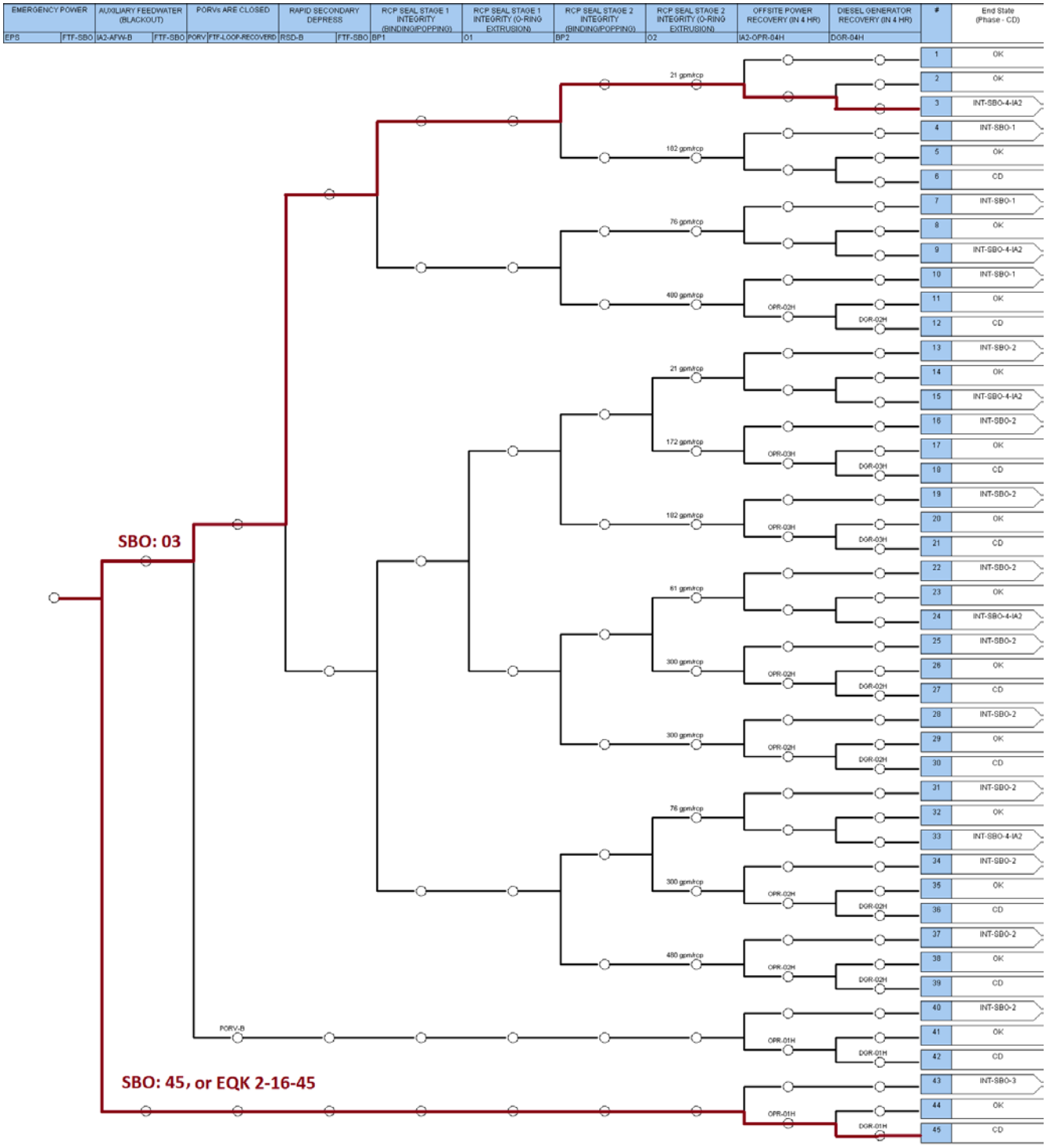

Figure 24. SBO Event Tree INT-SBO-IA2, Sequences 03 and 45 (EQK Sequence 2-16-45).

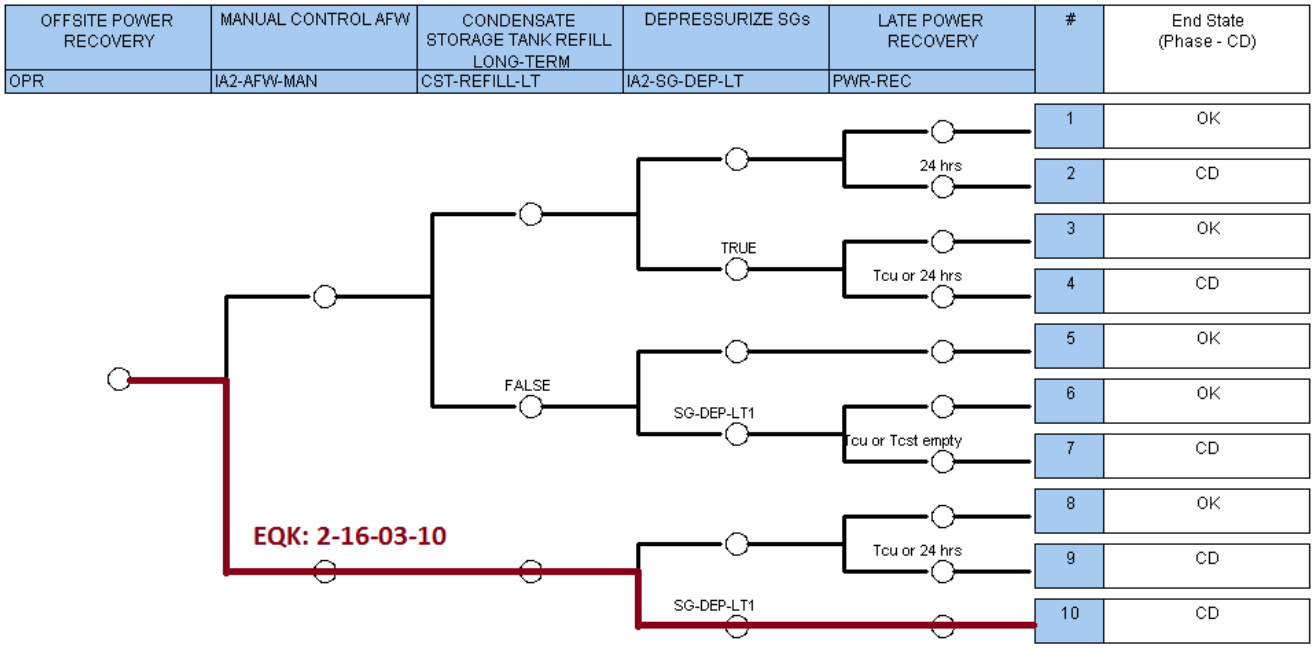

Figure 25. Event Tree INT-SBO-4-IA2, Sequence 10 (EQK Sequence 2-16-03-10).

3.2.1.3 Static PRA Model Results

After the above seismic sequences are selected, the associated fault tree models related to the event tree top events (such as EPS, AFW, LOSC, FAB, HPI-L) are reviewed and revised for simplification and easier to be converted to EMRALD model. Prefix IA2 is added to the name of the revised fault tree models. For example, revised EPS fault tree is renamed as IA2-EPS. The three seismic event trees are then quantified with SAPHIRE. Table 6 presents the quantification results for the four selected seismic sequences under each seismic bin event.

Table 6. SAPHIRE Quantification Results for Selected Seismic Sequences.

Seismic Bin	EQK Sequence	Sequence Frequency
BIN-1	2-02-05	2.74E-10
	2-15	4.60E-12
	2-16-03-10	5.26E-09
	2-16-45	3.99E-10
BIN-2	2-02-05	3.84E-09
	2-15	9.54E-09
	2-16-03-10	3.46E-08
	2-16-45	1.04E-07
BIN-3	2-02-05	1.04E-07
	2-15	3.76E-07
	2-16-03-10	2.77E-07
	2-16-45	1.58E-06

After the above base model is quantified, several other cases are considered. The first one is to consider the impact due to seismic induced pipe failures in switchgear room. The second one is to consider an alternative seismic hazard vector.

SEISMIC INDUCED PIPE FAILURES IN SWITCHGEAR ROOMS

INL has developed a 3D switchgear room model for simulation based dynamic study of the potential of seismic induced pipe failures (refer to (Parisi, et al. 2016) and (Coleman, et al. 2016)). Figure 26 displays the 3D model. The 3D dynamic model is used in the project to estimate the seismic induced pipe failure probabilities in switchgear rooms 1 and 2 which have different piping layout and different number of pipe joints.

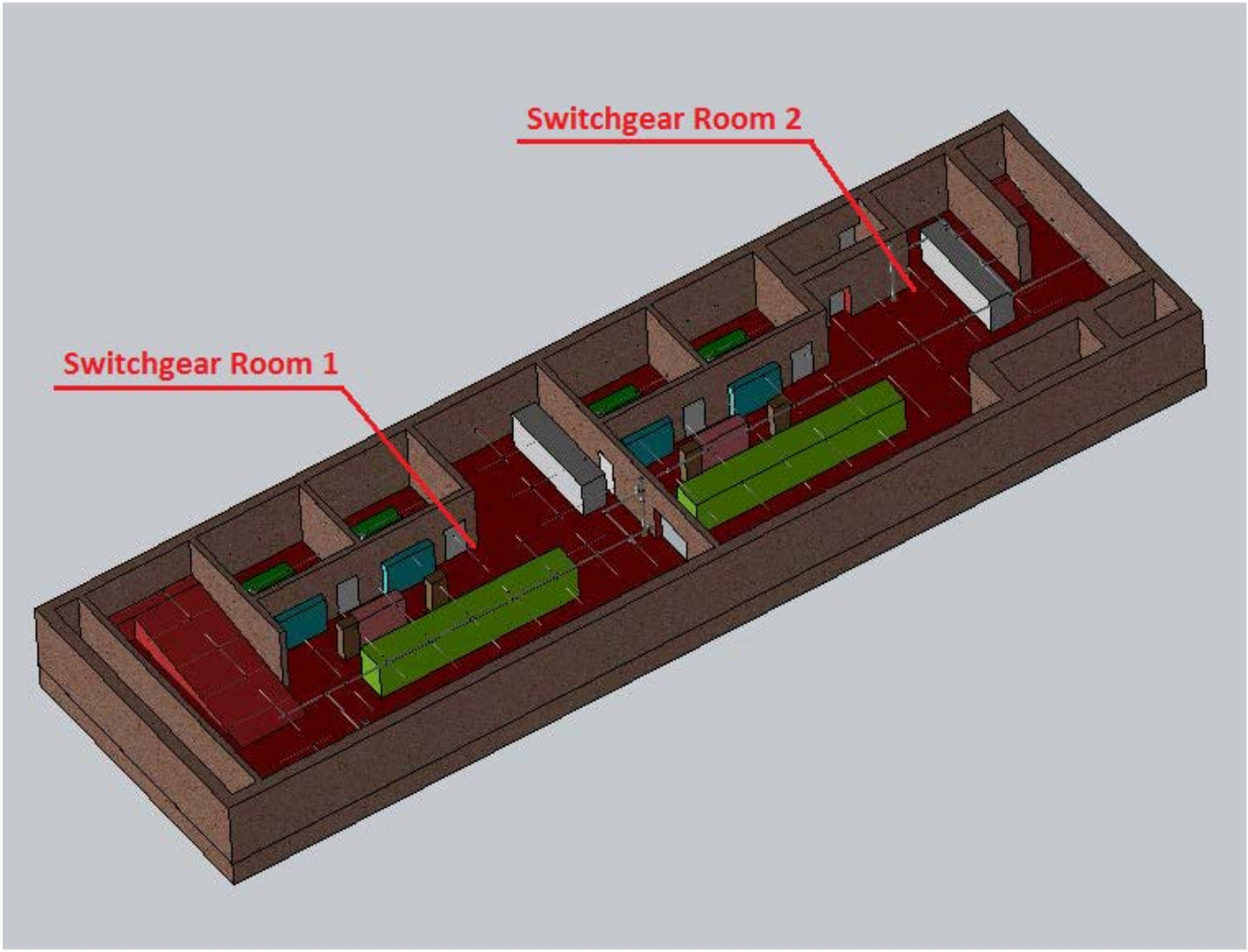

Figure 26. 3D Switchgear Room Model.

Table 7 shows the seismic induced pipe failure probabilities in switchgear rooms 1 and 2 from the 3D dynamic model. They are incorporated into the base SAPHIRE model with new seismic basic event EQx-SWGR1-FA and EQx-SWGR2-FA.

Table 7. Seismic Induced Switchgear Room Pipe Failure Probabilities.

Switchgear Room	Seismic Induced Pipe Failure Probability		
	BIN-1	BIN-2	BIN-3
Room 1	0.00E+00	3.817E-01	9.524E-01
Room 2	0.00E+00	0.000E+00	4.762E-02

ALTERNATIVE SEISMIC HAZARD VECTOR

The base SAPHIRE model uses the generic seismic hazard vector in Table 3 to calculate seismic initiating event frequencies and bin accelerations. The work in (Parisi, et al. 2016) uses a different seismic hazard vector shown in Table 8. This is similar to receiving new seismic data for a specific facility and applying it to the model.

Table 8. Alternative Seismic Hazard Vector.

Ground Acceleration (g)	Cumulative Exceedance Frequency (per year)
0.06	1.00E-02
0.21	1.00E-03
0.4	1.00E-04
0.6	1.00E-05
0.93	1.00E-06
1.4	1.00E-07

To apply this alternative seismic hazard vector to the SAPHIRE model with the same seismic bin accelerations, the vector can be fit to the curve with the following equation:

$$Freq = 2.0769x^2 - 6.712x - 1.6472$$

where $x = log_{10}(PGA)$.

The above alternative seismic hazard vector can thus be converted to the same three seismic bins as in Table 6, with the same bin accelerations but different bin frequencies. Table 9 shows the alternative seismic initiating event frequencies with the same bin categories.

Table 9. Alternative Seismic Initiating Event Frequencies and Bin Accelerations.

Ground Acceleration (g)	Exceedance Frequency	Seismic Bin	Bin Acceleration	Bin Frequency
0.05	1.053E-02	BIN-1 (0.05-0.3g)	0.122	1.019E-02
0.08	6.747E-03			
0.15	2.470E-03			
0.25	6.377E-04			
0.3	3.358E-04	BIN-2 (0.3-0.5g)	0.387	3.030E-04
0.4	1.001E-04			
0.5	3.281E-05	BIN-3 (>0.5g)	0.707	3.281E-05
0.65	7.370E-06			
0.8	2.053E-06			
1	5.220E-07			

SAPHIRE QUANTIFICATION RESULTS

To incorporate the seismic induced switchgear room pipe failure and the alternative seismic hazard parameters into the SAPHIRE model, two change sets, IA2-EQ-SWGR (Switchgear Component Failure due to Seismic-Induced Pipe Failure) and IA2-EQ-IE (Alternative Seismic Hazard Vector), are developed to quantify different cases:

- Case 1, no change set selected: base model, **generic** hazard vector, **no** seismic induced switchgear pipe failure
- Case 2, only select change set IA2-EQ-SWGR: **generic** hazard vector, **with** seismic induced switchgear pipe failure
- Case 3, only select change set IA2-EQ-IE: **alternative** hazard vector, **no** seismic induced switchgear pipe failure
- Case 4, both change sets selected: **alternative** hazard vector, **with** seismic induced switchgear pipe failure

Table 10 shows the SAPHIRE quantification results for all the four cases, which can be used for comparison with the results from dynamic PRA model.

Table 10. SAPHIRE Quantification Results for Different Cases.

Seismic Bin	EQK Sequence	Sequence Frequency			
		Case 1	Case 2	Case 3	Case 4
BIN-1	2-02-05	2.74E-10	2.74E-10	9.89E-09	9.89E-09
	2-15	4.60E-12	4.60E-12	4.07E-10	4.07E-10
	2-16-03-10	5.26E-09	5.26E-09	1.89E-07	1.89E-07
	2-16-45	3.99E-10	3.99E-10	1.67E-08	1.67E-08
BIN-2	2-02-05	3.84E-09	5.74E-09	9.26E-08	1.38E-07
	2-15	9.54E-09	7.29E-08	2.30E-07	1.76E-06
	2-16-03-10	3.46E-08	7.71E-08	8.32E-07	1.86E-06
	2-16-45	1.04E-07	2.85E-07	2.49E-06	6.85E-06
BIN-3	2-02-05	1.04E-07	2.32E-07	4.72E-07	1.06E-06
	2-15	3.76E-07	2.34E-06	1.71E-06	1.07E-05
	2-16-03-10	2.77E-07	4.37E-07	1.26E-06	1.99E-06
	2-16-45	1.58E-06	3.43E-06	7.19E-06	1.56E-05

3.2.2 Dynamic PRA Model

A dynamic PRA model was constructed and run using EMRALD. This model was built in several stages described in the following sections and linked the seismic data, the 3D fluid simulation and the thermal hydraulics data into the PRA analysis.

3.2.2.1 Dynamic Seismic Modeling

Initial Dynamic PRA modeling was done using the seismic data. Most SAPHIRE seismic models have a standard seismic hazard curve, for this analysis we are assuming new seismic hazard curve data was received and this new curve was modeled in EMRALD and used to sample for earthquake PGA levels. Next the fragility curves for piping failures were added. This model was run to determine the likelihood of piping failures for each of the seismic hazard bins.

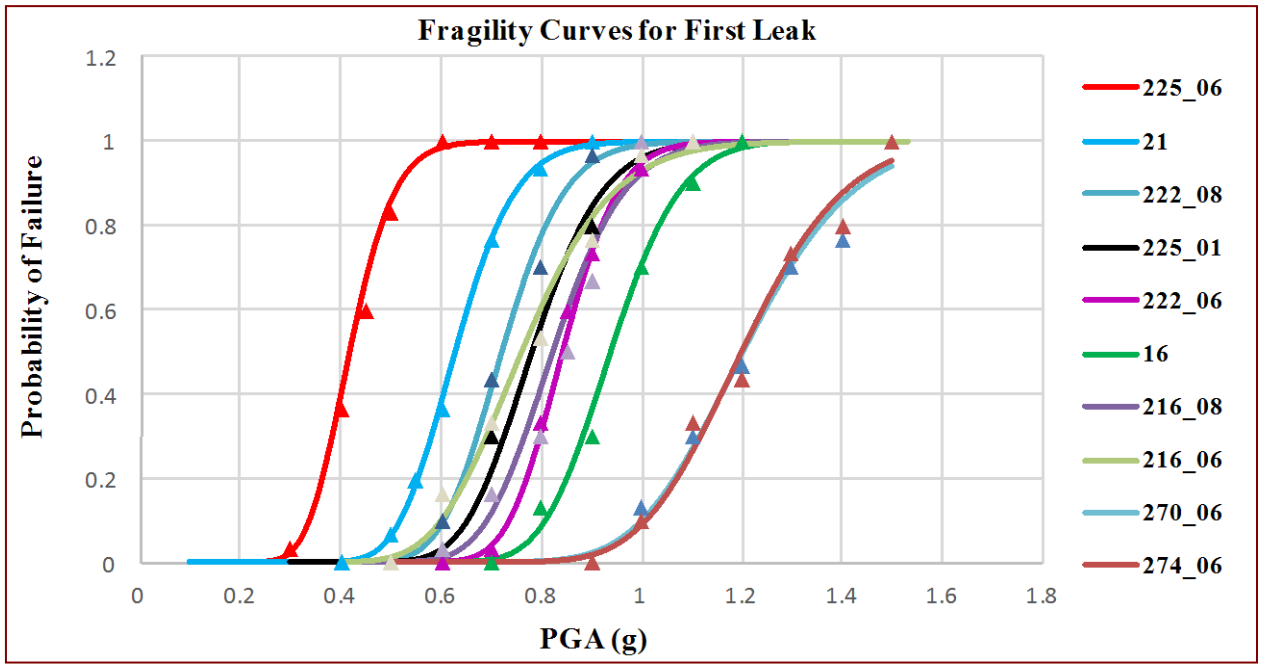

Figure 27. Seismic Fragility Curves for First Leak with X Direction Input.

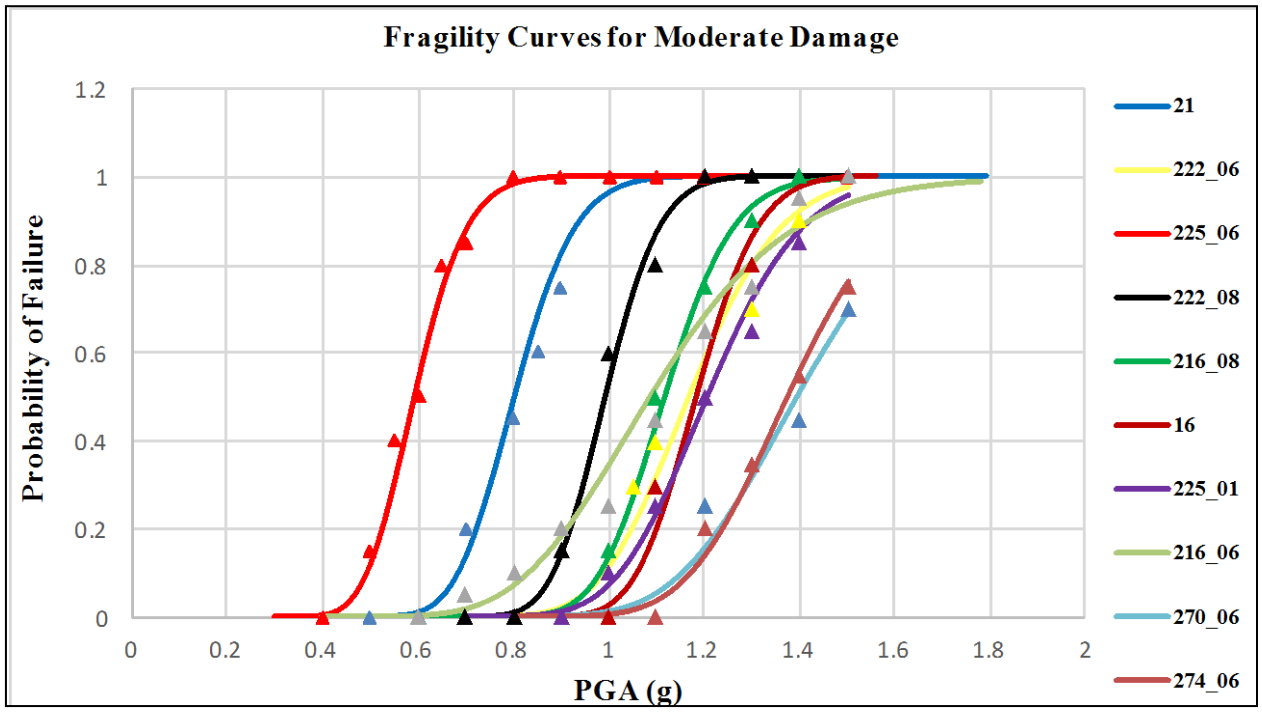

Figure 28. Seismic Fragility Curves for Moderate Damage for X Direction Input.

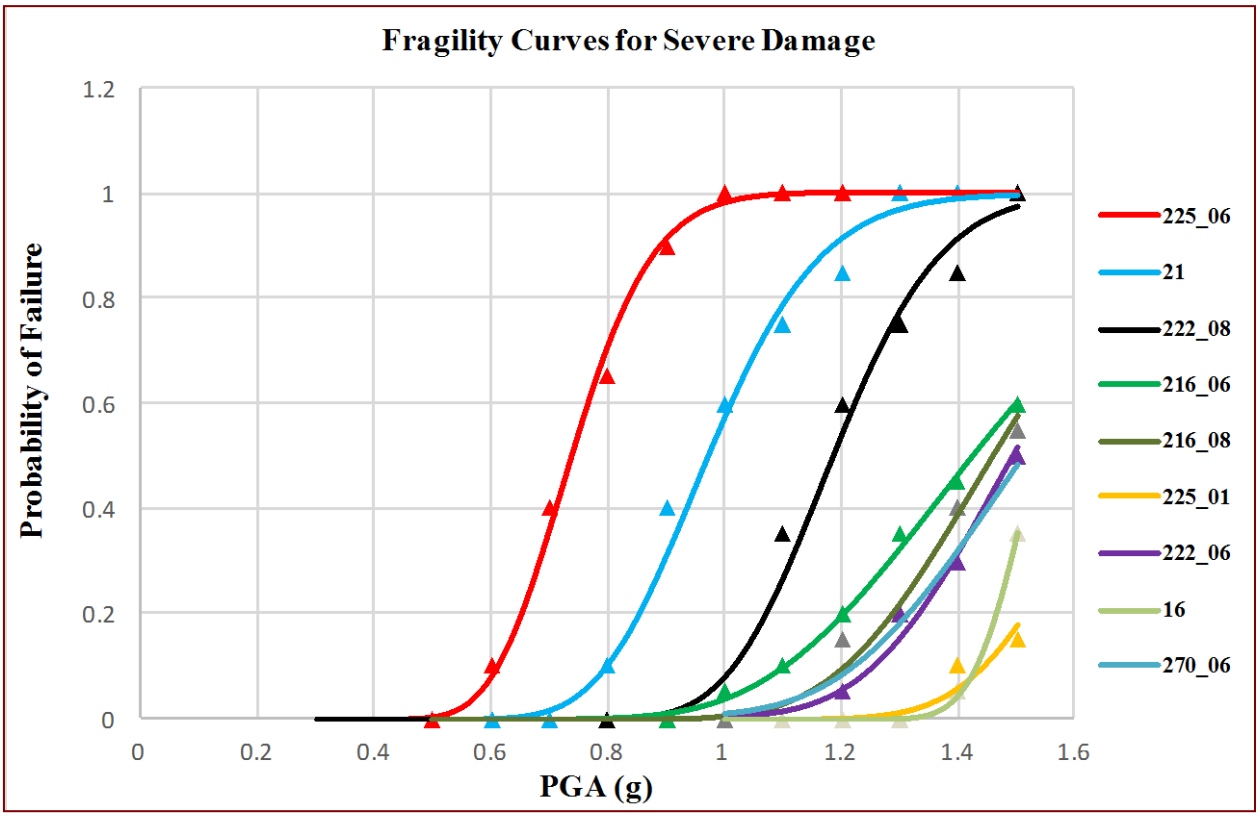

Figure 29. Seismic Fragility Curves for Severe Damage for X Direction Input.

This initial data was used to add additional failure rates to the flooding susceptible components in the SAPHIRE model. By comparing the change in CDF of the SAPHIRE model's sequences we determine which sequences could have the biggest effect from the dynamic modeling. Only these sequences need to be modeled, reducing the scope of the problem. If no sequences had a significant difference then no additional modeling would be necessary. Table 11 shows four sequences with different seismic hazard bins that had significant impact when adding seismically induced flooding of the Switch Gear Room.

Table 11. CDF Comparison between No Flooding and Max Damage Flooding in the Switch Gear Room (SWGR).

Sequence Case	New Hazard, No SWGR Pipe Failure	New Hazard, SWGR Pipe Failure	% difference
EQK-BIN-1-IA2:2-02-05	9.89E-09	9.89E-09	0.00%
EQK-BIN-1-IA2:2-15	4.07E-10	4.07E-10	0.00%
EQK-BIN-1-IA2:2-16-03-10	1.89E-07	1.89E-07	0.00%
EQK-BIN-1-IA2:2-16-45	1.67E-08	1.67E-08	0.00%
EQK-BIN-2-IA2:2-02-05	9.26E-08	1.38E-07	49.03%
EQK-BIN-2-IA2:2-15	2.30E-07	1.76E-06	665.22%

EQK-BIN-2-IA2:2-16-03-10	8.32E-07	1.86E-06	123.56%
EQK-BIN-2-IA2:2-16-45	2.49E-06	6.85E-06	175.10%
EQK-BIN-3-IA2:2-02-05	4.72E-07	1.06E-06	124.58%
EQK-BIN-3-IA2:2-15	1.71E-06	1.07E-05	525.73%
EQK-BIN-3-IA2:2-16-03-10	1.26E-06	1.99E-06	57.94%
EQK-BIN-3-IA2:2-16-45	7.19E-06	1.56E-05	116.97%

3.2.2.2 Dynamic System Models

The next stage of dynamic modeling consisted of modeling all the systems used in the significant sequences. Each system was modeled in EMRALD and tested against SAPHIRE results to verify the modeling was done correctly. Several factors contribute to the differences in the results shown in Table 12, including random sampling in EMRALD, min-cut upper bound estimation errors for high probability events, and failure timing modeling restrictions used in SAPHIRE.

Table 12. Comparison of SAPHIRE results.

System	SAPHIRE	EMRALD
AFW	6.320E-05	6.300E-05
EPS	3.078E-05	3.067E-05
FAB	5.653E-02	5.648E-02
HPI	3.211E-03	3.175E-03
LOSC	3.211E-03	3.183E-03

3.2.2.3 Coupling Thermal Hydraulics

For a couple of sequences it was determined that a TH model could provide more insight. As discussed in section 3.5.1 a limit surface for a couple aleatory parameters in the sequence, was pre calculated to provide quick evaluation with little computational costs.

If the simulation encountered the equivalent of sequence EQK-BIN-2-IA2:2-16-45 or EQK-BIN-1-IA2:2-02-05, then an equation based on the limit surface was used to determine if there was core damage on that sequence. Ideally we would call the limit surface directly, but project time restrictions required us a simplification of this through an equation approximation. This evaluation was done by adding a code evaluation event to the model with the code containing the approximation of the limit surface. If the code returns true, then the model moves to that sequence state, otherwise it is considered OK and the simulation continued.

3.2.2.4 Coupling the Flooding Model

The dynamic PRA model is the controller for the 3D flooding simulation model. An optional startup parameter for EMRALD is a NEUTRINO simulation file to run if needed. After a sampled seismic event the PGA is used to sample for any pipe failures and their locations as described in 3.2.2.1. If there are any pipe failures a flow rate and angle for the spray is sampled according to the size of the break. This data is then sent through the network connection to NEUTRINO so that the particle emitters can be assigned before the simulation starts. A

small break has a leak rate from 0.002 – 0.004 cubic meters per sec; a medium break from 0.004 – 0.006; and a large break from 0.006 – 0.008. Any water spray on susceptible components or flooding levels reached are sent back to EMRALD from NEUTRINO and registered as failed components in the simulation. See section 3.3 for more details on the Flooding model and 3D simulation.

3.2.2.5 Capturing Lower Probability Events

One drawback about simulation is that in order to accurately capture events with low probability, you must either run greater than (1/probability) simulations, or do some complex sampling and post processing to adjust the results. EMRALD does not have a complex sampling method, and because of the 3D simulation a very large number of simulations is also infeasible. To overcome this a method of repeatedly rerunning a section of the model was implemented. This works by putting a timing marker after the 3D Simulation but before running the rest of the model. After the 3D simulation finishes and the PRA model is evaluated, then the model backs up in time to the marker just after the 3D simulation, repeatedly reevaluating the PRA model. For this model it was done 10,000 of times and thus capturing events five orders of magnitude lower than without the sub-sampling. These sub-sampling results are then adjusted and multiplied back into the overall probability of the corresponding sequence.

3.2.2.6 Optimization

Several optimization items were added to the dynamic PRA model to reduce computational time. First, it was determined through 3D simulation tests that if the total flow from pipe fractures is less than 0.006 cubic meters per sec will not cause flooding damage to any components within the operator action time of shutting down the fire water system. This means that the simulation only needs to run long enough to determine component failures caused by spray.

Another optimization is done if there are no component failures from the 3D simulation. For this case, there is no need for dynamic simulation and the static value from SAPHIRE is used for the sequences this simulation run.

3.2.2.7 Full Dynamic Model

The dynamic PRA model consists of component diagrams, system diagrams, and a plant response diagram. Every component for the key systems was determined using the failure rates for each of the components basic events. (See Figure 30) The logic for the system diagrams was also modeled after the corresponding fault tree in along with all relevant common cause events added to the logic model. For more information on modeling using EMRALD see (Prescott, Smith and Samptah 2014).

Component	Component ID	Seismic Failure	FTS/FTO		TM		FTR			CCF_FTS		CCF_FTR		
4160 VAC BUS 1AA02	ACP_BAC_1AA02		FTS/FTO				_LP	4.00E-07	9.60E-06					
480 VAC BUS 1ABA	ACP_BAC_1ABA						_LP	4.00E-07	9.60E-06					
480 VAC BUS 1ABE	ACP_BAC_1ABE						_LP	4.00E-07	9.60E-06					
4160 VAC BUS 1BA03	ACP_BAC_1BA03						_LP	4.00E-07	9.60E-06					
480 VAC BUS 1BBA	ACP_BAC_1BBA						_LP	4.00E-07	9.60E-06					
480 VAC BUS 1BBE	ACP_BAC_1BBE						_LP	4.00E-07	9.60E-06					
SWITCHYARD AC BREAKER AA20	ACP_CRB_AA20	DCP_EQ	_CC	2.50E-03						ACP_CRB_CF_A2030	4.25E-05			
SWITCHYARD AC BREAKER BA30	ACP_CRB_BA30	DCP_EQ	_CC	2.50E-03						ACP_CRB_CF_A2030	4.25E-05			
ACCW HEAT EXCHANGER 001	ACW_HTX_001						_PG	6.00E-07	1.44E-05			ACW_HTX_CF_HTXS	5.62E-08	1.35E-06
ACCW HEAT EXCHANGER 002	ACW_HTX_002						_PG	6.00E-07	1.44E-05			ACW_HTX_CF_HTXS	5.62E-08	1.35E-06
ACCW PUMP 001	ACW_MDP_001	SWS_EQ	_FS	2.00E-03			_FR	5.00E-06	1.20E-04	ACW_MDP_CF_START	8.36E-05	ACW_MDP_CF_RUN	9.70E-08	2.33E-06
ACCW PUMP 002	ACW_MDP_002	SWS_EQ	_FS	2.00E-03	_TM	6.00E-03	_FR	5.00E-06	1.20E-04	ACW_MDP_CF_START	8.36E-05	ACW_MDP_CF_RUN	9.70E-08	2.33E-06
ACCW SURGE TANK	ACW_TNK_SURGE	RWST_EQ	_FC	4.80E-08										
AFW DISCHARGE CHECK VAVLES CCF	AFW_CKV_001214									AFW_CKV_CF_001214	5.80E-08			
AFW SUCKTION CHECK VAVLES CCF	AFW_CKV_0331358									AFW_CKV_CF_0331358	5.80E-08			
SG STOP CHECK VAVLES CCF	AFW_CKV_113456									AFW_CKV_CF_113456	1.12E-07			
SG ISOLATION CKV CCF	AFW_CKV_125678									AFW_CKV_CF_125678	1.12E-07			
AFW MOTOR-DRIVEN PUMP P4-4002	AFW_MDP_4002	AFW_EQ	_FS	1.50E-03	_TM	4.00E-03	_FR	2.24E-05	5.38E-04	AFW_MDP_CF_START	8.25E-05	AFW_MDP_CF_RUN	1.68E-07	4.04E-06
AFW MOTOR-DRIVEN PUMP P4-4003	AFW_MDP_4003	AFW_EQ	_FS	1.50E-03	_TM	4.00E-03	_FR	2.24E-05	5.38E-04	AFW_MDP_CF_START	8.25E-05	AFW_MDP_CF_RUN	1.63E-07	3.91E-06
AFW MDP B MINFLOW MOV 5154	AFW_MOV_FV5154		_OO	1.00E-03						AFW_MOV_CF_FV51545	7.57E-06			
AFW MDP A MINFLOW MOV 5155	AFW_MOV_FV5155		_OO	1.00E-03						AFW_MOV_CF_FV51545	7.57E-06			
AFW TURBINE DRIVEN FEED PUMP P4-001	AFW_TDP_4001	AFW_EQ	_FS	7.00E-03	_TM	5.00E-03	_FR	2.09E-04	5.00E-03			AFW_PMP_CF_RUN	5.45E-09	1.31E-07
CST TANK	AFW_TNK_CST1	CST_EQ					_FC	2.00E-09	4.80E-08					
OPERATOR FAILS TO MANUALLY INITIATE A	AFW_XHE_MANAFW		_XM	4.00E-03										
OPERATOR FAILS TO CONTROL AFW TDP AF	AFW_XHE_TDPBD		_XM	3.00E-01										
CVC-DIS CHECK VAVLE	CVC_CKV_CV013		_CC	1.20E-05										
CVC-SUC CHECK VAVLE	CVC_CKV_CV189		_CC	1.20E-05										
CHARGING PUMP 1A	CVC_MDP_1A	HPI_EQ	_FS	1.50E-03	_TM	4.00E-03	_FR	5.00E-06	1.20E-04	CVC_MDP_CF_START	6.27E-05	CVC_MDP_CF_RUN	9.70E-08	2.33E-06
CHARGING PUMP 1B	CVC_MDP_1B	HPI_EQ	_FS	1.50E-03	_TM	4.00E-03	_FR	5.00E-06	1.20E-04	CVC_MDP_CF_START	6.27E-05	CVC_MDP_CF_RUN	9.70E-08	2.33E-06
VCT MOV CCF	CVC_MOV_LV0112BC		_CF	2.28E-05										
POSITIVE DISPLACEMENT CHARGING PUMP	CVC_PDP_PDP		_FS	3.00E-03	_TM	3.00E-03	_FR	8.00E-06	1.92E-04					

Figure 30. List of Components and Events for Building the Component Diagrams in EMRALD.

The plant response diagram couples the system evaluations into the desired sequences along with the 3D simulation and the Thermal Hydrodynamics. The following steps explain the evaluation and movement done at each state of the model.

1. Normal_Op – Starting state for the main model. Here we set the 24 hour mission time and wait for an earthquake to sample the PGA and check for a loss of offsite power event (IE_LOOP_EQ).
2. Loop_EQ_Occured – an earth quake occurred along with the failure of offsite power. Now evaluate to see if there are any pipe ruptures for the sampled PGA value. Start any flooding evaluation sections. If it is a lower PGA go to seismic Bin2, if it is higher go to seismic Bin3.
3. EQ_Bin2 – an earthquake with a PGA between 0.3 and 0.5 occurred. If there were no pipe ruptures goto "Normal_Op" state otherwise go to "Pipe_Fail"
4. EQ_Bin3 – an earthquake with a PGA > 0.5 occurred. If there were no pipe ruptures goto "Normal_Op" state otherwise go to "Pipe_Fail"
5. Pipe_Fail - There was a pipe failure. Set the failure rate for components susceptible to seismic failure. Add the state to start the 3D simulation "Running_3D_Sim". Check for the loss of offsite Power and go to "LOOP" if there is no offsite AC Power.
6. LOOP - Lost offsite power, start evaluation of pieces for emergency power systems and components. Wait for the recovery of offsite power, if so go to "OSP_Recovered". Wait for diesel generator failure, if so go to "Station_Black_Out".
7. Station_Black_Out – No AC power from either outside or internal diesel generators. Set the time for the start of depleting the batteries. Wait battery failure, if so set "DC_Run_Time", Wait for diesel generator recovery, if so set "DG_Rec_Time". Wait for offsite power recovery, if so go to "OSP_Recovered".
8. OSP_Recovered – offsite power has been recovered, set the recovery time "OSP_Rec_Time"

9. Running_3D_Sim – Start the 3D NEUTRINO flooding simulation. Assign the pipe failure values for the 3D simulation. Start the systems and components to evaluate the overall model. Wait for mission time to be over, if go to "Subrun_PRA". If the pipe breaks are low flow then wait for 10 sec and add "Stopping_3D_Sim" state. Wait for firewater shutoff, then add "Stopping_3D_Sim".
10. Stopping_3D_Sim – the 3D simulation is done or no longer needed, so stop the 3D sim. Go to "Eval_PRA"
11. Eval_PRA – begin to evaluate the PRA model which in this state will include any 3D failed components. Save the current states and time so it can be rerun after this point. Add "Short_Circuit_Subruns" to the current states. Wait for EPS system failure, if so add "EPS" to current states. Wait for LOSC system failure, if so add "LOSC" to current states. Wait for AFW system failure, if so add "AFW" to current states.
12. EPS – Emergency power systems have failed. Wait for AFW system to fail, if so goto AFW-B.
13. AFW-B – Auxiliary Feed Water and EPS has failed. Evaluate the Thermal hydraulics for this sequence, if failed go to Seq2_16_45.
14. Seq2_16_45 – Sequence 2_16_45 has occurred, increment a counter for this sequence.
15. AFW - Auxiliary Feed Water has failed. Wait for FAB to fail, if failed go to Seq2_15.
16. Seq2_15 – Sequence 2_15 has occurred, increment a counter for this sequence.
17. LOSC – Loss of seal cooling has occurred. Sample and set the RCP leak rate. Wait for EPS system failure, if so go to HPI_L.
18. HPI_L – Loss of high and low pressure injection. Do a thermal hydraulics evaluation with the RCP leak rate and power recovery time, if failed go to Seq2_2_5.
19. Seq2_2_5 – Sequence 2_2_5 has occurred, increment a counter for this sequence.
20. Short_Curcuit_Subruns – evaluate if there were any 3D simulation failed components, if not then set the "Subrun_Cnt" variable to the max so to sub-runs are done.
21. Subrun_PRA – rerun the purely PRA part of the model to capture more rare events. Increment the "Subrun" couner. If enough runs are done then quit, else reset the time "Reset_Time" and evaluate this part of the model again.

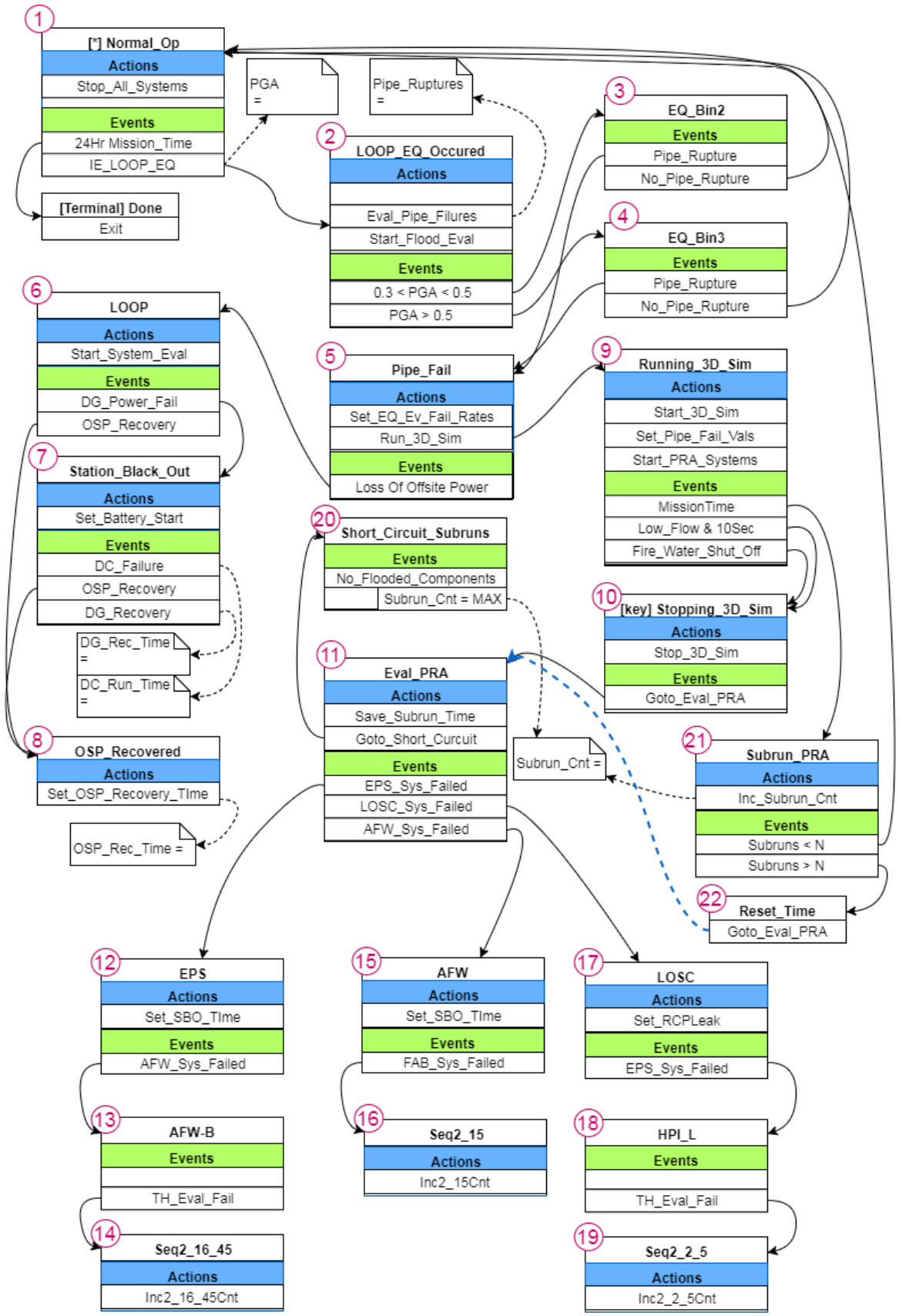

Figure 31. Plant Response Diagram for the Dynamic PRA Model.

3.3 Flooding Models

3.3.1 3D Model

For this demonstration the same 3-D model of the two switchgear rooms from the previous work was used (see Figure 32). This model consists of a 3-D polygon model of a floor of the facility and other rigid objects representing components, refer to (Coleman, et al. 2016) or more detail on the 3D model layout.

These critical components those susceptible to water damage, including four battery units, two 4kV switchgear units, two 125V DC distribution panels and four Uninterruptible Power Supply (UPS) units. Refer to report (Parisi, et al. 2016) for more detail on the layout of these components. Refer to Figure 33 to identify 3D component names and use Table 13 to identify the corresponding PRA model items. Effects of the components on the systems can be seen by referring to the fault trees in section 3.2.1.3 for information on the effects of their failures on the systems.

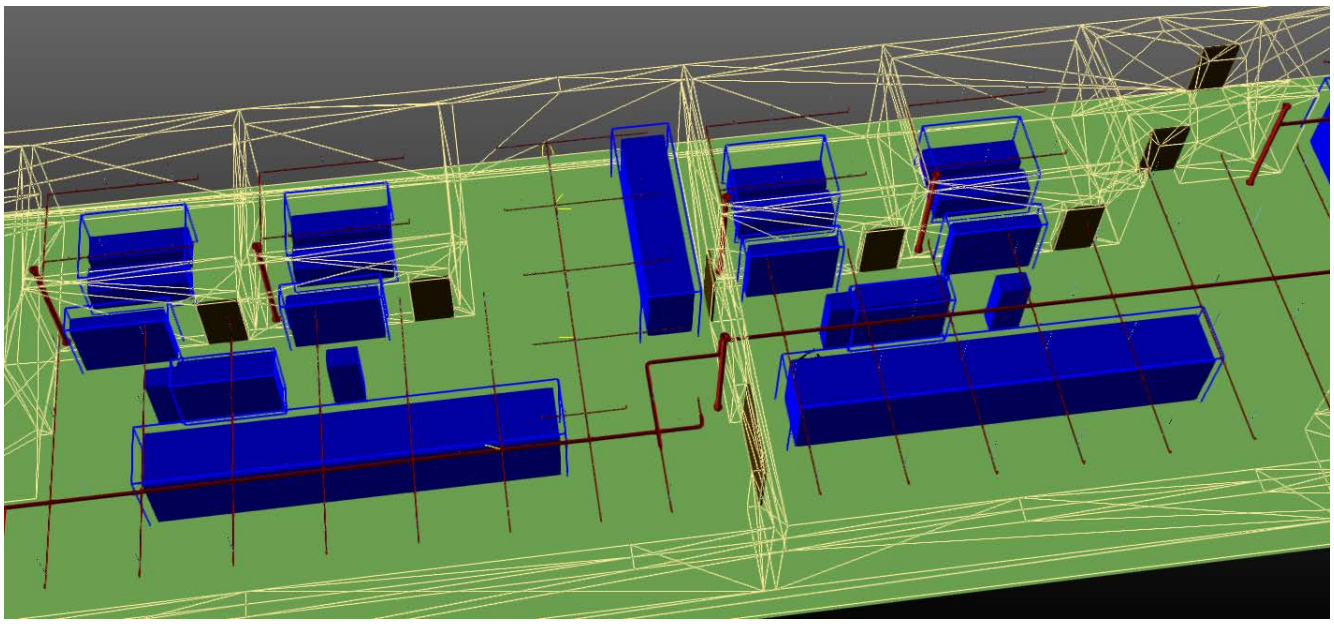

Figure 32. 3D Model of the Switch Gear Rooms.

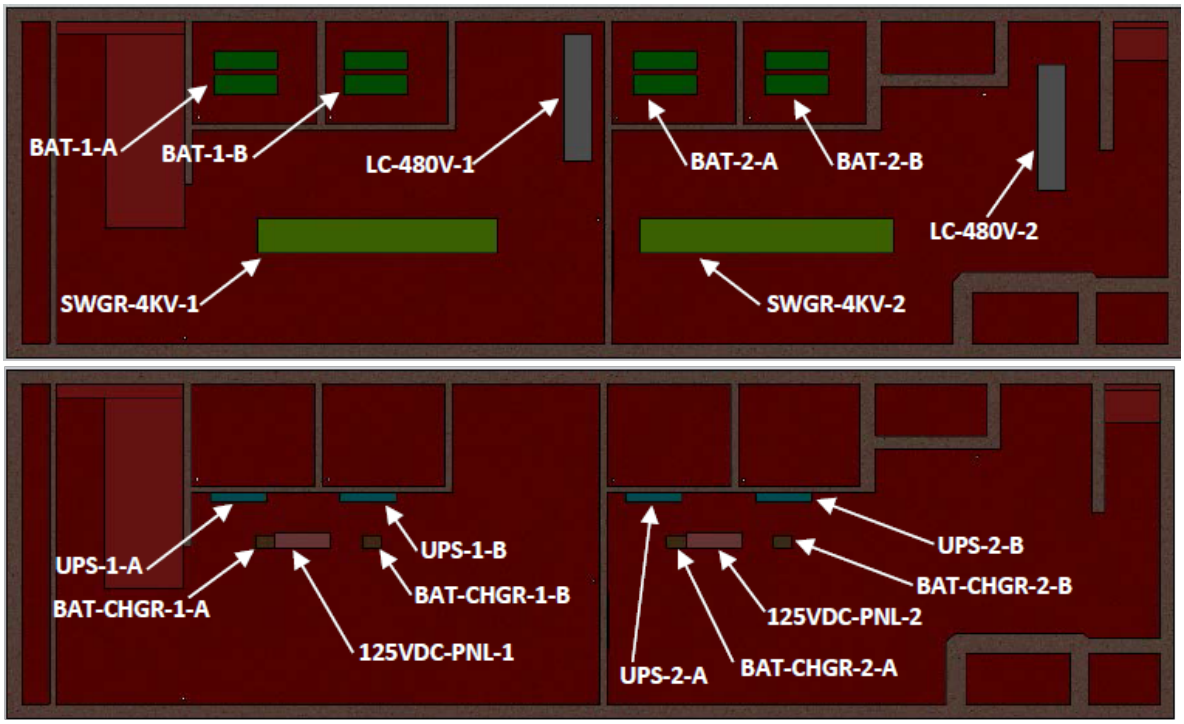

Figure 33. Component Identification or Layout.

Table 13. List of Corresponding Components to the Static PRA Model Component Names.

Component	Component ID	Flooding Model Component
4160 VAC BUS 1AA02	ACP_BAC_1AA02	SWGR_4KV_1
480 VAC BUS 1ABA	ACP_BAC_1ABA	LC_480V_1
480 VAC BUS 1ABE	ACP_BAC_1ABE	LC_480V_1
4160 VAC BUS 1BA03	ACP_BAC_1BA03	SWGR_4KV_2
480 VAC BUS 1BBA	ACP_BAC_1BBA	LC_480V_2
480 VAC BUS 1BBE	ACP_BAC_1BBE	LC_480V_2
125 VDC PANEL 1AD1	DCP_BDC_1AD1	UDC_125VDC_PNL_1
125 VDC PANEL 1BD1	DCP_BDC_1BD1	UDC_125VDC_PNL_2
125 VDC PANEL 1CD1	DCP_BDC_1CD1	UDC_125VDC_PNL_2
BATTERY CHARGER 1AD1CA	DCP_BCH_1AD1CA	UPS_1_A
BATTERY CHARGER 1AD1CB	DCP_BCH_1AD1CB	UPS_1_B
BATTERY CHARGER 1BD1CA	DCP_BCH_1BD1CA	UPS_2_A
BATTERY CHARGER 1BD1CB	DCP_BCH_1BD1CB	UPS_2_B

3.3.2 Simulation

Dynamic particle emitters are used to simulate a rupture from the water based fire suppression system. For this setup, only the top 10 pipe break locations were added to the simulation model. These locations were determined by the seismic analysis described in section 4.2 of (Coleman, et al. 2016). The locations shown in Figure 34 are modeled in the simulation using particle emitters.

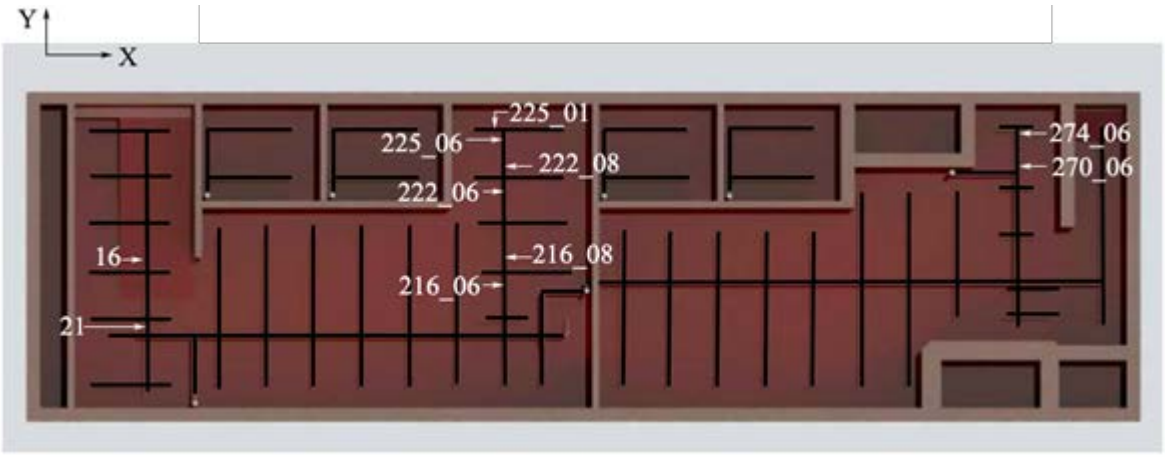

Figure 34. Top Fracture and Leak Probabilities for the Fire Suppression System.

Almost all the NEUTRINO properties can be adjusted dynamically through the network communication link see Figure 35. The flow rate and spray angle of these particles is set dynamically by EMRALD before the simulation starts. In order to run faster simulations, larger particle sizes (0.05m) were used. Modifications were made to allow for the velocity of larger particles to more closely match what would be sprayed out of small openings with fine particles.

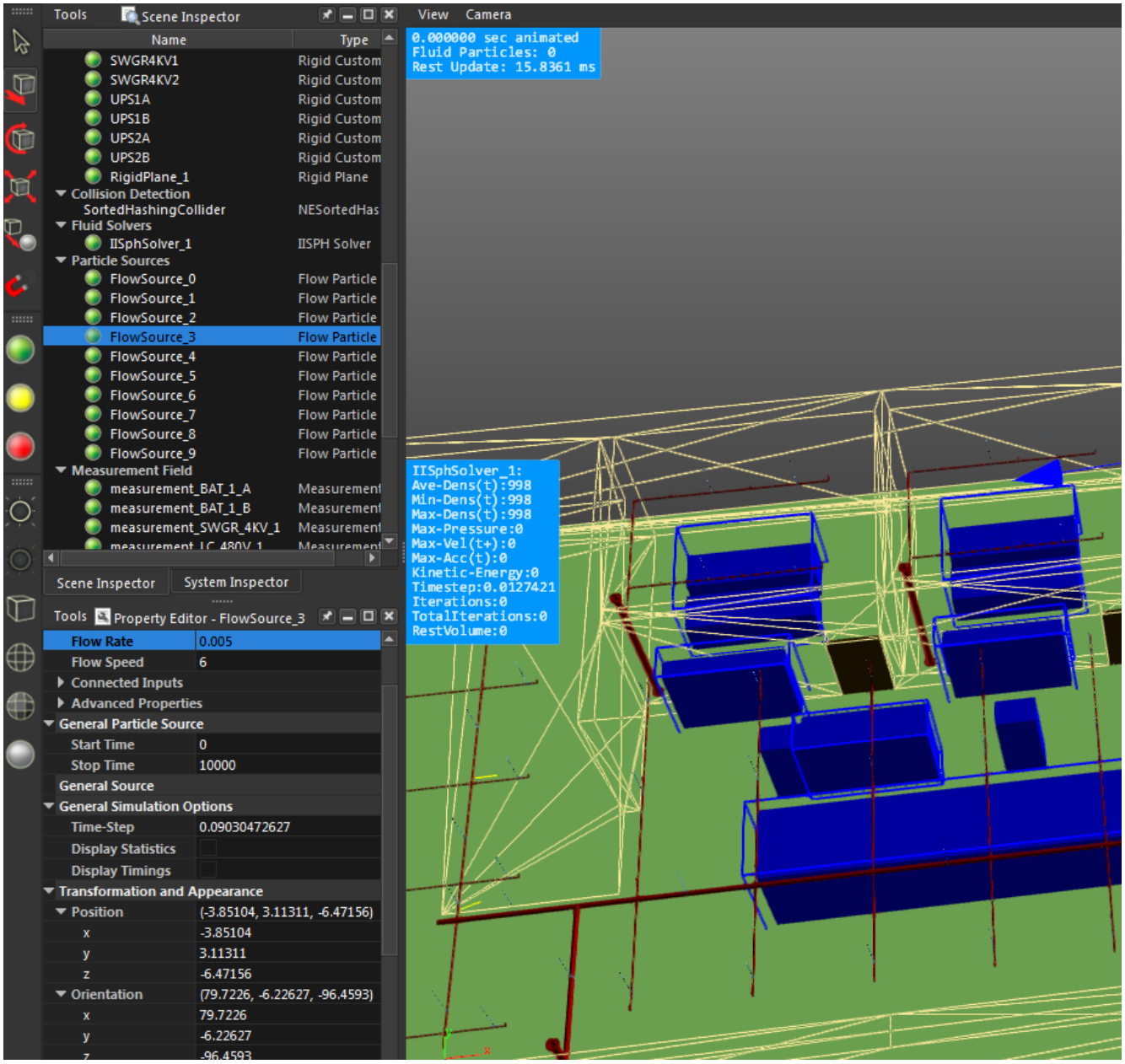

Figure 35. Item Properties Can Be Edited Dynamically Before or During a NEUTRINO Simulation.

When the simulation is loaded, the desired events data is also loaded. This indicates what measurement field events are needed and are to be sent back to EMRALD. In this model each component has a failure for critical water height failure and a possible spray failure. As a simulation runs, it monitors fluid interaction with component measurement fields. If a component's failure criteria are met, a failure message is sent through the network communication to EMRALD. Initial simulations were done to determine that no components would fail due to flooding with a combined leak rate less than 0.006 cubic meters per sec.

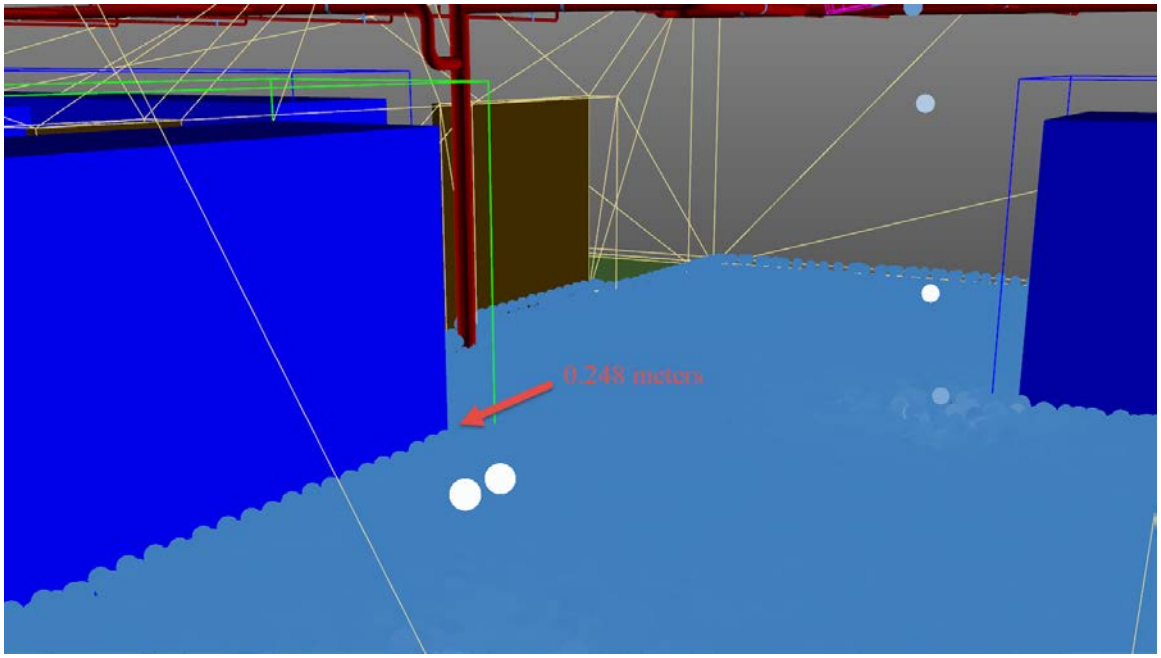

Figure 36. NEUTRINO Measuring Flood Height at 0.248 Meters.

3.3.3 Spray Enhancements

This example uses random sampling of a logical direction for the pipe break (5-40 deg. from perpendicular on either side of the cyclic movement) and is meant to show the basics of incorporating spray failures. Pipe break and spray is a very advanced field of study needs more research. Once more data on pipe break and spray patterns has been done, this information can be used to produce better simulation spray results.

3.4 System TH Model

3.4.1 The INL Generic PWR Model

The RELAP5-3D system TH code models a generic 2.5 GWth 3-loops Westinghouse PWR, representative of the US LWR fleet. The NPP model, also called IGPWR, is described in detail in (Szilard, et al. 2016). In the table below it is reported the main design parameters. The 3-loop unit was chosen because of the large amount of publicly available data, e.g. (Dominion 2007), (US NRC, SOARCA Project. Volume 2. Surry Integrated Analysis 2013) which allowed to develop and validate a realistic model.

Table 14. Relevant Design Parameters of the IGPWR.

Parameter	Value (SI units)	Value (British units)
Core Power [MW_{th}]	2,546	
Reactor Inlet / Outlet Temperature [^oC / ^oF]	282 / 319	540 / 606
Number of Fuel Assemblies	157	
Rod Array	15x15	
RCS Coolant Flow [kg/s / lb_m/hr]	12,738	101.6E+8
Nominal RCS Pressure [MPa /psia]	15.5	2,250
Number of SG	3	
Secondary Pressure [MPa / psia]	5.405	785
Secondary Side Water Mass @ HFP [kg / lb_m]	41,639	91,798
SG Volume [m^3 / ft^3]	166	5,868
SG Steam Flow rate @ HFP [kg/s / lb_m/hr]	473.0	3.756E+6
FW Temperature [^oC / ^oF]	228	443
Main FW pump [m^3/s / gpm]	2 x 6.513 (at 518 m)	2 x 13,800 (at 1,700 feet)
Turbine-driven AFW pump [m^3/s / gpm]	1 x 0.3304 (at 832 m)	1 x 700 (at 2,730 feet)
Emergency Condensate Storage Tank [m^3 / ft^3]	416	14,691
Accumulator Water Volume [m^3 / ft^3]	3 x 27.61	3 x 975
Accumulator Pressure [MPa /psig]	4.14-4.59	600-665
High Head Safety Injection [m^3/s /gpm]	3 x 0.0708 (at 1,767 m)	3 x 150 (at 5,800 ft)
Low Head Safety Injection [m^3/s /gpm]	2 x 1.416 (at 68.6 m)	2 x 3,000 (at 225 ft)
Containment Volume [m^3 / ft^3]	50,970	1,800,000
Containment Design Pressure [MPa /psig]	0.31	45
Containment Operating Pressure [MPa /psia]	0.062 to 0.071	9 to 10.3

The RELAP5-3D model developed for analyzing LOOP and SBO-like events is based on an input-deck describing:

- reactor pressure vessel (RPV);
- three main circulation circuits (MCC), including the main coolant pumps (MCP) and the steam generators (SG);

- pressurizer (PRZ), and its main valves (PORV and SV);
- connections for the emergency core cooling system (ECCS) and the auxiliary feed-water (AFW);
- secondary part of the SGs up to the SG outlet, including the main valves (PORV and SV);
- main feed-water (MFW)
- ECCS including High and Low Pressure Injection Systems (HPIS and LPIS) and accumulators

The sketches of the RPV and of the MCC, including the secondary side of the SGs, are given in Figure 37 and Figure 38. Three independent TH channels representing the central, the middle and the periphery of the core are used. A sketch of the three-channel core region subdivision is given in Figure 39, together with the number of the fuel assemblies and their relative radial power. 214 hydraulic volumes connected by 257 junctions and coupled to 240 heat structures compose the RELAP5-3D nodalization. The total number of mesh points, discretizing the heat structures, is 1312. The model is based on a nodalization developed for the RELAP/SCDAP code for SBO analyses (Bayless 1987).

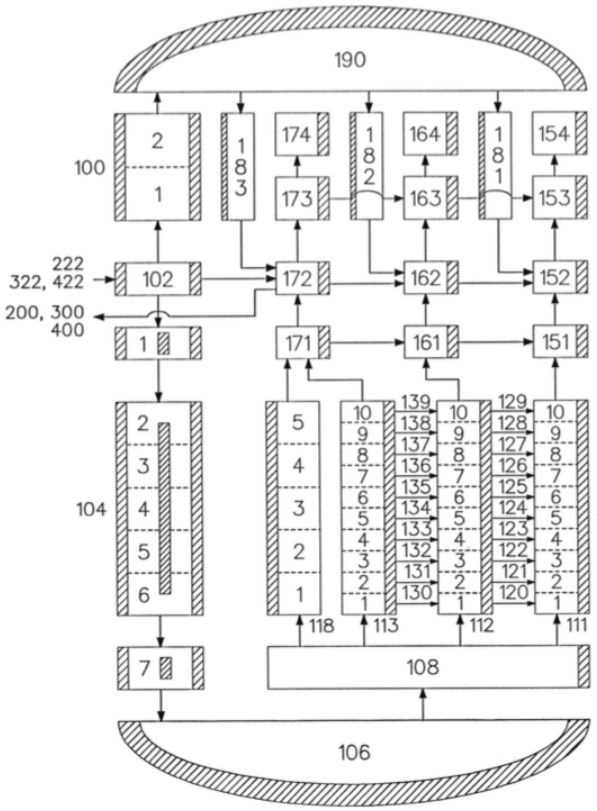

Figure 37. RELAP5-3D RPV Model.

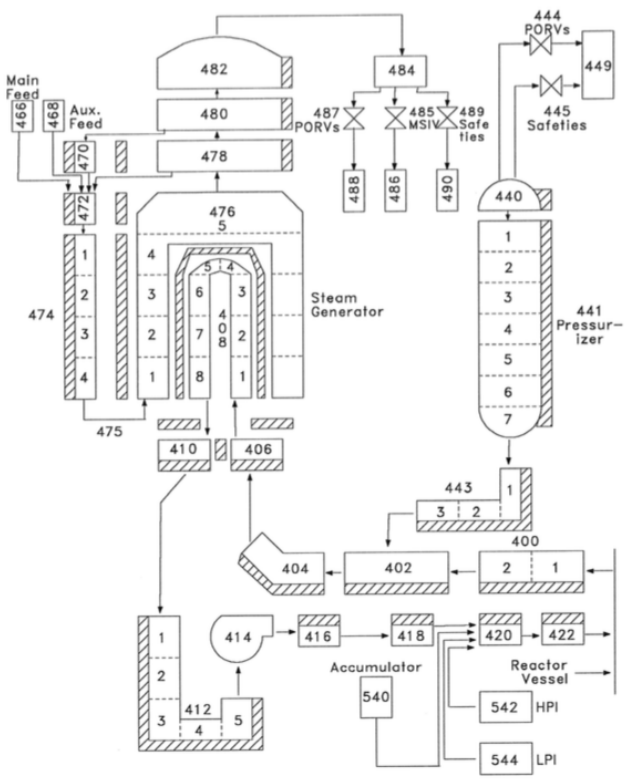

Figure 38. RELAP5-3D MCC & SG Model.

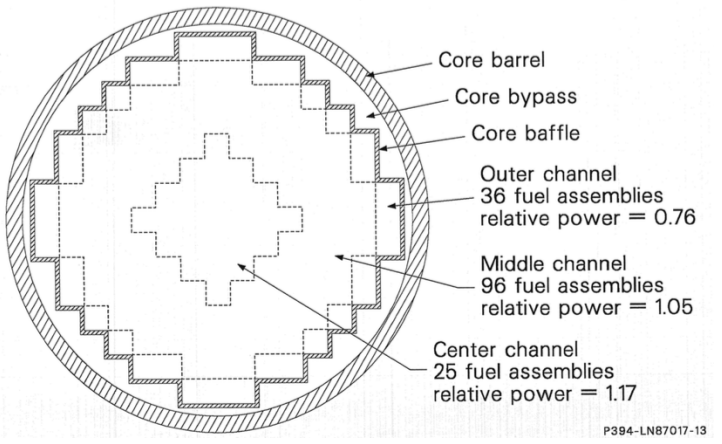

Figure 39. RELAP5-3D Core Model.

The possible operator actions (SG cool-down, feed and bleed, AFW flow control, HPIS/LPIS actuation) are implemented through the RELAP5-3D control logic. RELAP5-3D control variables calculate the derived parameters for the control logic and for the transients' analyses.

3.4.2 Model Qualification

Steady state and on-transient validation has been achieved for the RELAP5-3D model. Details of qualification results are provided in (Parisi, et al. 2016). A null-transient of 1000 s was calculated for validating the steady-state solution. Comparison between RELAP5-3D calculated values and IGPWR reference data are provided in Table 15. Deviations of calculated values are negligible, resulting in an excellent agreement. (Parisi, et al. 2016) provides the trend of the main parameters and the on-transient calculations with code-to-code validation.

Table 15. RELAP5-3D SS Calculation of Main Parameters.

Parameter	Reference Value	RELAP5-3D value	Deviation (%)
Reactor Power (W)	2,546	2,546	imposed
PRZ Pressure (MPa)	15.5	15.5	imposed
Total RCS Coolant Loop Flowrate (Kg/s)	12,738	12,738	0.0
CL Temperature (K)	555.6	557.3	0.3
		557.3	0.3
		557.3	0.3
HL Temperature (K)	591.8	593.1	0.2
		593.1	0.2
		593.1	0.2
Feed-water Temperature (K)	501.5	501.5	imposed
		501.5	imposed
		501.5	imposed
Steam Flowrate per SG (K)	473.	470.1	-0.6
		470.7	-0.5
		471.0	-0.4
Steam Pressure at the Outlet Nozzle (MPa)	5.405	5.405	imposed
		5.405	imposed
		5.405	imposed
Liquid Mass per SG (Kg)	41,639	41,640	0.0
		41,638	0.0
		41,638	0.0
Steam Temperature (K)	542	542	0.0
		542	0.0
		542	0.0

3.4.3 Sequence of Events

Two of the sequence identified by the SAPHIRE PRA analysis, required a TH simulation. Each of those main sequences can branch-off in other different sub-branches depending by the type of failures (e.g. the MCP seal leakage rate, battery failure time), the operator/emergency crew actions (emergency injection time, recovery of ECCS). Therefore, the RELAP5-3D code was used for deterministic calculations of such events as function of selected parameters. In the following two sections, results from the two selected sequences are reported. Details can be found in Appendix B of this report.

3.4.3.1 Loss of Offsite Power – Sequence 2-02-05 of PRA

LOOP event (sequence 2-02-05) is the simultaneous loss of electrical power to all unit safety buses (emergency buses, Class 1E buses, and vital buses) requiring all emergency power generators to start and supply power to the safety buses. The nonessential buses may also be de-energized as a result of this (US NRC, LOOP Glossary 2017). The sequence studied is initiated by an off-site event (earthquake). In the main LOOP sequence, RELAP5-3D calculates the main TH parameters of the plant, simulating the list of events that lead to core damage.

Table 16. LOOP 2-02-05 Sequence: RELAP5-3D Timing.

EVENT DESCRIPTION	TIME [hh:mm]
Initiating event LOOP – loss of electrical power to safety buses. EDG start.	00:00
Reactor trip MSIVs close RCP seals initially leak at 21 gpm/pump (~1 Kg/s)	00:00
TD-AFW auto initiates at full flow	00:01
RCP seals leak increase at 182 gpm/pump (~8.7 Kg/s)	00:13
First SG SRV opening	00:15
Operators control AFW to maintain level	00:15
Upper plenum water level starts to decrease	00:36
Offsite Power is not recovered	02:00
HPIS fails to provide make-up water	02:00
Core Damage	~07:43

In this sequence, the operator does not initiate controlled cooldown of secondary at ~100 F/hr (~55.5 C/hr). Mass is lost through the MCP seal break and fuel is damaged after ~7.5 hrs. In the next figures, some of the most important TH parameter trends of the sequence are reported. Details of the calculations are provided in Appendix B of this report.

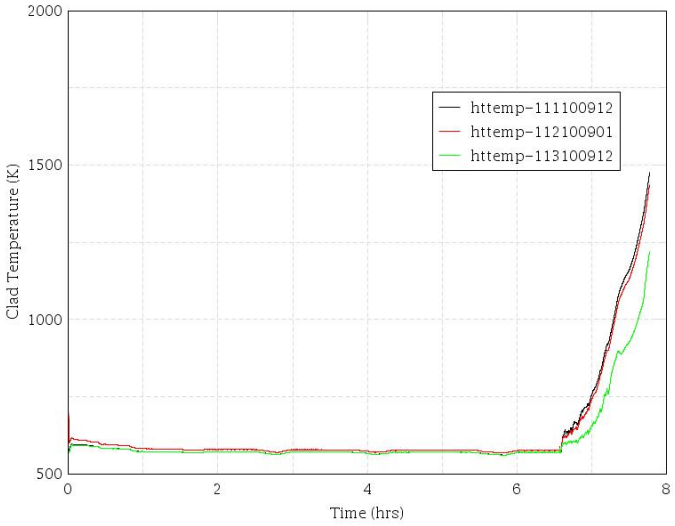

Figure 40. LOOP 2-02-05: Cladding Temperatures.

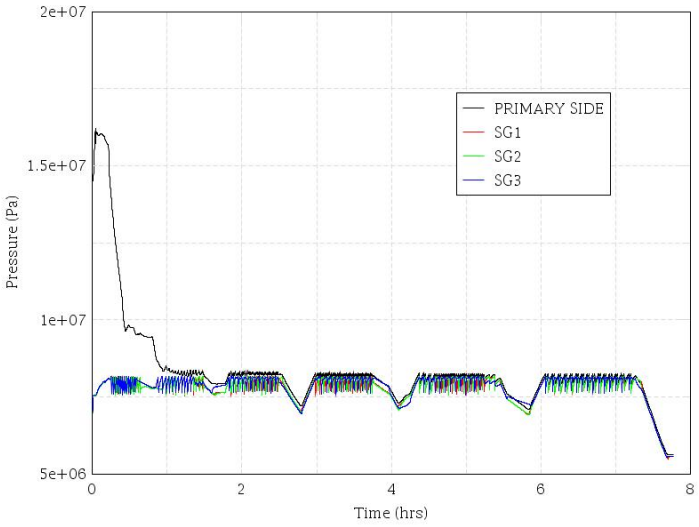

Figure 41. LOOP 2-02-05: Pressure Trends.

This sequence of events was further investigated using the RELAP5-3D/RAVEN coupling for identifying a Limit Surface (LS) as function of MCP seal leakage versus SG depressurization time (see section 3.5.1.2).

In fact the sequence of events that do not terminate with core damage involve a proper actuation of the SG depressurization by the operator, see e.g. the sequence of events reported in Table 17 and e.g., Figure 42 and Figure 43

Table 17. LOOP 2-02-05-noCD Sequence: RELAP5-3D Timing.

EVENT DESCRIPTION	TIME [hh:mm]
Initiating event LOOP – loss of electrical power to safety buses. EDG start.	00:00
Reactor trip MSIVs close RCP seals initially leak at 21 gpm/pump (~1 Kg/s)	00:00
TD-AFW auto initiates at full flow	00:01
RCP seals leak increase at 182 gpm/pump (~8.7 Kg/s)	00:13
Operators control AFW to maintain level	00:15
Upper plenum water level starts to decrease	00:36
Offsite Power is not recovered	02:00
HPIS fails to provide make-up water	02:00
Operator successfully perform controlled cooldown of secondary at ~100 F/hr (~55.5 C/hr)	06:38
Cladding temperature start to decrease	~07:33

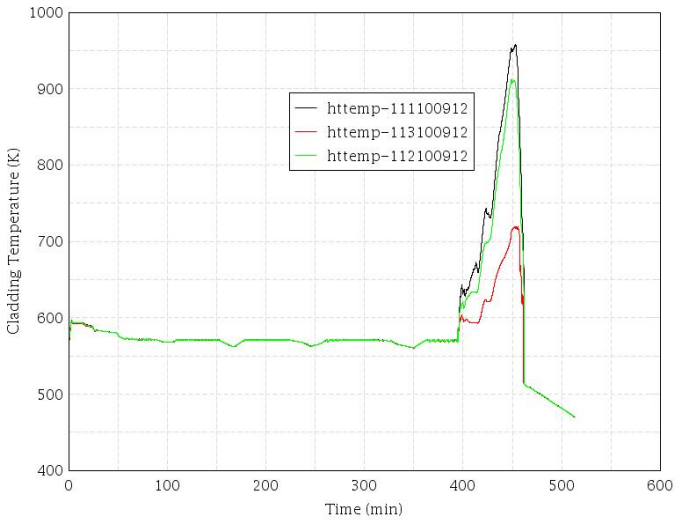

Figure 42. LOOP 2-02-05-noCD: Cladding Temperatures.

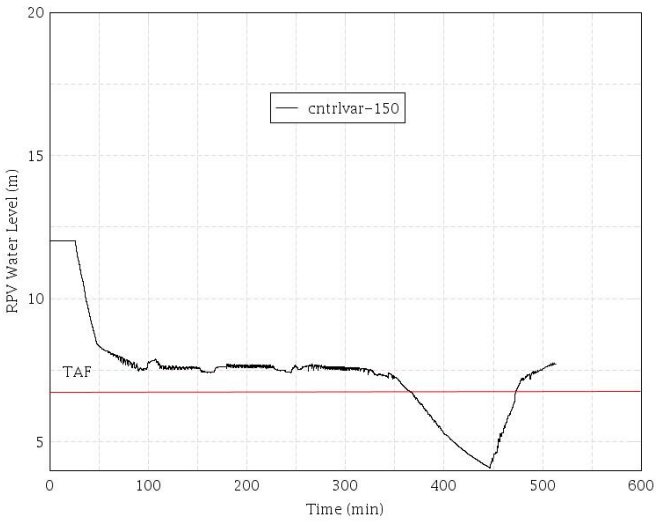

Figure 43. LOOP 2-02-05-noCD: RPV Water Level.

3.4.3.2 SBO – Sequence 2-16-45 of PRA

The SBO event (sequence 2-16-45) is the complete loss of AC power to safety buses. SBO involves the LOOP concurrent with the failure of the onsite emergency AC power system. It should be noted that it does not include the loss of available AC power to safety buses fed by station batteries through inverters (US NRC, LOOP Glossary 2017). Generally the SBO case assumes that no DC power is lost and the operator is able to perform reactor cool-down using feed-and-bleed procedure on the secondary side.

In this sequence it is assumed that a pipe failure in the switchgear room causes a flooding that knockdown the DC power during the first hour. If emergency actions are not promptly actuated, core damage is occurring in few hours. E.g., the assuming that DC power is lost after 25 minute, the following sequence has been calculated (see Table 18).

Table 18. SBO+DC Loss Sequence (2-16-45 of PRA): RELAP5-3D Timing.

EVENT DESCRIPTION	TIME [hh:mm]
Initiating event Station blackout – loss of all onsite and offsite AC power	00:00
Reactor trip. MSIVs close. RCP seals initially leak at 21 gpm/pump (~1 Kg/s)	00:00
TD-AFW auto initiates at full flow	00:01
RCP seals initially leak at 182 gpm/pump (~8.7 Kg/s)	00:13
First SG SRV opening	00:15

Operators control TD-AFW to maintain level	00:15
Pipe rupture and flooding in the switchgear knockdown DC power. TD-AFW is lost.	00:25
RPV water level below TAF	02:33
Core Damage occur	~03:10

RELAP5-3D results are shown in Figure 44 and Figure 45.

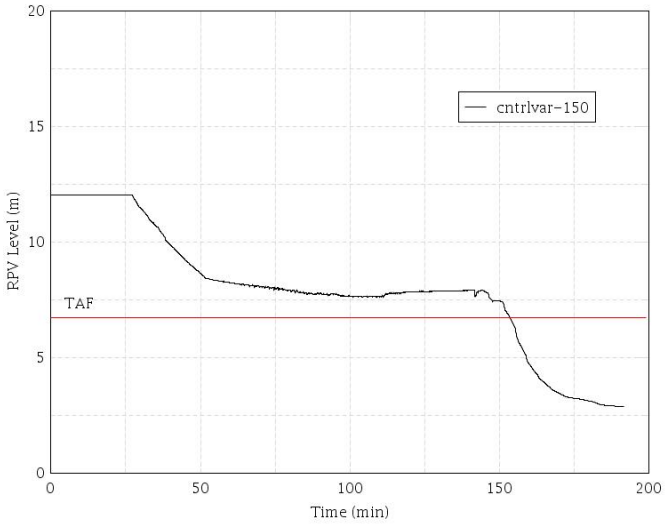

Figure 44. SBO 2-16-45-CD: RPV Water Level.

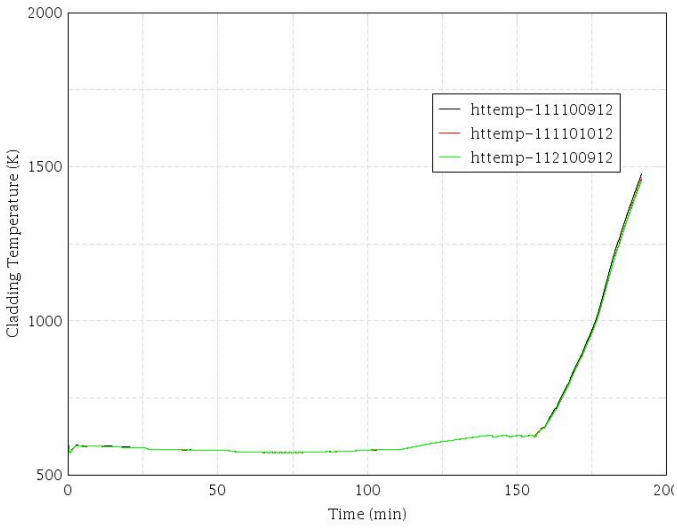

Figure 45. SBO 2-16-45-CD: Cladding Temperatures.

Emergency crew can be deployed to manually actuate the AFW and the SG PORV using mobile emergency equipment (e.g., spare batteries, compressed-air bottles). RELAP5-3D/RAVEN is used for calculating the LS as function of the DC failing time versus the emergency crew recovery time (see section 3.5.1.3). The following

table and figures report the case in which the DC power is lost after 25 minutes and the emergency crew successfully recover TD_AFW and SG PORVs after ~2 hours and 45 minutes. Details of calculations are provided in Appendix B of this report.

Table 19. SBO+DC Loss Sequence (2-16-45 of PRA): RELAP5-3D Timing.

EVENT DESCRIPTION	TIME [hh:mm]
Initiating event Station blackout – loss of all onsite and offsite AC power	00:00
Reactor trip. MSIVs close. RCP seals initially leak at 21 gpm/pump (~1 Kg/s)	00:00
TD-AFW auto initiates at full flow	00:01
RCP seals initially leak at 182 gpm/pump (~8.7 Kg/s)	00:13
First SG SRV opening	00:15
Operators control TD-AFW to maintain level	00:15
Pipe rupture and flooding in the switchgear knockdown DC power. TD-AFW is lost.	00:25
RPV water level below TAF	02:33
Emergency crew succeeds in performing blackrun of TDAFW and SG PORV operation. Controlled cooldown of secondary at ~100 F/hr (~55.5 C/hr)	02:45
Fuel Temperatures and Primary/Secondary pressures start to decrease	02:50
Accumulators begin injecting	03:30
RPV water level at bottom of HL/CL	~04:00

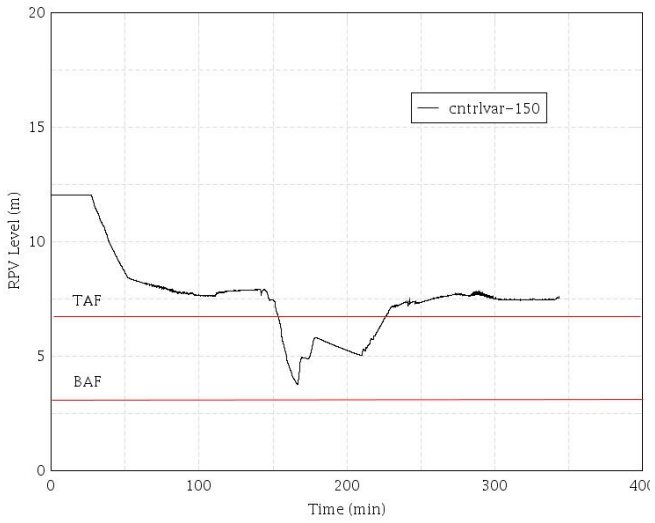

Figure 46. SBO 2-16-45-noCD: RPV Water Level.

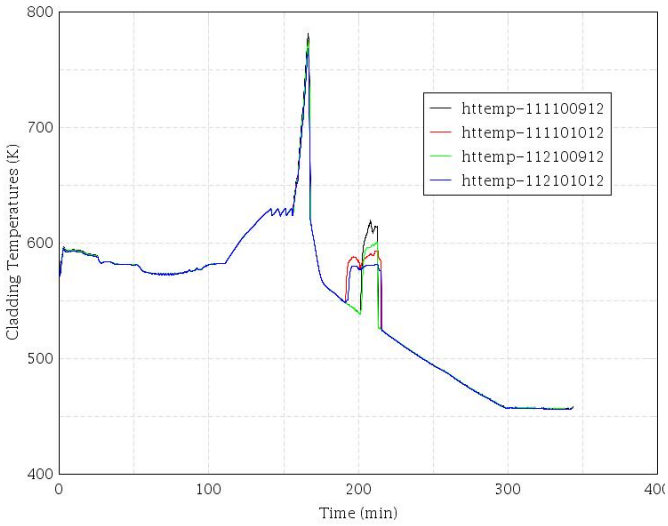

Figure 47. SBO 2-16-45-noCD: Cladding Temperatures.

3.5 Limit Surface Search and UQ Model

3.5.1 Limit Surface Search

3.5.1.1 Theoretical Background

Quick and automatic determination of a LS (i.e., the surface, in the n-dimensional space of our problem, dividing the safe fuel conditions from the failed ones) has been performed using RAVEN LimitSurfaceSearch algorithm. LS search is based on the use of a Reduced Order Model (ROM) or Surrogate Model (SM). The initial observations (in this case, RELAP5-3D calculations) are used for training the ROM, which is then employed for

the determination of the LS. Exploration of the n-dimensional space of the problem using the ROM is not-computationally expensive and several algorithms from machine learning are available. The workflow of the LS search is presented in Figure 48.

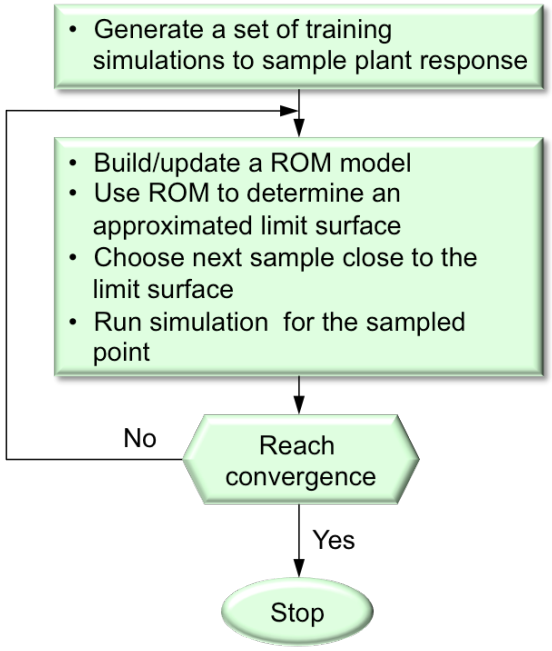

Figure 48. Limit Surface Search Workflow in RAVEN.

Among the multiple ROM algorithms available, we selected the Support Vector Machine/Support Vector Classifier (SVM/SVC) ROM (Cortes and Vapnik 1995) from the Scikit-Learn external Python library (Scikit-Learn 2017). The fit time complexity is more than quadratic with the number of samples, which makes it hard to scale to dataset with large number of samples. In our cases, the number was quite small (maximum order of one thousands), so there were no problems in applying SVM/SVC. Different kernels are available (linear, polynomial, exponential, sigmoid, e.g. see Figure 49).

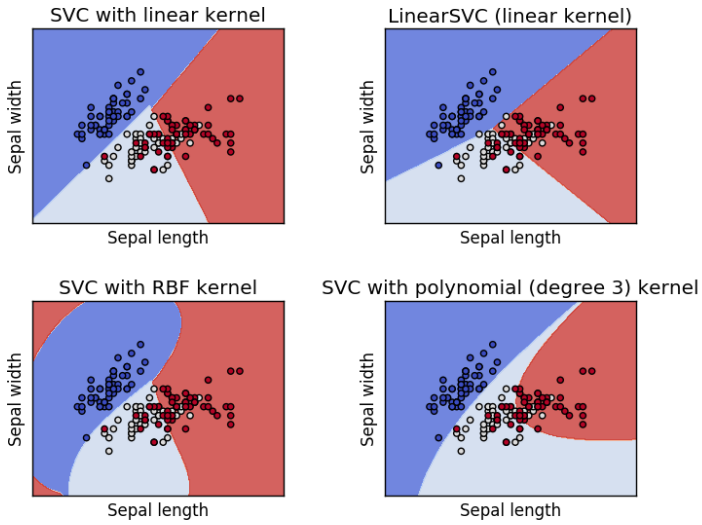

Figure 49. Different Available Kernels from SVM/SVC – Scikit-Learn.

After several tests, we selected the exponential kernel (see following equation):

$$e^{(-\gamma|x-x'|^2)}$$

with the following kernel parameters, C=50, γ=10. These set of parameters allowed a fast and smooth identification of the LS. Several runs were also performed for assessing the effect of the convergence parameters. It should be noted that the LS algorithm identifies, more than the real LS, a region that bound the LS. The identification of the different points of the regions (fail/safe) is performed using a "goal function', which in this case is:

$$if\ (CladTemp_i < 1480\ K)\ then\ \text{goal function} = 1;\ else = -1$$

for all the selected *i* values of the clad temperatures calculated by RELAP5-3D. A convergence acceleration of the LS search is also possible in RAVEN using an adaptive refined sub-grid (Alfonsi, et al. 2017).

3.5.1.2 Limit Surface for LOOP 2-2-05

Automatic LS search for the PRA LOOP 2-02-05 sequence was performed. The parameters that were sampled are:

- MCP Seal Leakage rate: 6 points in the interval: 21 to 480 gpm (corresponding to 782.6 to 802.8 seconds on the Figure 50). The assigned distribution was uniform.
- SG depressurization time: 16 points in the interval: 13000 to 42000 seconds (~3.6 hr to ~1.6 hr). The assigned distribution was uniform.

Results of the LS search are given in Figure 50. It should be noted that the "loop" in the top right part of the figure constitute a zone of non convergence of the LS algorithm calculations.

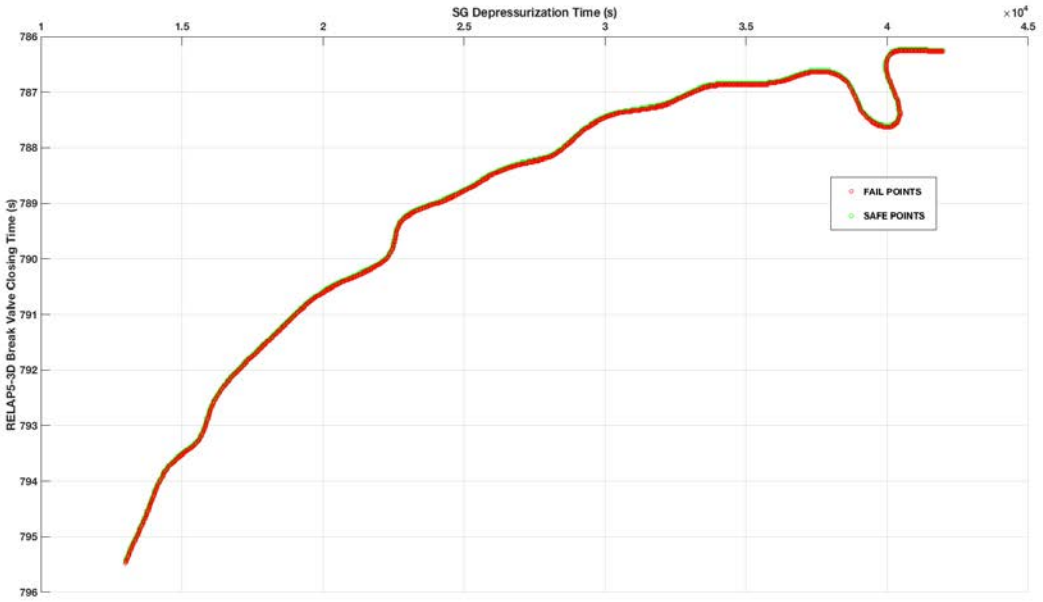

Figure 50. Limit Surface for LOOP 2-2-05-noCD.

3.5.1.3 Limit Surface for SBO 2-16-45

RELAP5-3D/RAVEN was also used for the PRA SBO 2-16-45 sequence. In this case, the parameters which were sampled are the Battery Failure Time and Operator Recovery Time. The parameters grid was:

- Battery Failure time: 4 points in the interval: 0.0 to 3600 seconds. The assigned distribution was uniform.
- Emergency Crew Recovery time: 4 points in the interval: 7200.0 to 14400 seconds. The assigned distribution was uniform.

The Limit Surface is given in Figure 51.

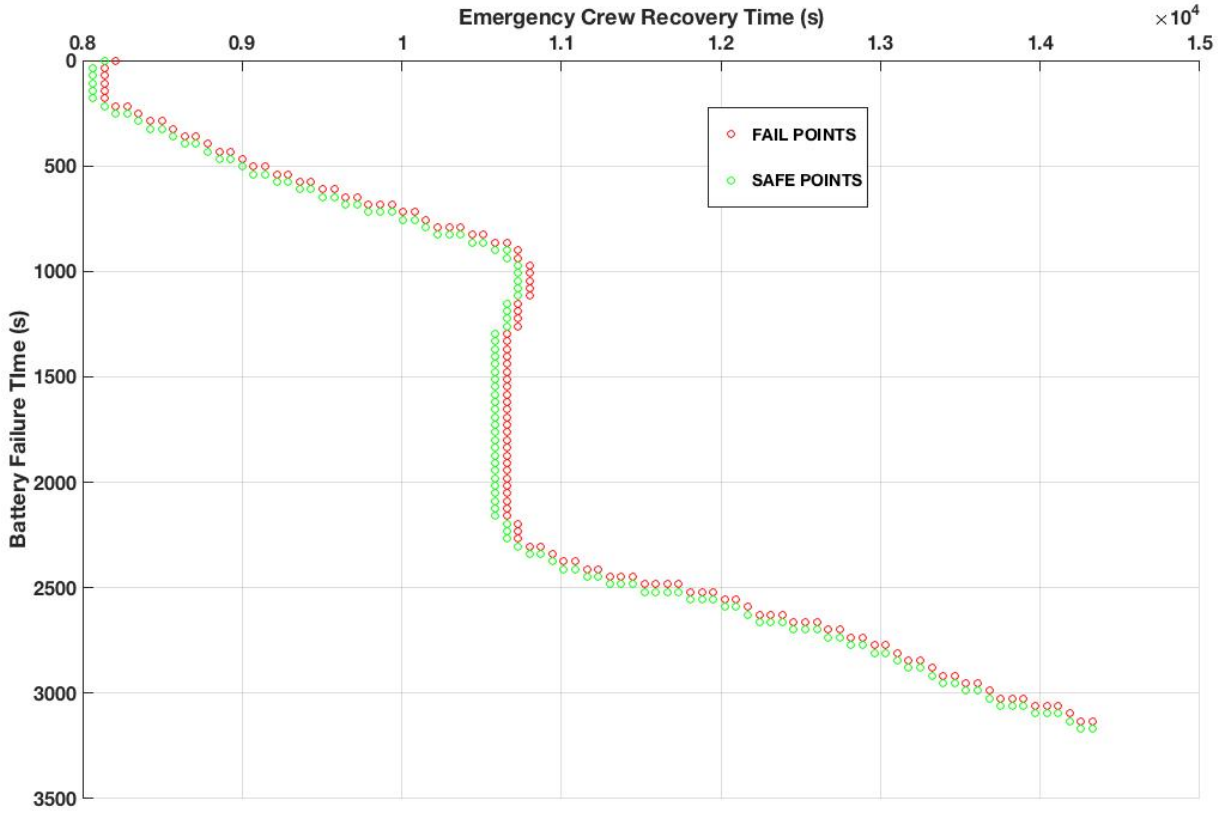

Figure 51. Limit Surface for SBO 2-16-45-noCD.

3.5.2 Uncertainty Quantification

3.5.2.1 General Considerations

The use of BE plus Uncertainty (BEPU) calculations is required when a risk-informed safety analysis is being performed (IAEA 2009). The simplified uncertainty analysis reported hereafter is intended to show the coupled RELAP5-3D/RAVEN capabilities in dealing with BEPU. As reported in (Nutt and Wallis 2004) and (Frepoli 2008), the uncertainty quantification (UQ) applied based the use of Wilks` formula (Wilks 1941) – order statistics require a minimum number of calculations given by:

$$\beta = 1 - \sum_{i=N-m+1}^{N} \frac{N!}{(N-i)!\, i!} \gamma^i (1-\gamma)^{N-i}$$

where γ=0.95 is the percentile of the bounding value of the PCT, β=0.95 is the confidence value, N is the number of calculation runs, m is the number of outputs in the γ^{th} quartile.

For this analysis, we assumed γ=0.95, β=0.95 and m = 1 and m = 4. Therefore, according to the above formula, we run 59 and 153 calculations for each UQ. Figure of merit (FOM) was the peak cladding temperature (PCT).

Since it was a simplified UQ, RELAP5-3D closure laws were not perturbed. The identification of the relevant parameters was based on the Phenomena Identification and Ranking Table (PIRT) of the CSAU methodology (Boyack, et al. 1990). RAVEN capabilities were exploited for perturbing uncertainty parameters, for analyzing results using basic statistics and for post-processing the large calculation databases. RELAP5-3D/RAVEN was run on INL Falcon HPC machine for achieving fast parallel calculations.

For IA2, RELAP5-3D relevant input parameters and their uncertainty distributions were selected, considering the main phases (e.g. reactor scram, SG depressurization, etc.) and the main phenomena involved during a LOOP/SBO scenario (e.g., natural circulation in the RCS, critical flow at the MCP seal break and on PRZ and SG PORV/SRV, heat transfer in the SGs).

The effect of the variation of these parameters (independent variables) on the RELAP5-3D output (dependent variable, in this case the clad temperature) was assessed, providing an indication of the calculation uncertainty. The list of perturbed parameters and their distribution is given in Table 20.

Table 20. List of Perturbed Parameters and Distribution.

Sensitivity Parameter	Associated Phenomenon	Distribution	Range (±σ or min/max)
Power Table	Decay Heat	Normal	±7%
Core Pressure Losses	RPV internal circulation	Uniform	±40%
SG PORV/SRV valve flow areas	Critical Flow / Loss of Secondary Side Mass	Uniform	±30%
PRZ PORV/SRV valve flow areas	Critical Flow / Loss of Primary Side Mass	Uniform	±30%
MCP seal break area	Critical Flow /Loss of Primary Side Mass	Uniform	±20%
SG HX Multiplier	Primary/Secondary Side Heat Exchange	Normal	±20%

RAVEN “Basicstatistics” module was applied for determining the importance of the selected parameters in respect to the FOM. Results for both scenarios are provided in Table 22 and Table 21.

Table 21. Basic Statistics for LOOP-2-02-05-noCD.

Sensitivity Parameter	Sensitivity	Covariance	Pearson
Decay Power	2.45E-05	1.34	0.0872
Core Pressure Losses	8.85E-04	48.6	0.0723
SG / PRZ PORV/SRV valve flow areas	-1.91E-4	-10.5	-0.258
SG HX Multiplier	9.17E-05	5.03	0.247

Table 22. Basic Statistics for SBO-2-16-45-noCD.

Sensitivity Parameter	Sensitivity	Covariance	Pearson
Decay Power	2.02E-04	19.2	0.948
Core Pressure Losses	-1.02E-04	-9.74	-0.011
SG / PRZ PORV/SRV valve flow areas	-1.17E-06	-0.111	-0.002
SG HX Multiplier	1.44E-05	1.37	0.051

3.5.2.2 Results for LOOP 2-2-05

In Figures 52-53, we show the trend Latin-hypercube sample of LOOP 2-02-05. As reported in the previous sections, 59 and 153 Latin Hypercube sampling were performed, obtaining first and fourth order statistics of the FOM. The PCT derived from 59 calculations and 153 is 1460.8 K and 1462.8 K, respectively. So the UQ analysis shows that there is a probability that some fuel damage could occur since few runs resulted in the temperature range above 1450s K.

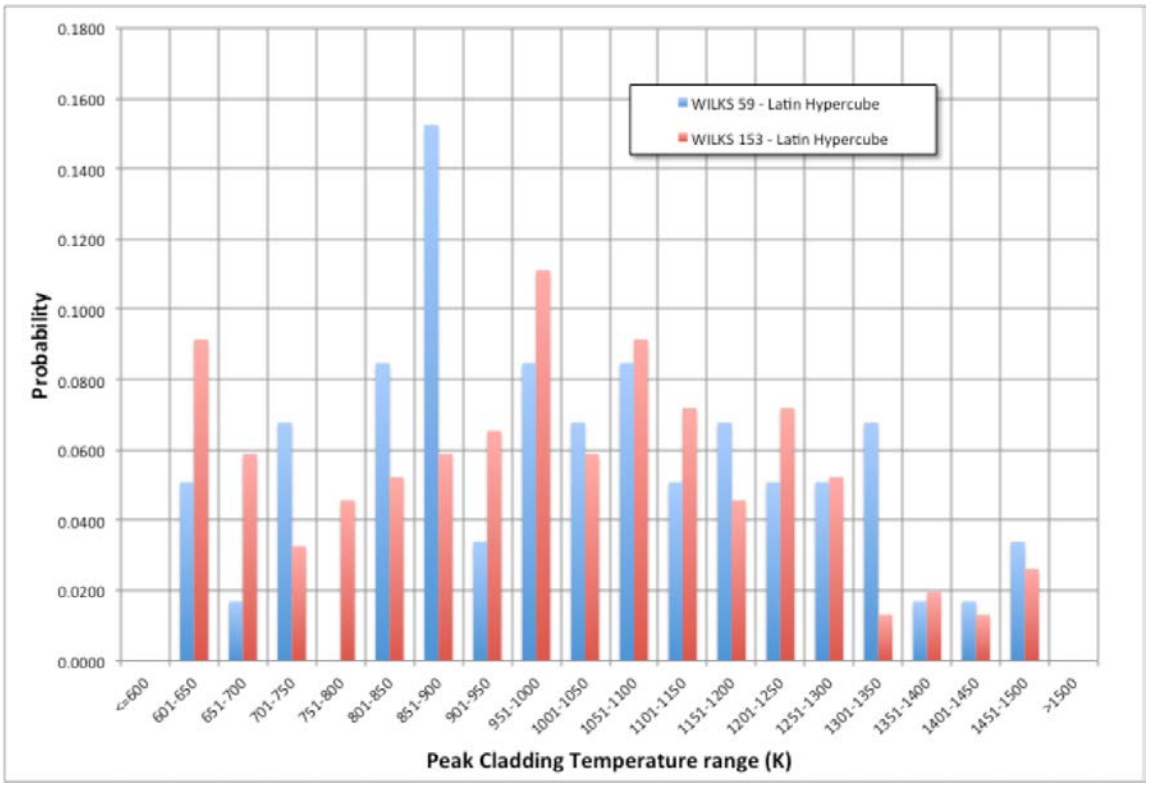

Figure 52. PCT for LOOP 2-2-05-noCD: MC/Latin Hypercube for 59 and 153 Calculations.

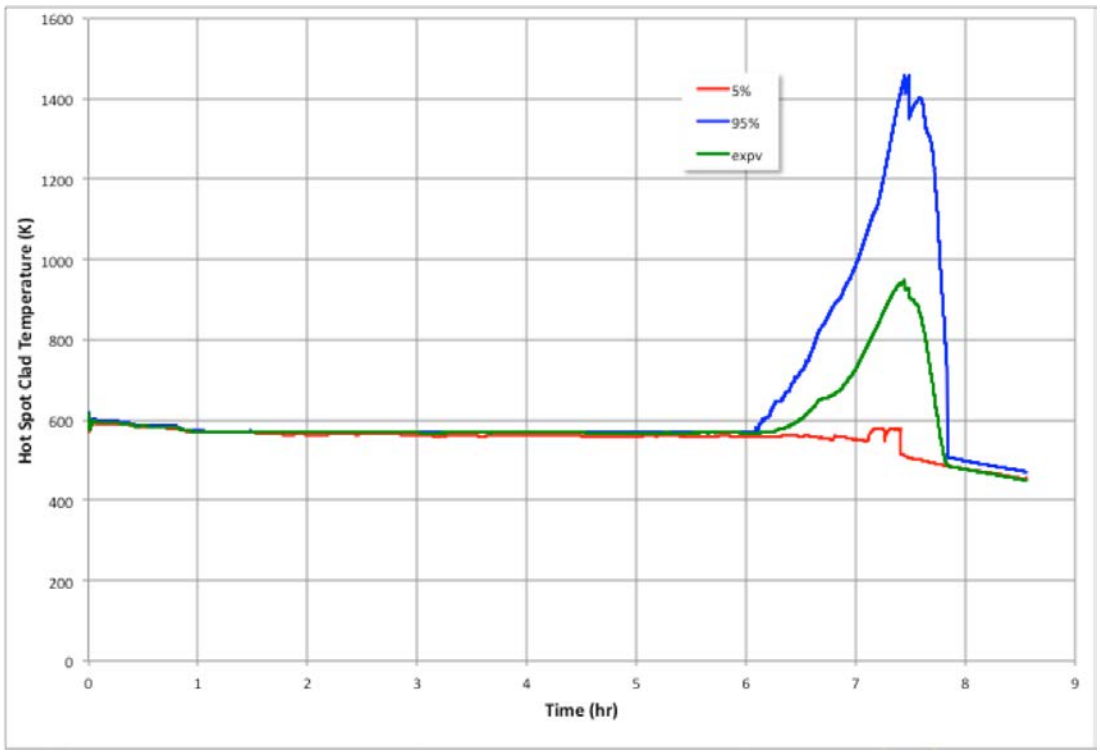

Figure 53. Distribution of PCT Trends for 59 Runs of LOOP 2-2-05-noCD.

3.5.2.3 Results for SBO 2-16-45

In Figures 54-55, we show the trend Latin-hypercube sample of SBO 2-16-45. As reported in the previous sections, 59 and 153 Latin Hypercube sampling were performed, obtaining first and fourth order statistics of the FOM. The PCT derived from 59 calculations and 153 is 1475.8 K and 1469.3 K, respectively. So the UQ analysis shows that there is a probability that some fuel damage could occur since some runs resulted in the temperature range above 1450s K.

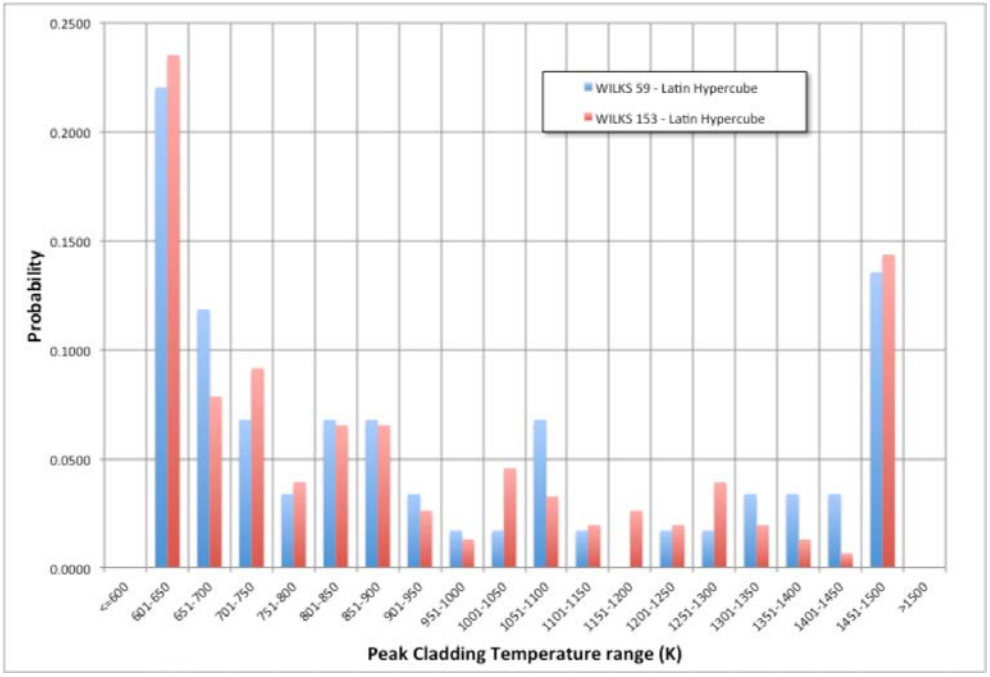

Figure 54. PCT for SBO 2-16-45-noCD: MC/Latin Hypercube for 59 and 153 Calculations.

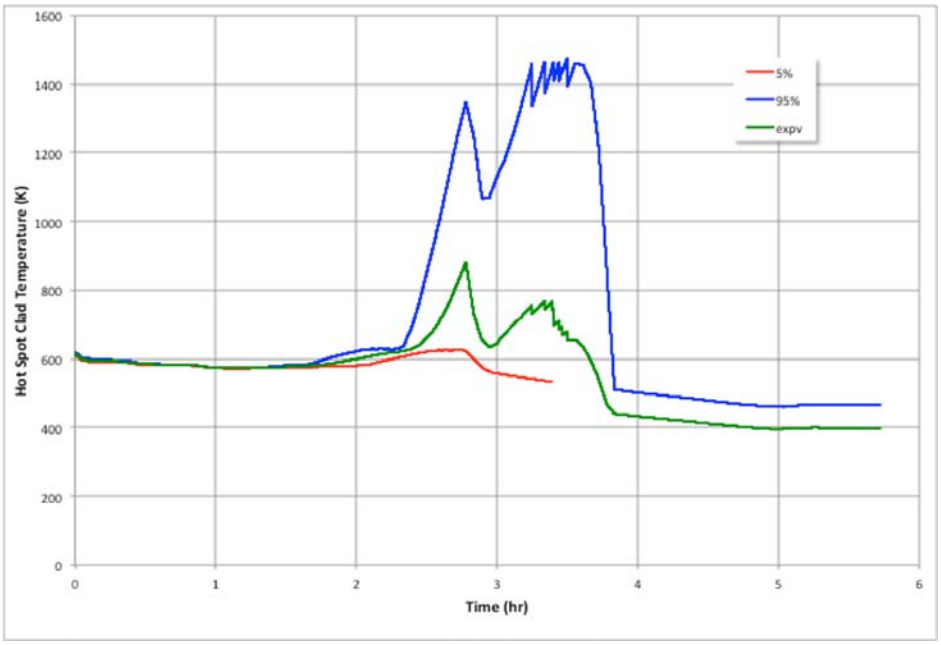

Figure 55. Distribution of PCT Trends for 59 Runs of SBO 2-16-45-noCD.

3.5.2.4 Limit Surface with Epistemic Uncertainties: The SBO Case

A demonstration of the LS search including the epistemic uncertainties was performed. We applied the "EnsembleForward" sampler of RAVEN, which allowed grid and Latin hypercube sampling of the problem space. Results of "EnsembleForward" sampling were then used for training the ROM. The perturbed parameters were stochastic uncertainties (e.g., battery failure time and crew recovery time) and epistemic uncertainties (core power, pressure losses, heat exchange in SGs, critical flow at the valves). The identified LS was a 6-dimensional surface, so we projected the fail points on a two dimensional surface (battery failure time vs crew recovery time).

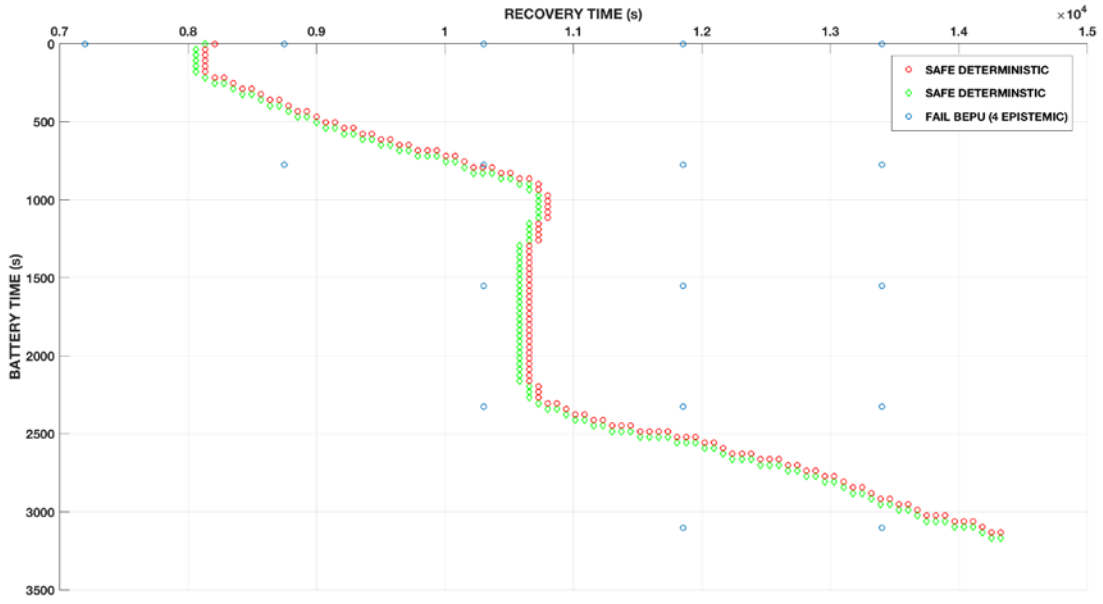

Figure 56. Limit Surface for SBO Including Epistemic Uncertainties.

We can notice in Figure 56 that the "safe" are is become smaller, with the projection of the LS moving toward the left side. The coarse mesh obtained is being refined in future calculations by decreasing the tolerance limit and performing grid acceleration.

4. Results of External Hazards Advanced PRA Demonstration

The results from SAPHIRE are used as a base comparison for the EMRALD results. The EMRALD model results are obtained from the computation of 3 workstations with a total of about 2 million runs. Many of the results presented here are a combination or comparison of both the SAPHIRE model and the EMRALD simulation results.

Table 23 shows a summary of the EMRALD simulations using combined 3D simulation in NEUTRINO and results from input to the RELAP5-3D-derived limit surfaces. Rows 3 and 4 show how often core damage is reached versus how often SAPHIRE estimates core damage for the two main LOOP and SBO sequences. These results demonstrate the sensible reduction in the level of conservatism that can be obtained using RISMC approach and toolkit.

Table 23. Likelihood of failures when event sequences required deterministic calculations.

Pipe Failure % if EQ and LOOP	2.12%
3D Simulation Comp Failure %	78.20%
Seq 2-02-05 TH Eval. Failure %	92.7%
Seq 2-16-45 TH Eval. Failure %	66%

Each pipe break and location was counted in the simulation and the likelihood of break at each location is shown in Table 24. This percentage is based on the number of simulations with a pipe break. It should be noted that often there was more than one break location in a simulation so the sum of percentages is totaling more than 100%.

Table 24. Likelihood of a Break occurring at a given location.

Break Location	Counts	Break %
16	103	0.242%
21	1107	0.000%
225_01	287	0.656%
225_06	39294	88.733%
225_08	407	0.963%
222_06	191	0.483%
216_08	236	0.585%
216_06	422	0.656%
274_06	20	0.071%
270_06	21	0.099%

The events from the NEUTRINO calculations coming into EMRALD are also saved and can track which components failed for every simulations ran. The simulation results in Table 25 show that 3D components LC_480V_1 (the 480 VAC buses 1ABA and 1ABE) in Switchgear Room 1 are most likely to be failed by seismic induced pipe rupture and flooding. However, when trying to determine such impacts on the SAPHIRE model, it was realized that the 480 VAC bus failure logic has been simplified and represented only by the 4160 VAC bus failure logic. This simplification occurred during the review process of the original PRA model. While the simplified model does include the single 480 VAC bus failure basic events (i.e., ACP-BAC-LP-1ABA and ACP-

BAC-LP-1ABE) in the model, they were not widely populated to all the associated fault tree logic because their very low random failure probability, 9.6E-6. This is a good lesson learned for future external event simulation works: when converting PRA model to EMRALD model, the very low random failure probability could be increased significantly due to the effect of external events.

Table 25. Component Failures from the 3D Flooding Simulation.

3D Component	Count	Failure %
LC_480V_1	30320	97.0768%
UPS_1_B	209	0.6692%
125VDC_PNL_1	515	1.6489%
SWGR_4KV_1	160	0.5123%
LC_480V_2	27	0.0864%
UPS_1_A	2	0.0064%

SAPHIRE bins the results according to the earthquake level, while EMRALD sampled on a curve and counted how many times earthquakes of BIN2 and BIN3 occurred. However all sequences were grouped together. The results in Table 26 include both BIN2 & BIN3 for the SAPHIRE results. BIN1 results were ignored because of the optimization process and because any EQs sampled in EMRALD that had a lower than 0.3 PGA were ignored. The two SAPHIRE column results show the original model. In particular, the second column shows the conservative or max failure rate increase if all flooding susceptible components fail during a seismic induced pipe failure. The EMRALD results are shown in the third column. EMRALD calculated the increase in CDF caused by component failures considering the 3D flooding and the Best-Estimate results for Sequences 2-02-05 and 2-16-45.

Table 26. SAPHIRE and EMRALD Results.

Sequence Case	CDF No SWGR Pipe Failure, SAPHIRE	CDF Increase from, SAPHIRE SWGR Pipe Failure	CDF Increase from EMRALD & 3D flooding & TH
Seq 2-02-05	6.19E-07	4.580E-08	8.540E-09
Seq 2-15	8.76E-06	1.525E-06	3.51E-09
Seq 2-16-03-10	2.82E-06	1.023E-06	1.48E-09
Seq 2-16-45	1.81E-05	4.360E-06	4.560E-10

These results show that the increase in CDF from the Fire Suppression system using a conservative approach (failure of all the components in the room when there is a water leak) could be significant. The results of the dynamic PRA and the physics based simulations show instead that the increase is insignificant.

However, the most commonly failed component (480 VAC busses), was not fully represented in the model. As described earlier, some simplification of the SAPHIRE PRA model included some effects of LC_480V_1 failure, so the impact of a NEUTRINO-calculated failure of the component was, in some way, decreased. This could have some impact on the outcome of the considered sequences. Modifications to the SAPHIRE and EMRALD models can be refined and simulations rerun in order to adjust these results.

5. SUMMARY AND PATH FORWARD

In this report we presented a demonstration of External Hazards analysis. First we proposed a toolkit and a methodology for performing a risk-informed safety analysis, focusing on earthquake-induced accidents. Then we showed the developed models, which are based on advanced tools. The results presented in the previous sections, demonstrate our capabilities in performing multi-physics and multi-scale simulations combining advanced seismic, PRA and BEPU analyses. The following relevant points could be highlighted from this work:

1) our methodology has the ability to use existing models and data. This can result in a work optimization and in an efficient use of resources when e.g., new data is available (see Figure 2);

2) the use of HPC and machine-learning algorithms can significantly help the safety analyst in handling the large amount of data that is generated when dealing with such complex problems (e.g. see Figure 51);

3) the combination of advanced PRA and BEPU can allow the industry to sensibly improve their procedures, the safety analysis margins and can help in find out new scenarios (e.g., see Table 23). The level of conservatism can be dramatically reduced, enhancing the economy and the safety level of a NPP;

4) further improvements could be obtained in the future by carrying out all calculations (deterministic and probabilistic) on a single HPC machine, leveraging a parallel calculation architecture.

In the following sections, we make some recommendations for future work, based on the experience we gathered during the development of the different tasks of the demonstration analysis.

5.1 Seismic

One of the open questions in the nuclear industry is can a high frequency wave, caused by impact of adjacent nuclear power plant structures during an earthquake, cause an adverse response in safety critical SSCs. A model was developed above that simulates the impact of adjacent NPP structures during earthquakes. Initial models show that the structures have potential to impact during the input motion, but it is unclear is the high frequency wave travels to locations of interest. Future model runs will attempt to determine how far these waves travel. Using the outline described in Figure 3, these seismic failures can be added to the static PRA model to determine a maximum change in CDF. If this maximum change is significant, the seismic failures due to high frequency could be added to the Dynamic PRA model.

5.2 Coupled Dynamic and Static PRA

One main drawback of simulation PRA vs. static PRA methods is the computational costs. With standard Monte Carlo sampling, it can take millions to billions of simulations to capture low probability events. One method others have used to overcome this is through targeted or smart sampling and then adjusting the results accordingly. This can add a lot of complexity to the modeling and code.

Another issue is the difficulty to find design errors in the model. Small mistakes can often go unnoticed they are lost in the mass of simulations that are done. Staged modeling with testing helps with this, but is not a solution.

We propose a hybrid Dynamic and Static PRA method as a solution to address both of these problems. Currently detailed static PRA models exist and produce a lot of valuable data. The main thing missing is time related data and the influence of physics based simulations. A dynamic model could be simplified greatly if it could just simulate the dynamic parts and use information from the static model for the other failure data. This may be achieved by running the simplified or specific dynamic model to get initial failures from things like physics based simulations and time coupled events, then applying those failures to the static PRA model to determine the new top sequence cut sets. These new top cut sets can give the failure rate for the current simulation run, and if

further event failure timing is needed then the events of those cut sets could be sampled for failure times and inserted into the event timeline.

With this method, the dynamic model is simplified and represents only the time dependent pieces. Modeling and runtime is reduced because the large portion of simulation time once used to evaluate standard systems is now done quickly using existing and fast static models.

5.3 Best-Estimate Plus Uncertainty

Concerning BEPU parts, no major issues were detected. RELAP5-3D constitutes the state-of-the-art for the Best Estimate analysis of LWR and all the sequences and the sensitivities were runs without problems. However, we identified the following key-points, which, if developed in the future, could greatly enhance the BEPU part. The key-points are:

1) a module for directly perturbing RELAP5-3D closure laws without accessing the source code should be developed. This would allow the possibility of performing reliable and extensive uncertainty analyses;

2) RELAP5-3D/RAVEN interface should be improved adding the capability by RAVEN of directly accessing the binary restart file of RELAP5-3D;

3) RAVEN Limit Surface algorithms should be systematically evaluated when introducing epistemic uncertainties;

4) RAVEN/EMRALD direct coupling would allow the direct transfer of information between BEPU and Dynamic-PRA modules (see Figure 2).

6. BIBLIOGRAPHY

Alfonsi, A., et al. *RAVEN Theory Manual and User Guide.* Idaho National Laboratory, Idaho Falls: Idaho National Laboratory, 2017, 76.

Bayless, P. D. *Natural Circulation during a Severe Accident: Surry Station Blackout.* EG&G, Idaho Falls: EG&G, 1987.

Boyack, B. E., I. Catton, R. B. Duffey, and et al. "Quantifying reactor safety margins - 1: an overview of the code scaling, applicability, and uncertainty evaluation methodology." *Nuclear Engineering and Desing* (ELSEVIER) 119, no. 1 (1990): 1-15.

CentroidLab. *"Neutrino Dynamics".* http://www.centroidlab.com/neutrinodynamics/ (accessed July 28, 2017).

Coleman, J. L., et al. *MASTODON Theory Manual.* Idaho National Laboratory, Idaho Falls: Idaho National Laboratory, 2017.

Coleman, Justin L., et al. *Multi-Hazard Advanced Seismic Probabilistic Risk Assessment Tools and Applications.* Idaho National Laboratory, Idaho Falls: Idaho National Laboratory, 2016.

Cortes, C., and V. Vapnik. "Support-vector networks." *Machine Learning* (Springer) 20, no. 3 (09 1995): 273-297.

Dominion. *Surry Power Station Units 1 and 2. Updated Final Safety Analysis Report. Rev. 39.* ADAMS, Virginia Electric and Power Company (Dominion), Washington, DC: US NRC, 2007.

Frepoli, Cesare. "An Overview of Westinghouse Realistic Large Break LOCA Evaluation Model." *Science and Technology of Nuclear Installations* (Hindawi Pubblishing Corporation) 2008 (2008): 15.

Gaston, D., G. Hansen, and C. Newman. “MOOSE: A Parallel Computational Framework for Coupled Systems for Nonlinear Equations.” *International Conference on Mathematics, Computational Methods, and Reactor Physics.* Saratoga Springs, NY: American Nuclear Society, 2009.

IAEA. *Deterministic Safety Analysis for Nuclear Power Plants.* Specific Safety Guide, IAEA, Vienna: IAEA, 2009.

LS-DYNA. *LS-DYNA Software Version smp R7.00.* Livermore Software Technology Corporation, Livermore: Livermore Software Technology Corporation, 2013.

Matev, A. "Analysis of Operator Response to Station Blackout." *International RELAP5-3D User Group Meeting* . West Yellowstone: Idaho National Laboratory, 2006.

Nutt, William T., and Graham B. Wallis. "Evaluation of nuclear safety from outputs of computer codes in the presence of uncertainties." *Reliability Engineering & System Safety* (ELSEVIER) 83 (2004): 57-77.

Parisi, Carlo, Steven R. Prescott, Ronaldo H. Szilard, Justin L. Coleman, Robert E. Spears, and Abhinav Gupta. *Demonstration of External Hazards Analysis.* Idaho National Laboratory, Idaho Falls: Idaho National Laboratory, 2016.

Prescott, S., C. Smith, and R. Samptah. *Incorporating dynamic 3D simulation into PRA.* Idaho National Laboratory, Idaho Falls: Idaho National Laboratory, 2014.

Prosek, A., and L. Cizelj. "Long-Term Station Blackout Accident Analyses of a PWR with RELAP5/MOD3.3." *Science and Technology of Nuclear Installations* 2013 (April 2013).

Sampath, R., N. Montanari, and N. Akinci. "Large-scale solitary wave simulation with implicit incompressible SPH." *Journal of Ocean Engineering and Marine Energy,* 2016.

Schultz, R. R. *RELAP5-3D(c) Code Manual Volume V: User`s Guidelines.* Idaho National Laboratory, Idaho Falls: Idaho National Laboratory, 2015, 620.

Scikit-Learn. 2017. http://scikit-learn.org/stable/ (accessed 07 28, 2017).

Smith, C. L., and al. *Risk-Informed Safety Margin Characterization (RISMC) Pathway Technical Program Plan.* Idaho National Laboratory, Idaho Falls: Idaho National Laboratory, 2015.

Smith, C. L., and S. T. Wood. *Systems Analysis Programs for Hands-on Integrated Reliability Evaluations (SAPHIRE).* Idaho National Laboratory, Idaho Falls: US NRC, 2011.

Spears, R. E., and J.L. Coleman. *Nonlinear Time Domain Seismic Soil-Structure Interaction (SSI) Deep Soil Site Methodology Development.* Idaho National Laboratory, Idaho Falls: Idaho National Laboratory, 2015.

Szilard, R. H., Justin L. Coleman, Steven R. Prescott, Carlo Parisi, and Curtis L. Smith. *RISMC Toolkit and Methodology Research and Development Plan for External Hazards Analysis.* Idaho National Laboratory, Idaho Falls: Idaho National Laboratory, 2016.

Szilard, R.H., and al. *Industry Application - External Hazard Anlyses - Problem Statement.* Idaho National Laboratory, Idaho Falls: Idaho National Laboratory, 2015.

The RELAP5-3D(c) Code Development Team. *RELAP5-3D code Manual Volume I: Code Structure, System Models and Solution Methods.* Manual, Idaho National Laboratory, Idaho Falls: Idaho National Laboratory, 2015, 662.

US NRC. "Loss of Offsite Power." *US NRC.* 2017. http://nrcoe.inel.gov/resultsdb/publicdocs/LOSP/loop-glossary.pdf (accessed 07 28, 2017).

US NRC. *Risk Assessment of Operational Events Handbook Volume 2 - External Events.* Washington, DC: United States Nuclear Regulatory Commission, 2008.

US NRC. *SOARCA Project. Volume 2. Surry Integrated Analysis.* NUREG, US NRC, Washington, DC: US NRC, 2013.

Wilks, S. S. "Determination of Sample Sizes for Setting Tolerance Limits." *The Annals of Mathematical Statistics* 12, no. 1 (1941): 91-96.

APPENDIX A – PRA MODEL

While section 3.2.1 provides the event trees used for the project, this appendix presents the main fault trees developed for this report. The end of this appendix also provides an example of the change sets IA2-EQ-SWGR and IA2-EQ-IE.

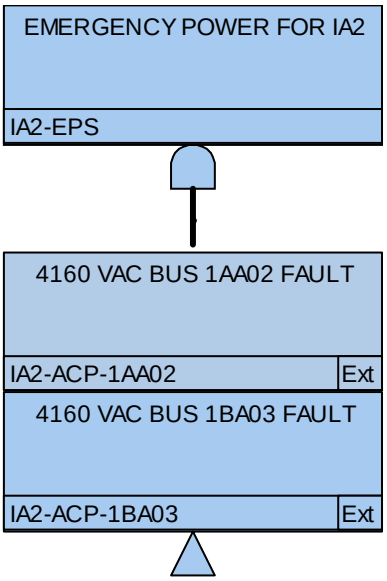

Figure 57. IA2 Fault Tree EPS.

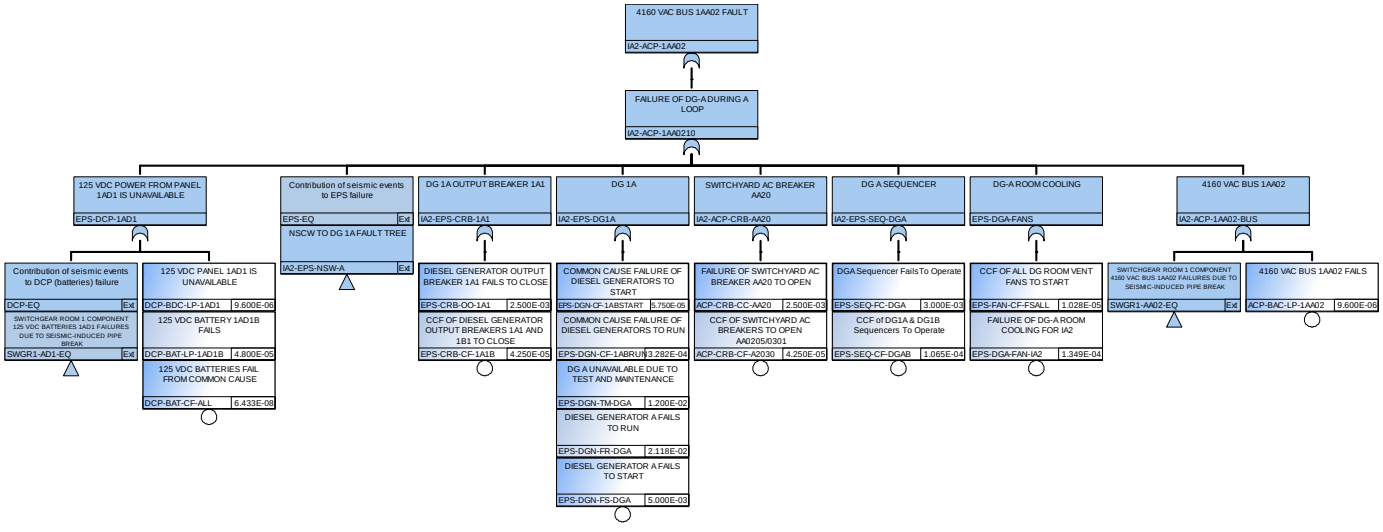

Figure 58. IA2 Fault Tree ACP-1AA02.

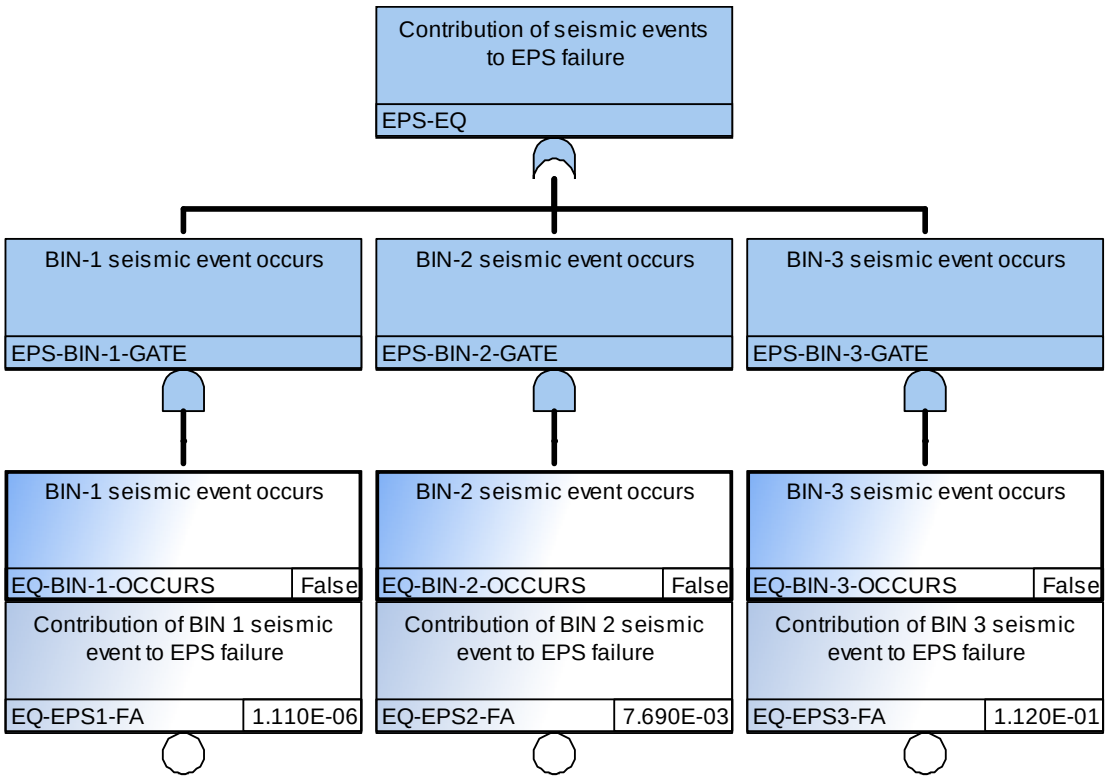

Figure 59. IA2 Fault Tree EPS-EQ.

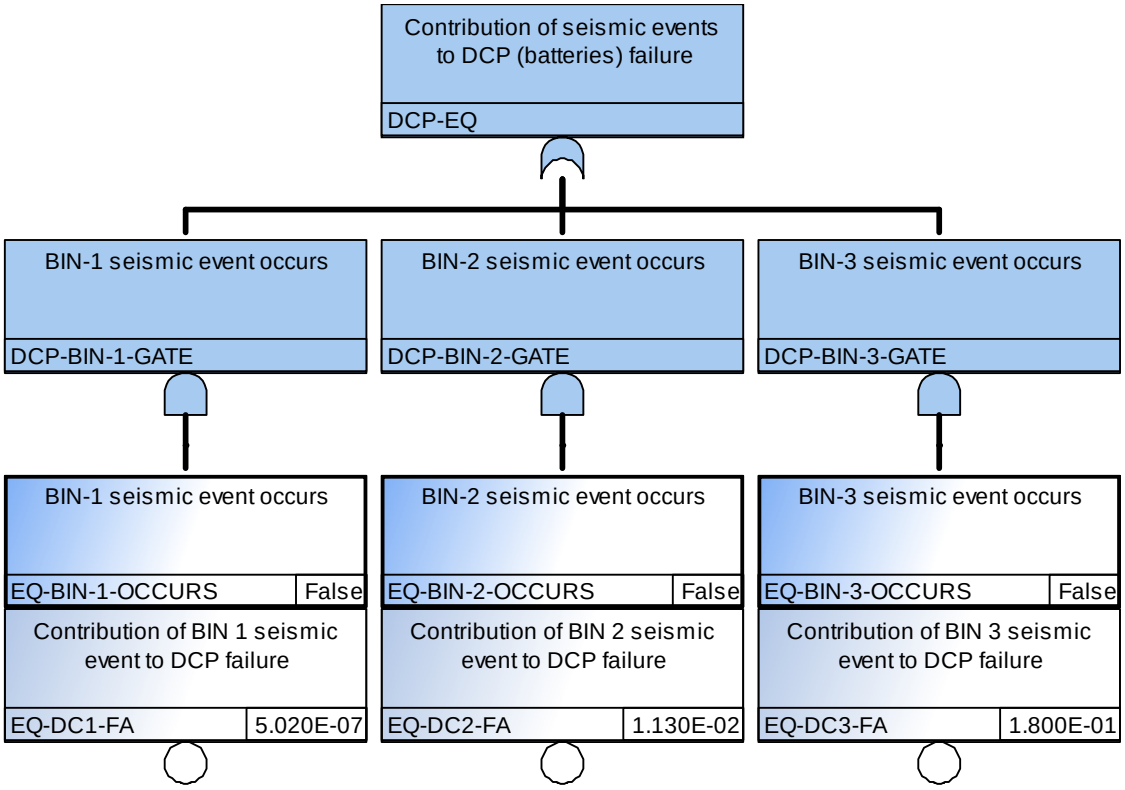

Figure 60. IA2 Fault Tree DCP-EQ.

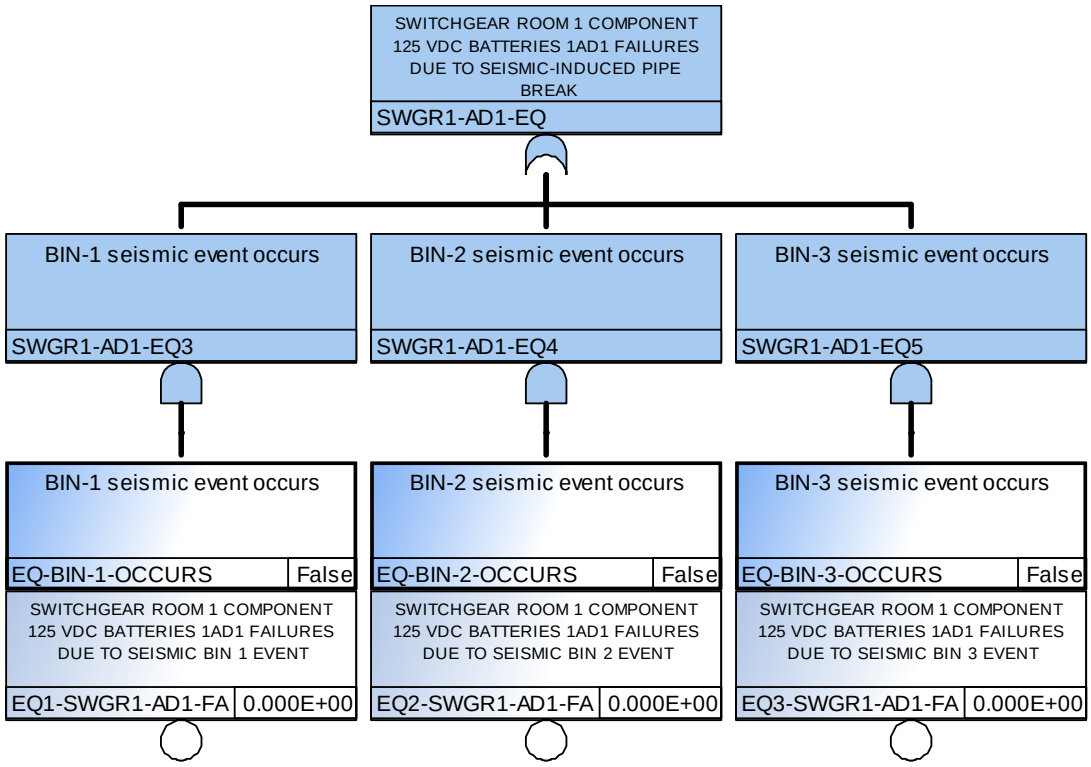

Figure 61. IA2 Fault Tree SWGR1-AD1-EQ.

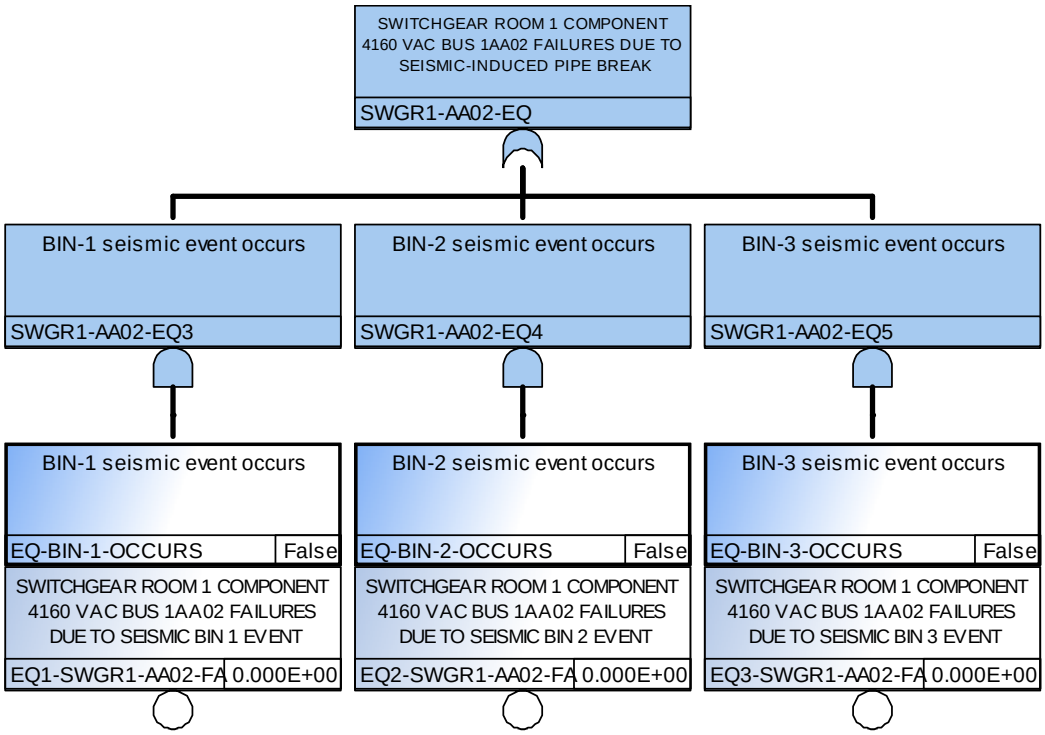

Figure 62. IA2 Fault Tree SWGR1-AA02-EQ.

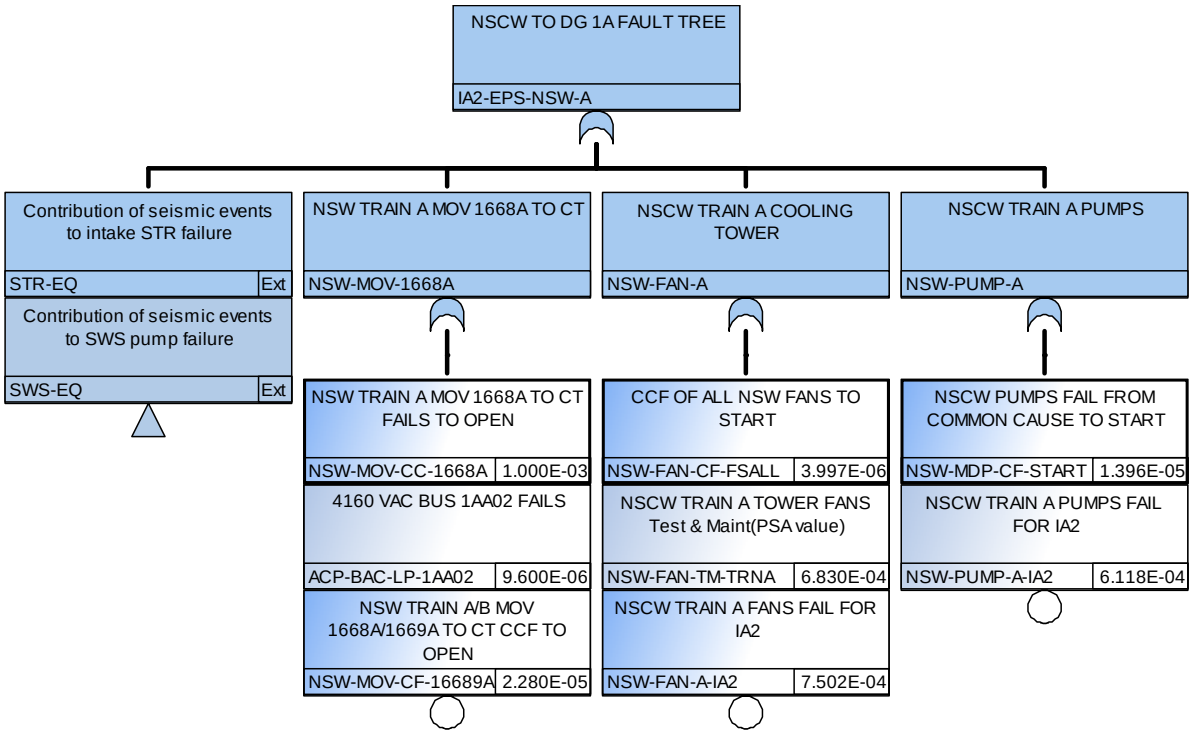

Figure 63. IA2 Fault Tree EPS-NSW-A.

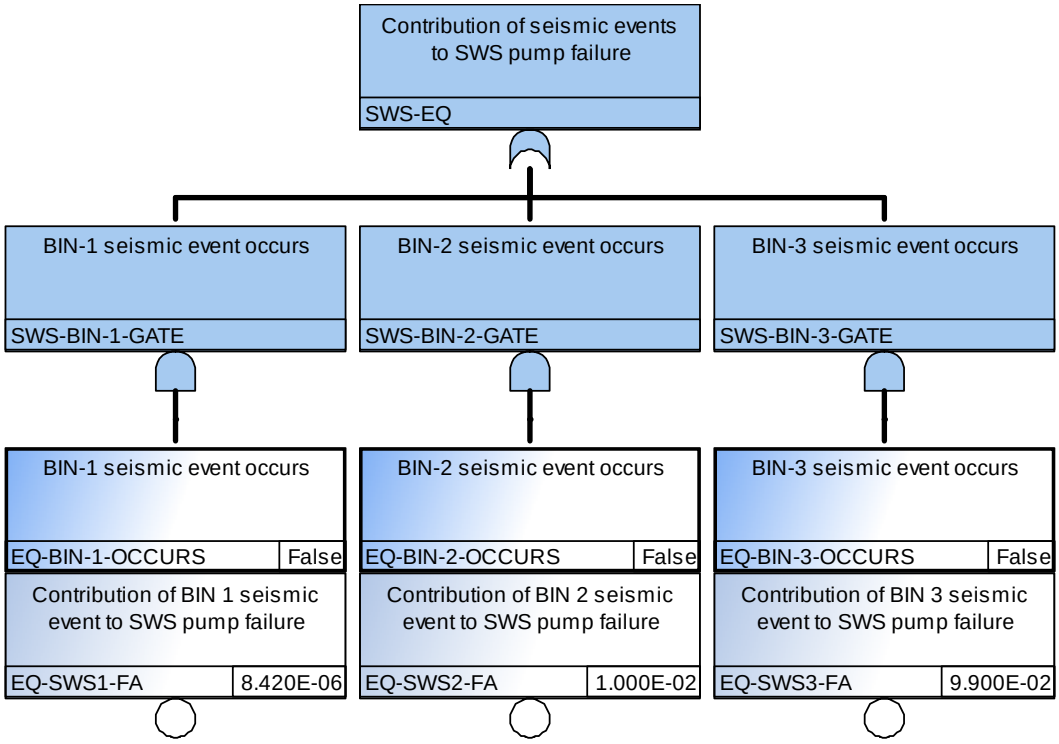

Figure 64. IA2 Fault Tree SWS-EQ.

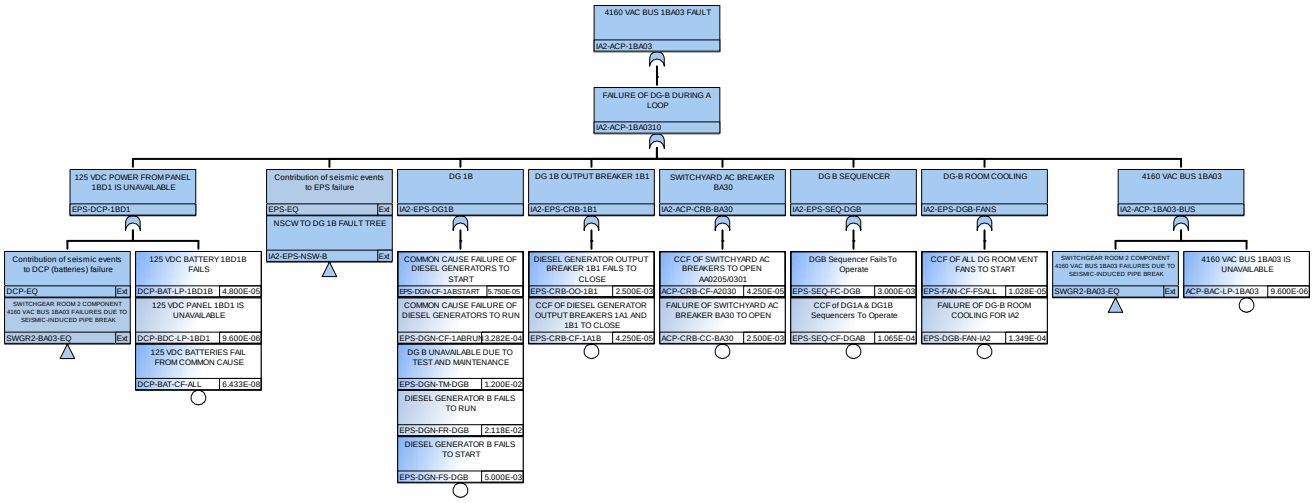

Figure 65. IA2 Fault Tree ACP-1BA03.

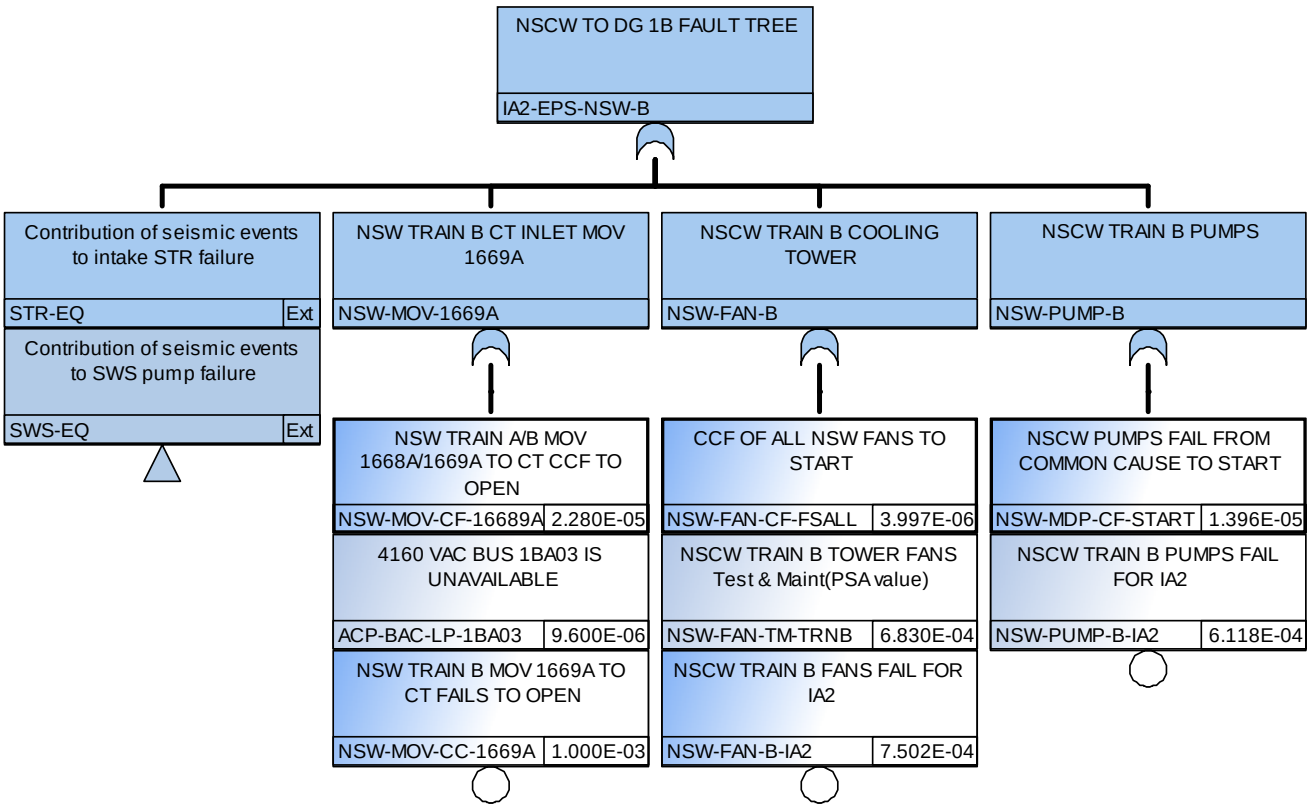

Figure 66. IA2 Fault Tree EPS-NSW-B.

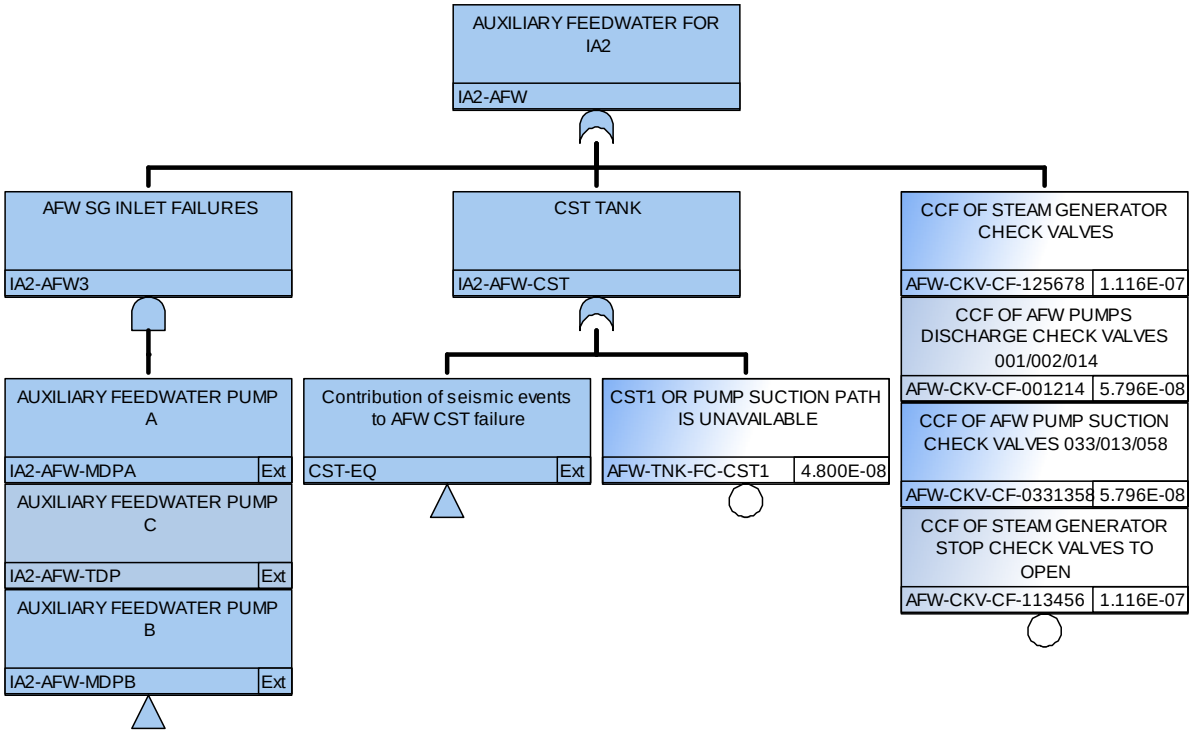

Figure 67. IA2 Fault Tree AFW.

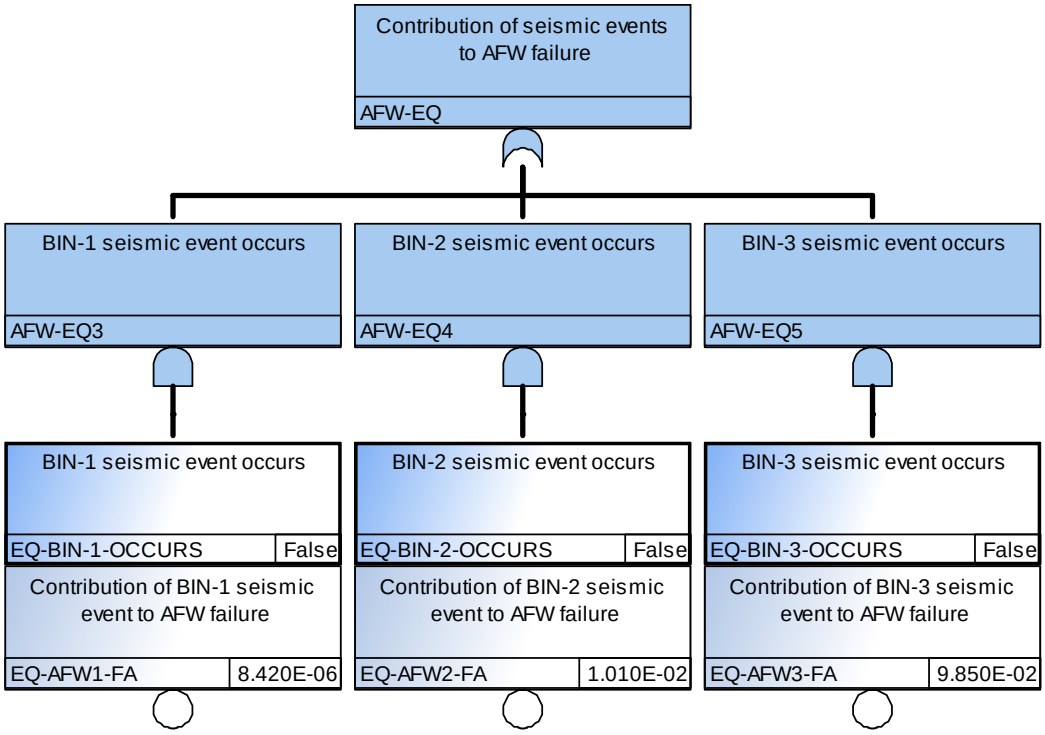

Figure 68. IA2 Fault Tree AFW-EQ.

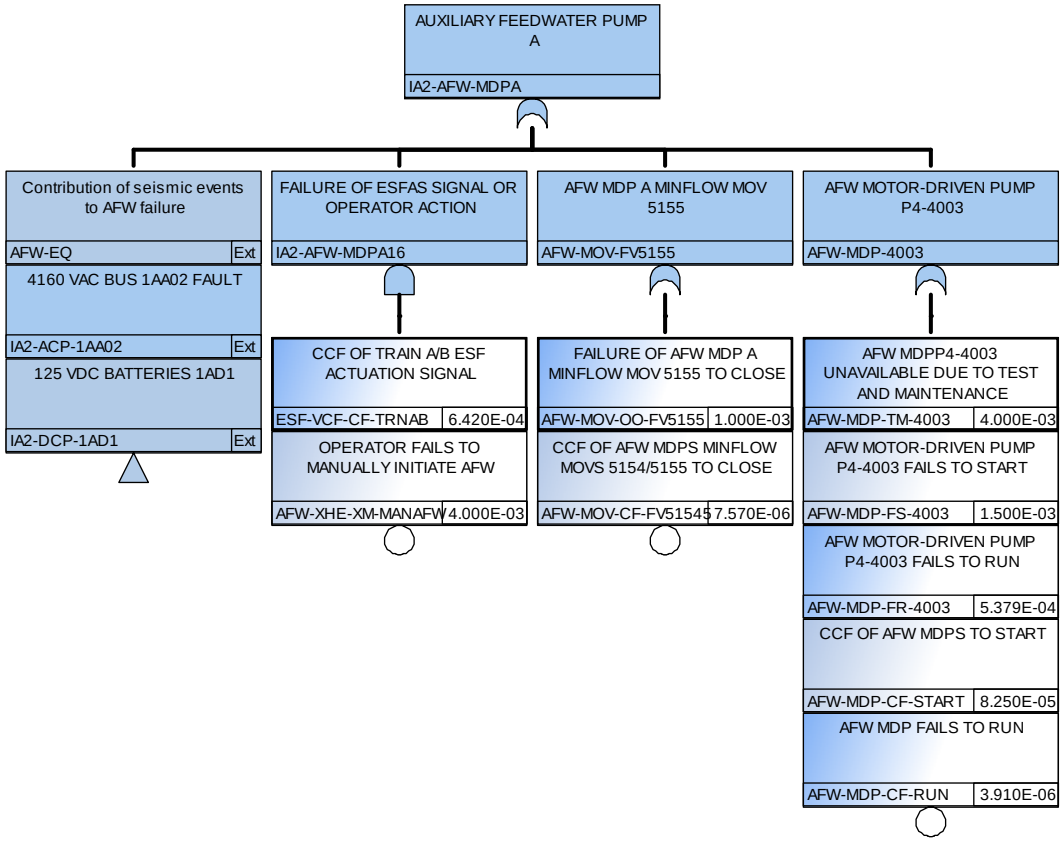

Figure 69. IA2 Fault Tree AFW-MDPA.

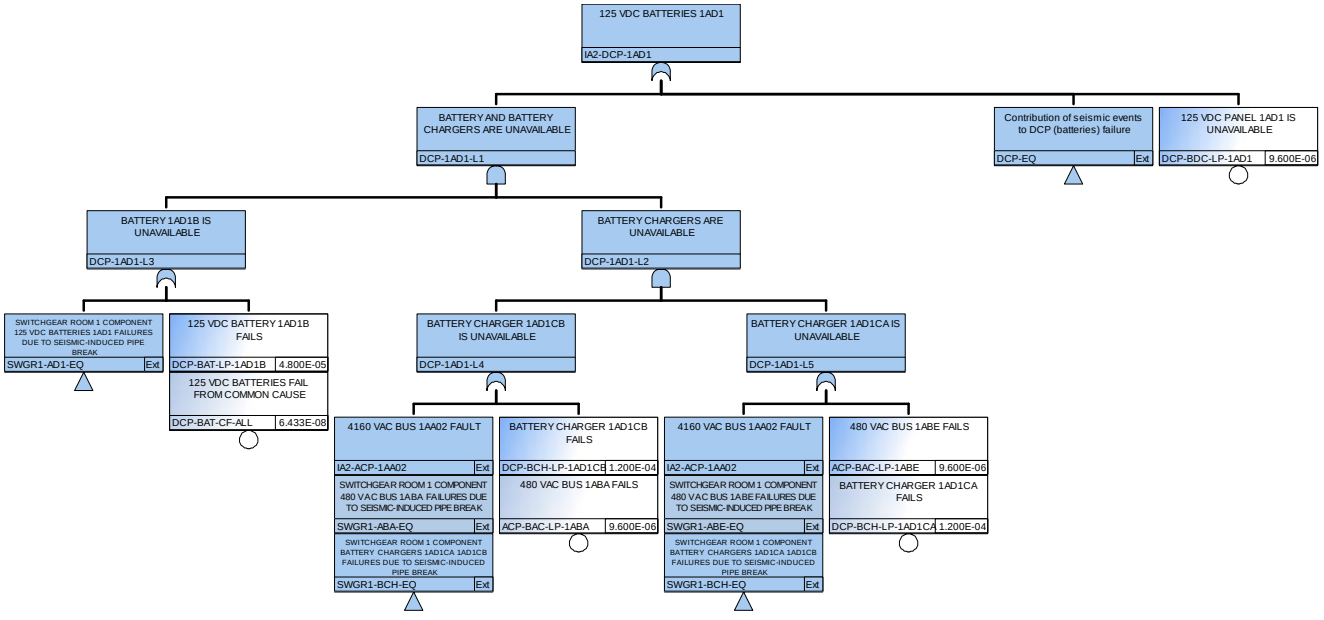

Figure 70. IA2 Fault Tree DCP-1AD1.

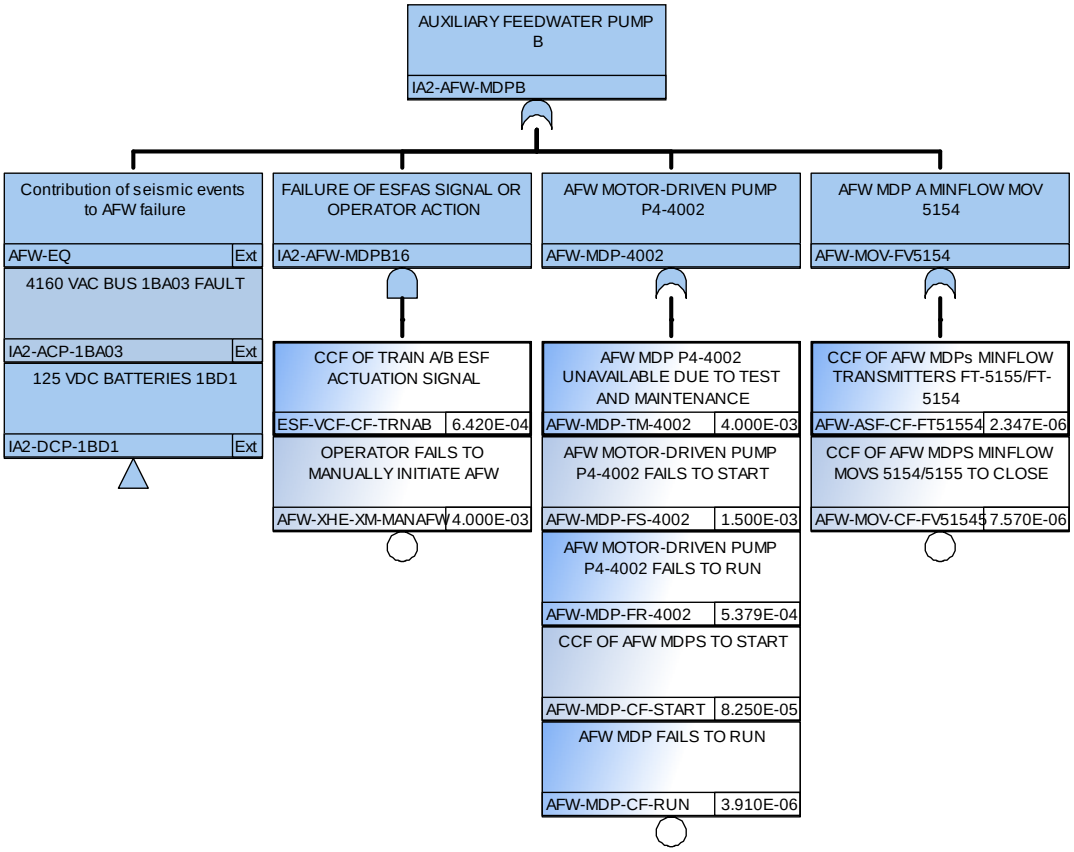

Figure 71. IA2 Fault Tree AFW-MDPB.

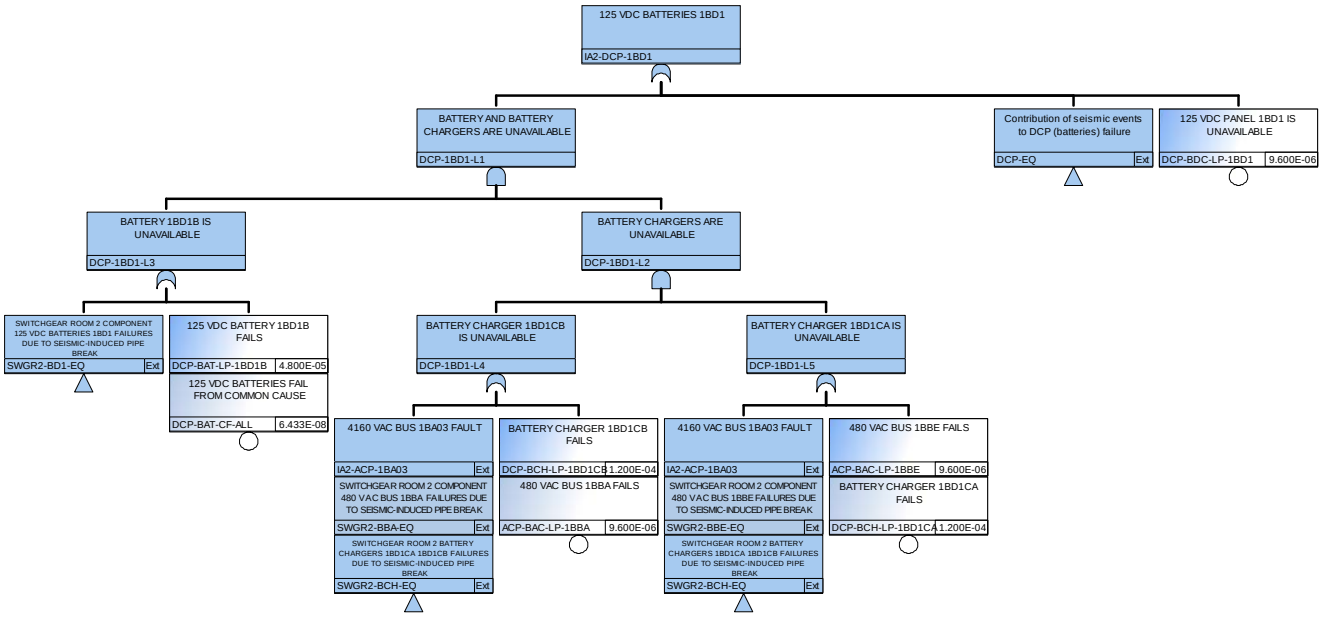

Figure 72. IA2 Fault Tree DCP-1BD1.

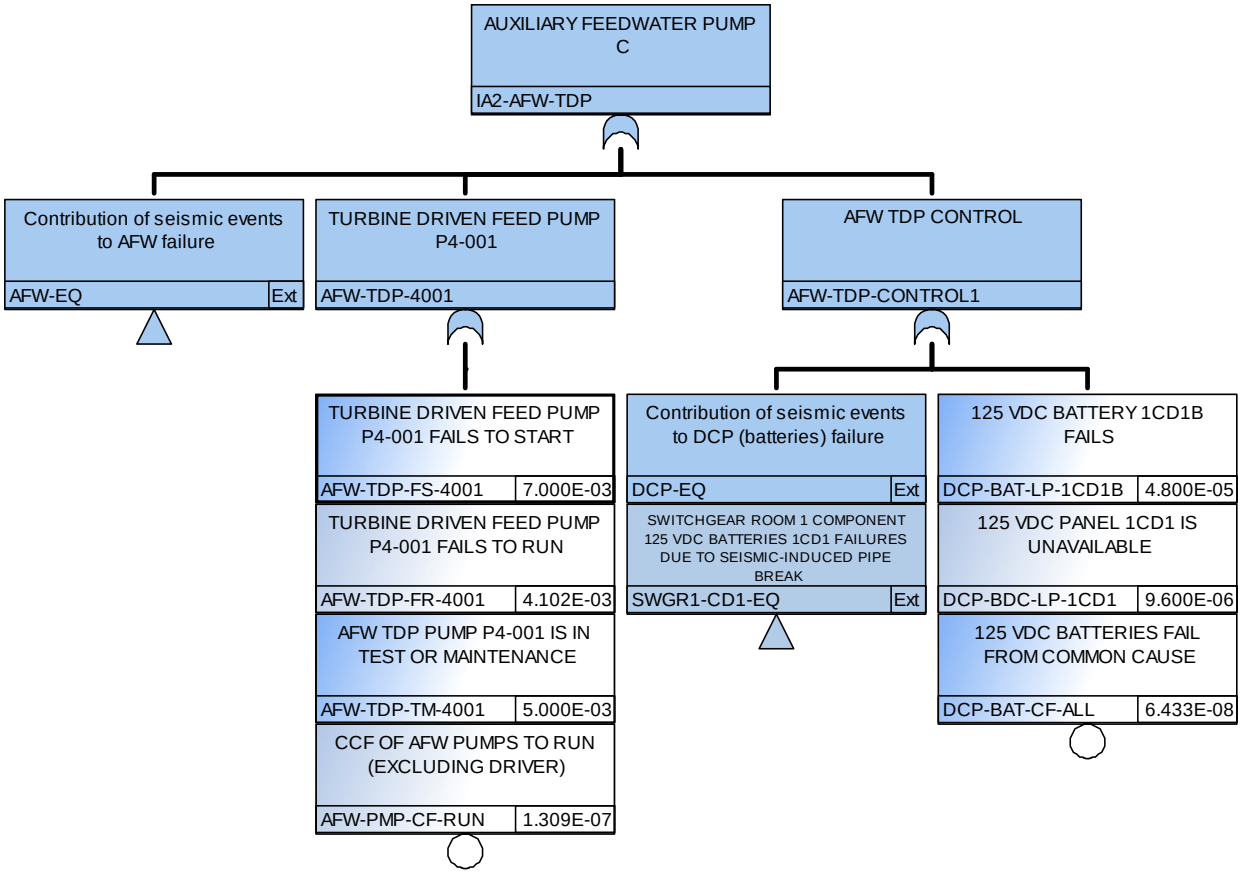

Figure 73. IA2 Fault Tree AFW-TDP.

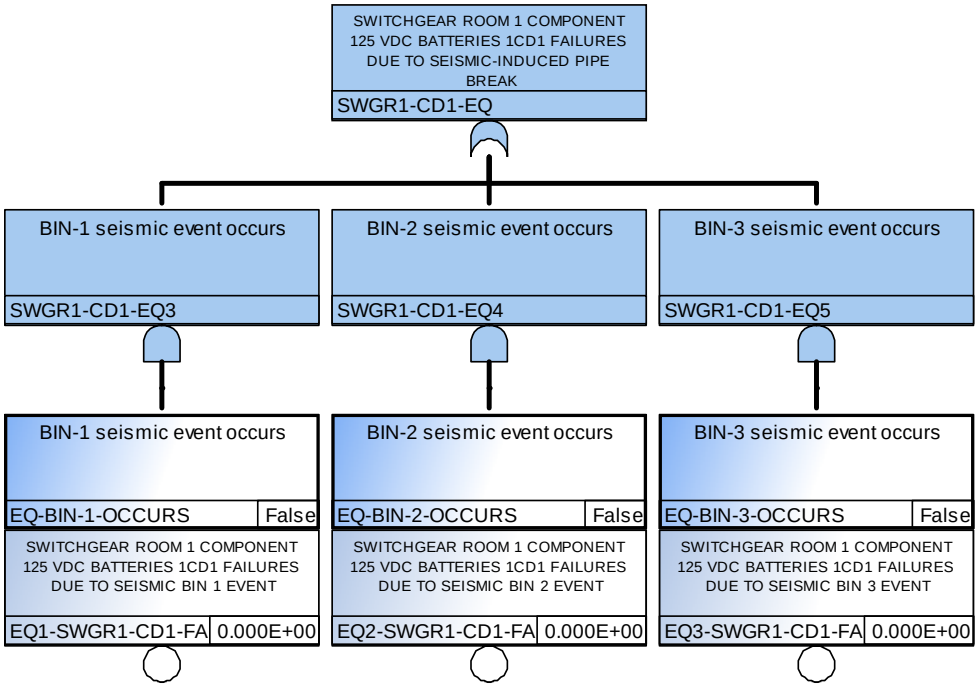

Figure 74. IA2 Fault Tree SWGR1-CD1-EQ.

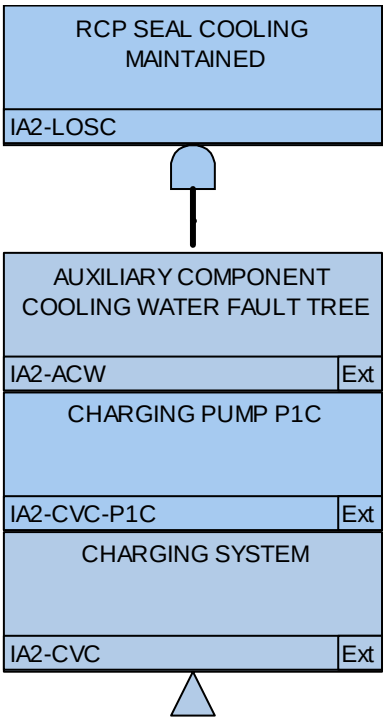

Figure 75. IA2 Fault Tree LOSC.

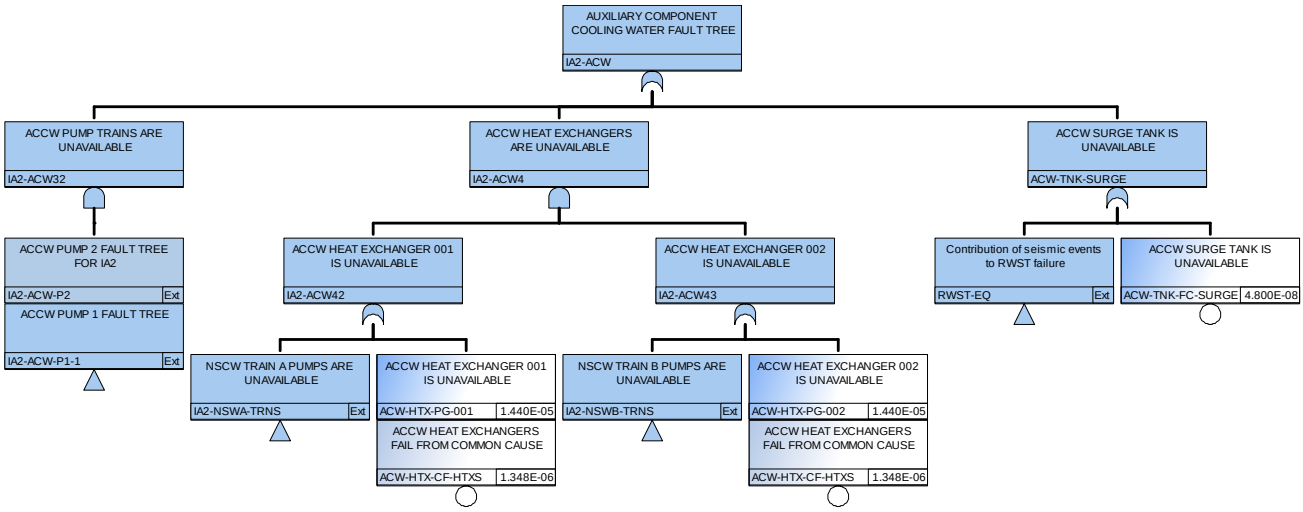

Figure 76. IA2 Fault Tree ACW.

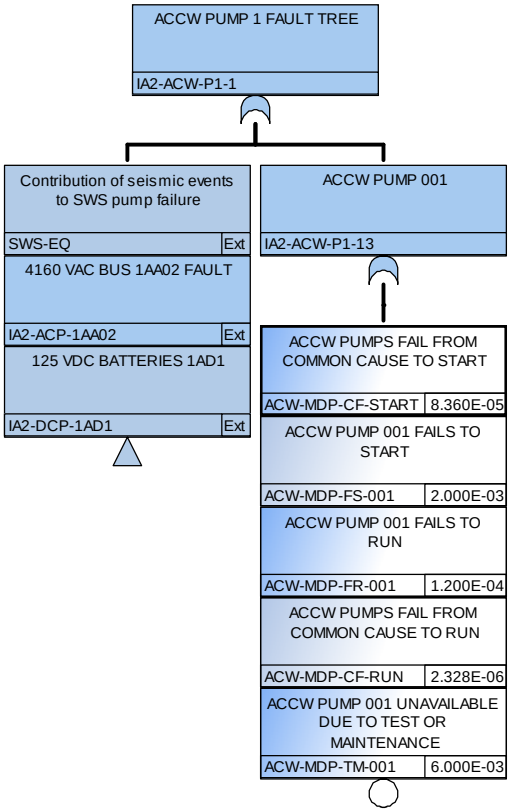

Figure 77. IA2 Fault Tree ACW-P1.

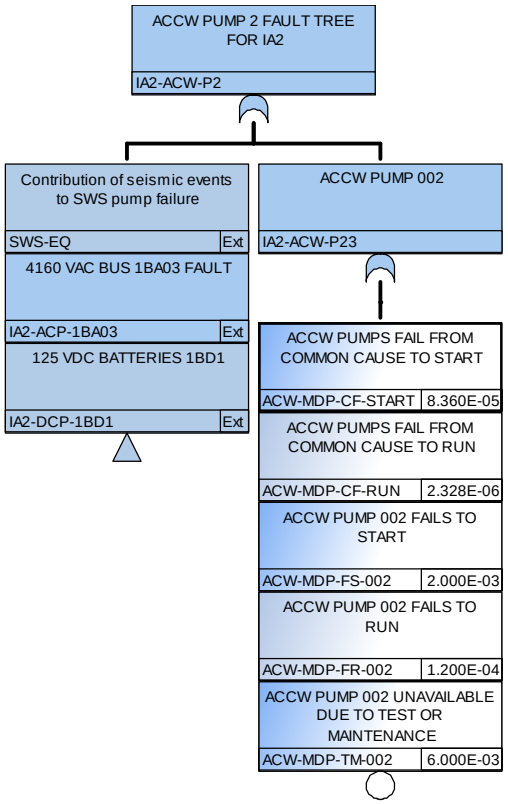

Figure 78. IA2 Fault Tree ACW-P2.

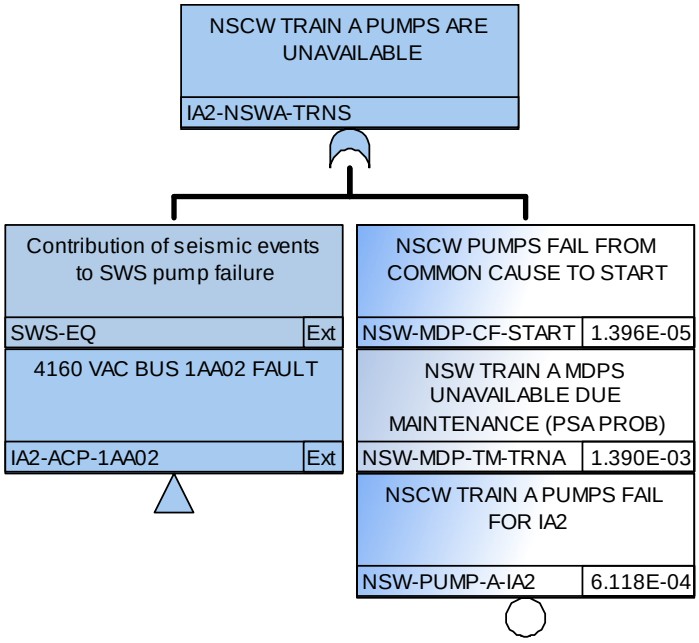

Figure 79. IA2 Fault Tree NSWA-TRNS.

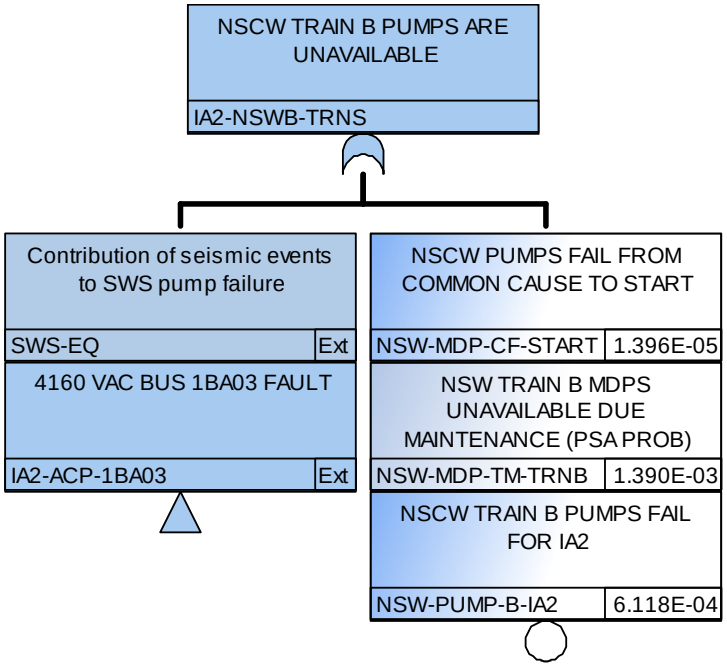

Figure 80. IA2 Fault Tree NSWB-TRNS.

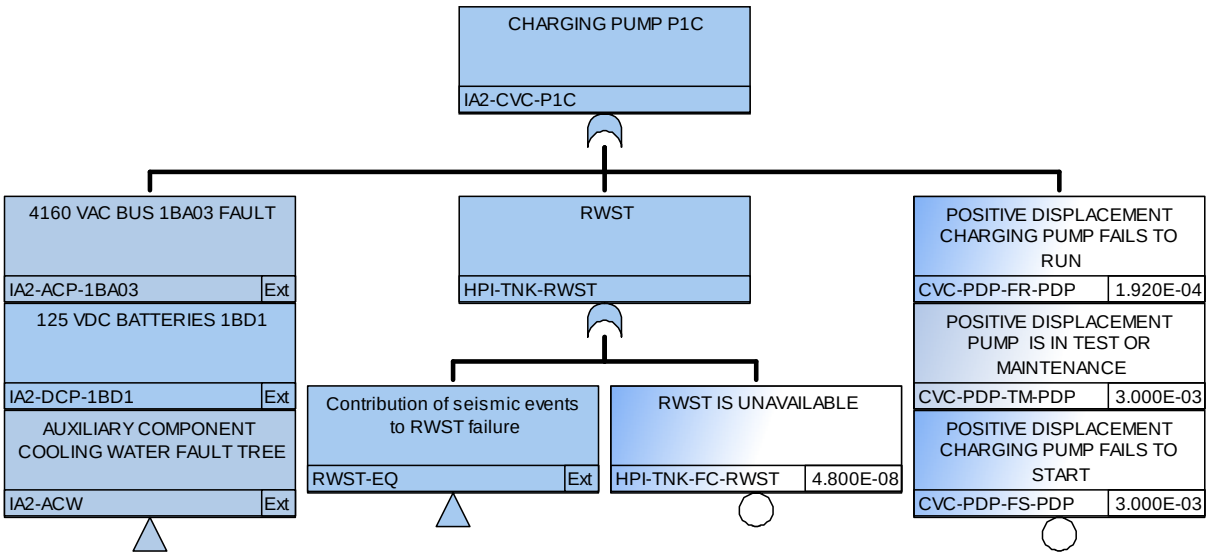

Figure 81. IA2 Fault Tree CVC-P1C.

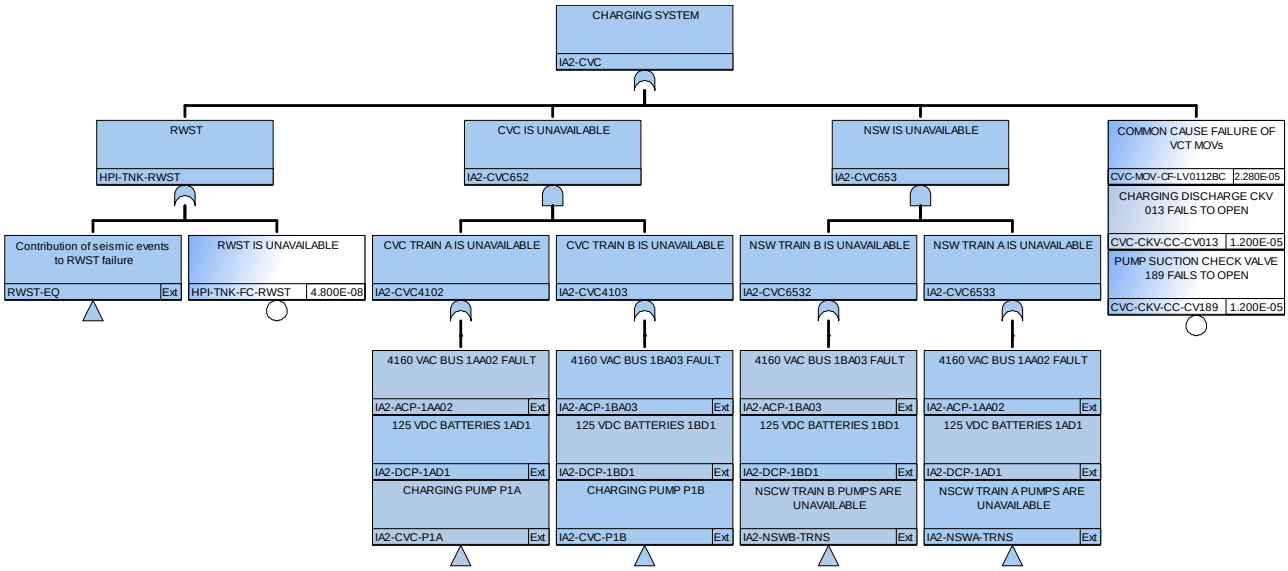

Figure 82. IA2 Fault Tree CVC.

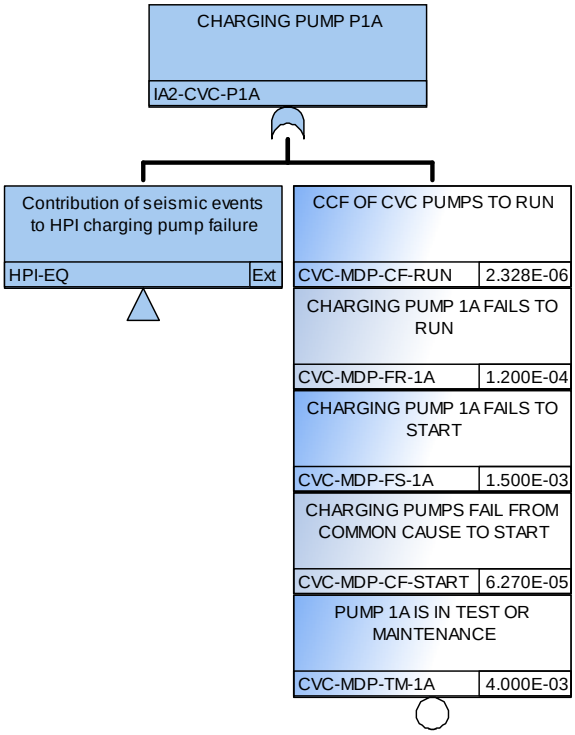

Figure 83. IA2 Fault Tree CVC-P1A.

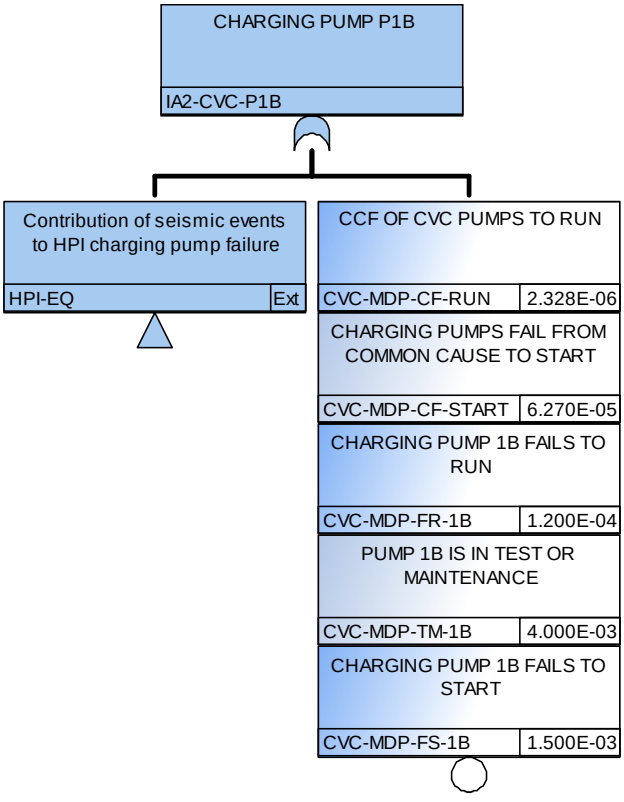

Figure 84. IA2 Fault Tree CVC-P1B.

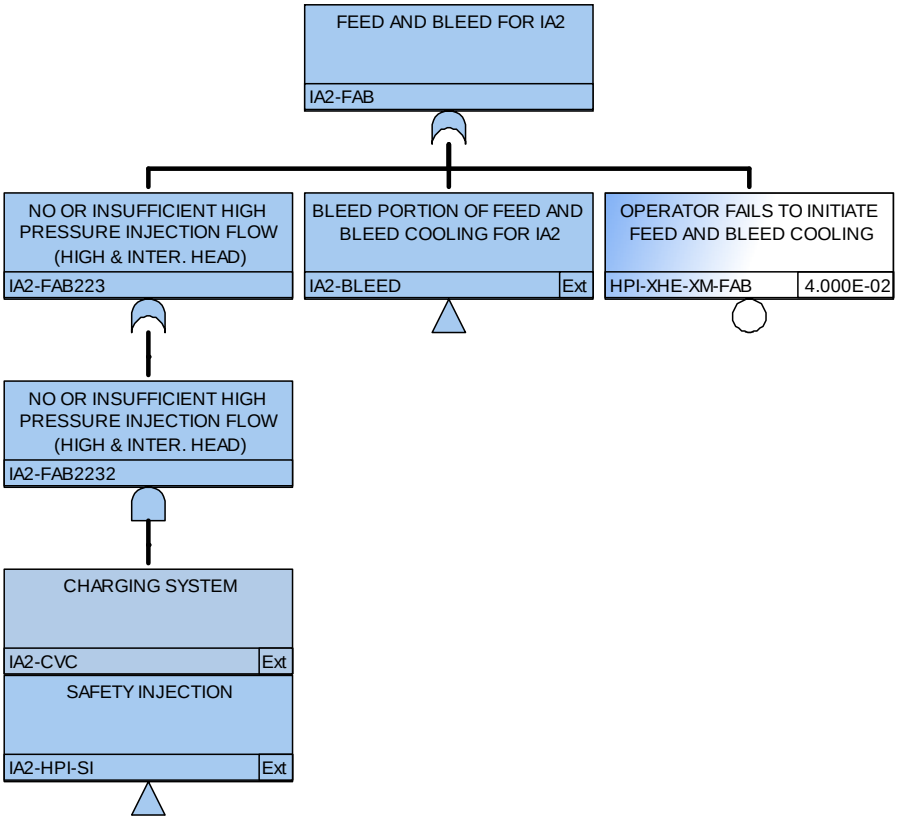

Figure 85. IA2 Fault Tree FAB.

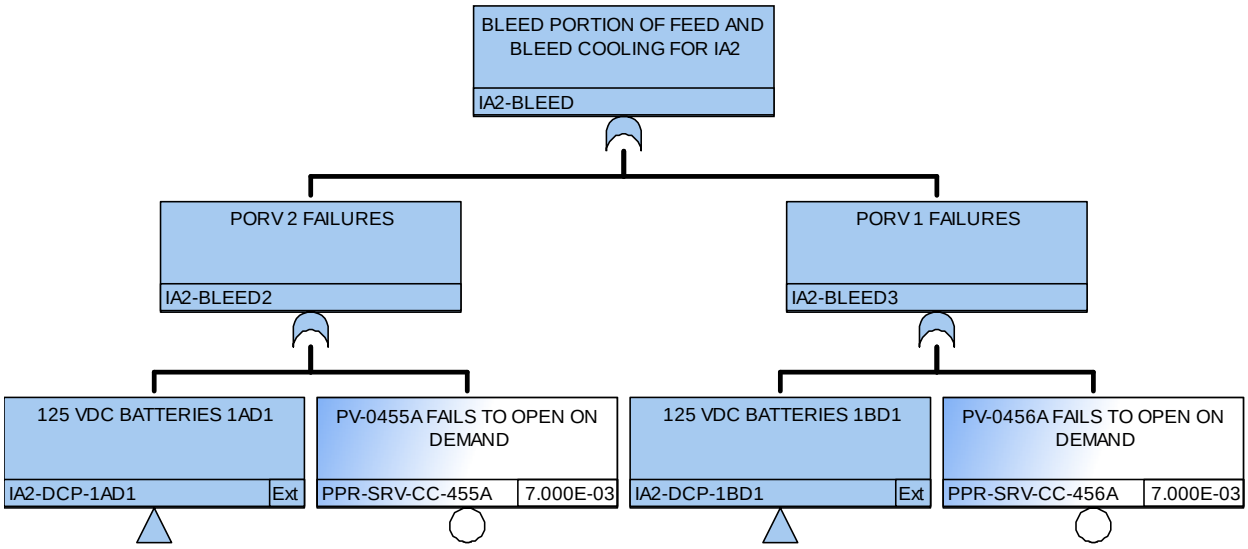

Figure 86. IA2 Fault Tree BLEED.

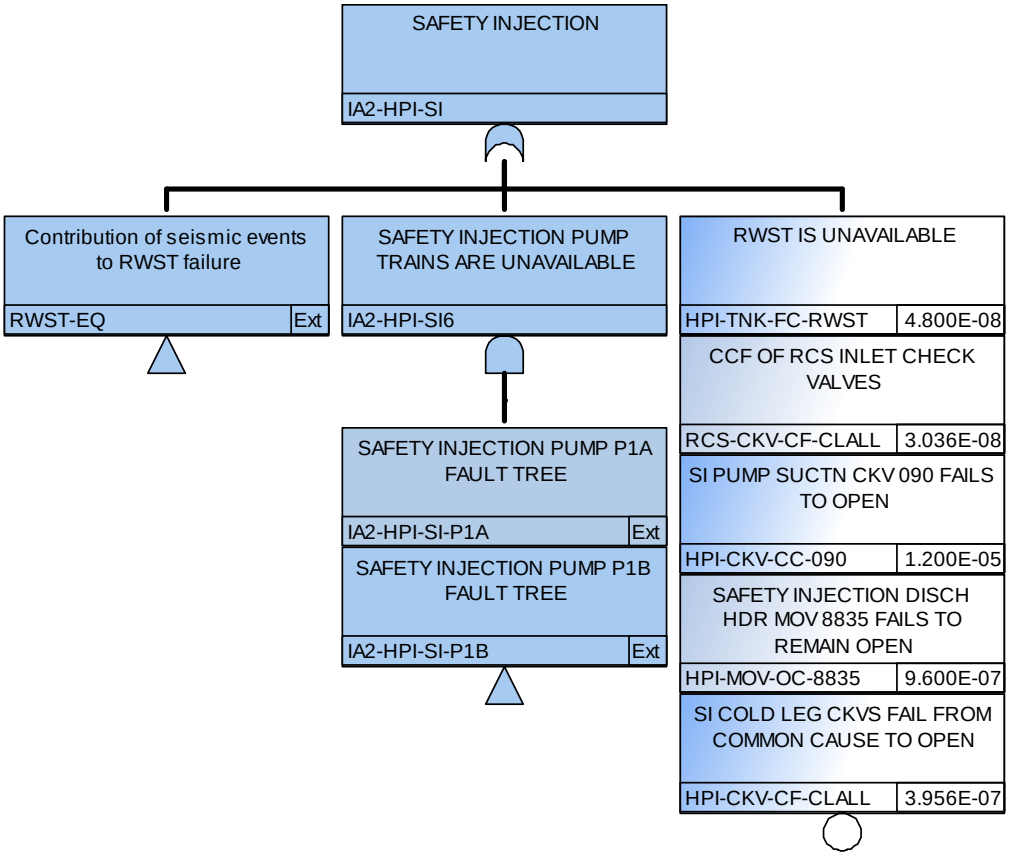

Figure 87. IA2 Fault Tree HPI-SI.

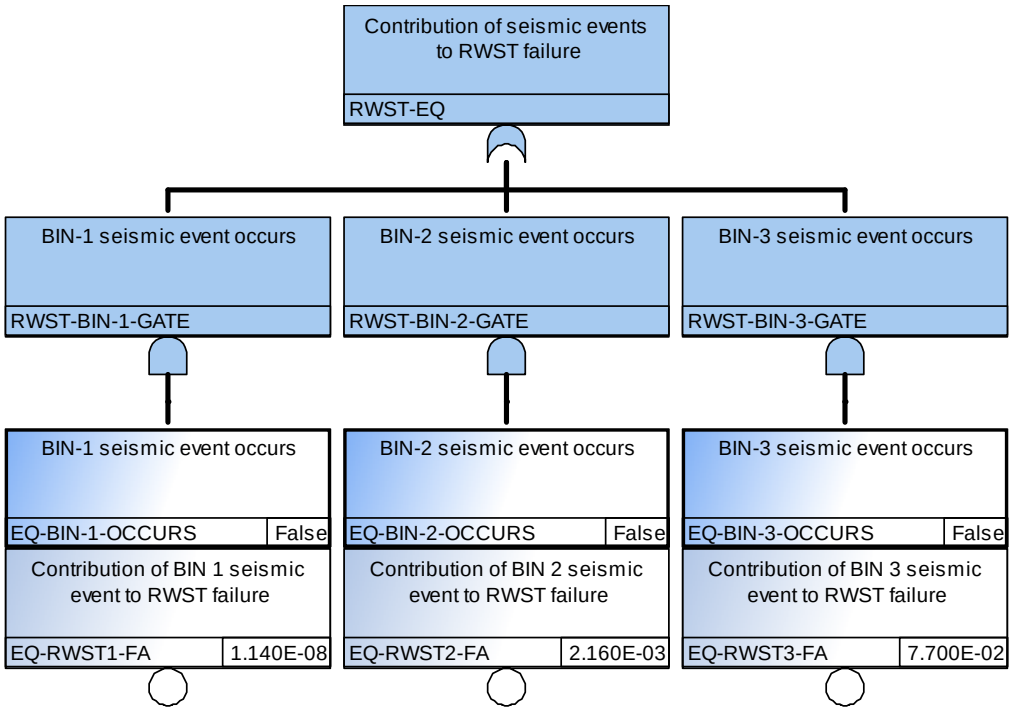

Figure 88. IA2 Fault Tree RWST-EQ.

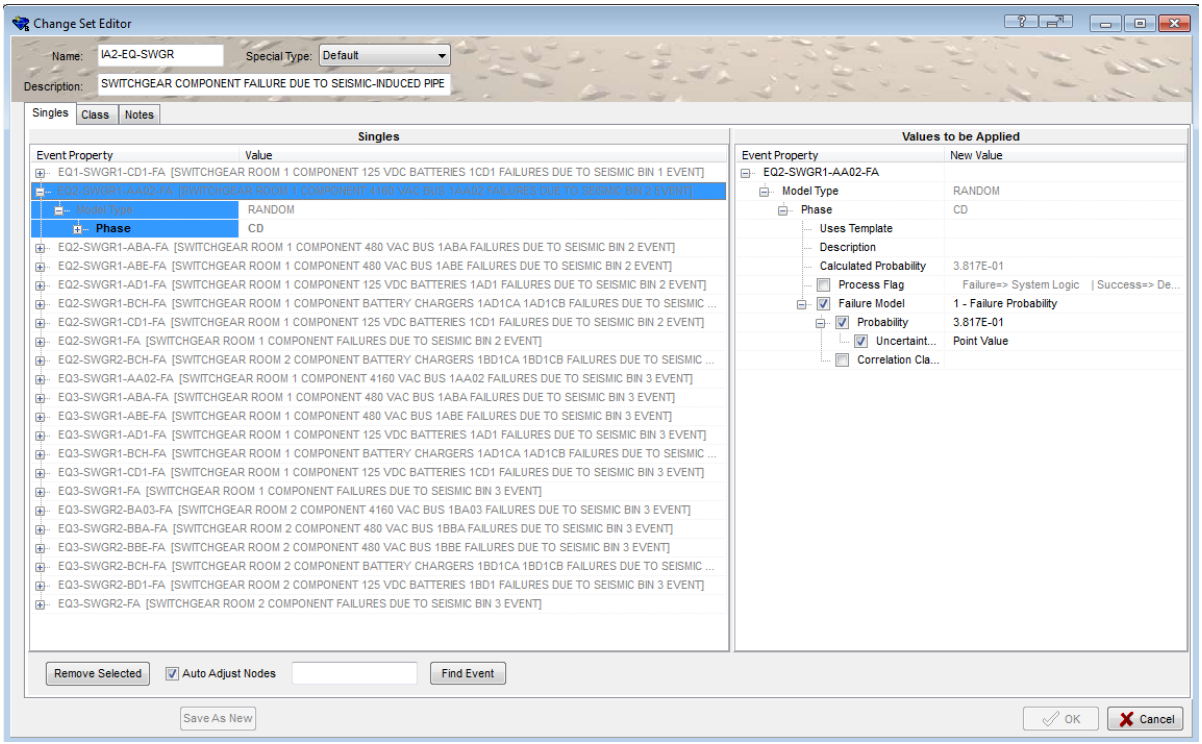

Figure 89. IA2 Change Set IA2-EQ-SWGR.

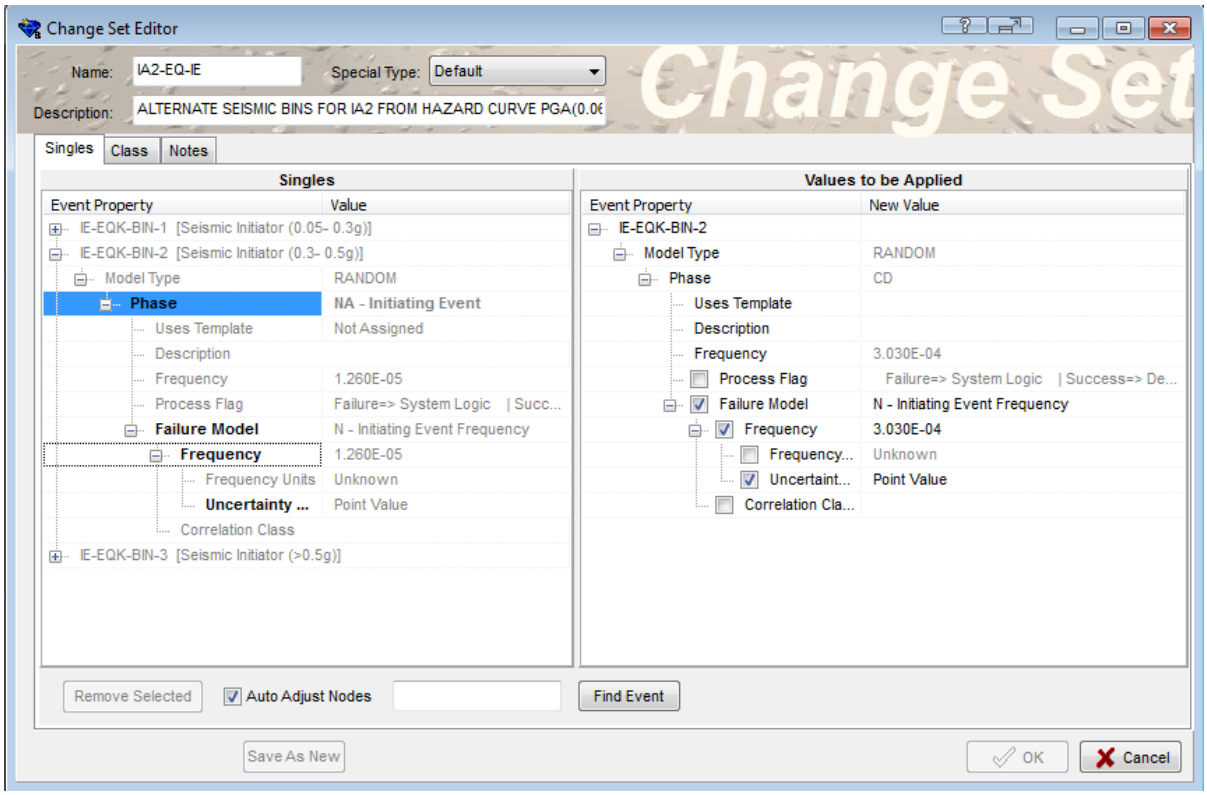

Figure 90. IA2 Change Set IA2-EQ-IE.

APPENDIX B – RELAP5-3D TRANSIENT RESULTS

In the following Figures, we reported the charts of the main parameters calculated by the RELAP5-3D code for the main PRA sequences.

LOOP: Sequence 2-02-05-no Core Damage

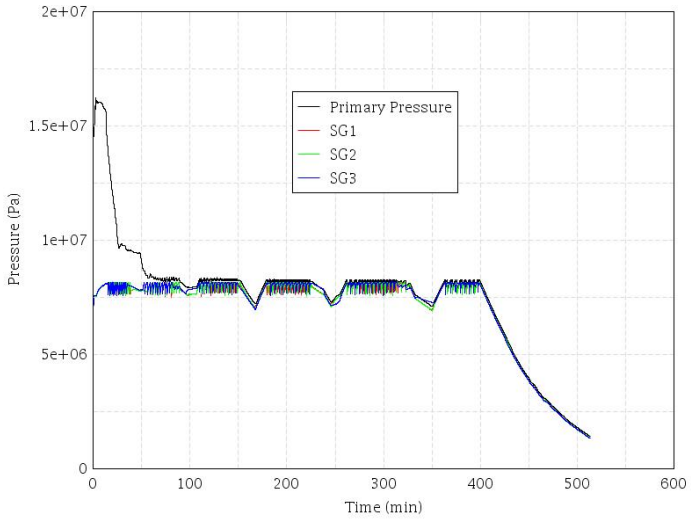

Figure 91. System Pressures.

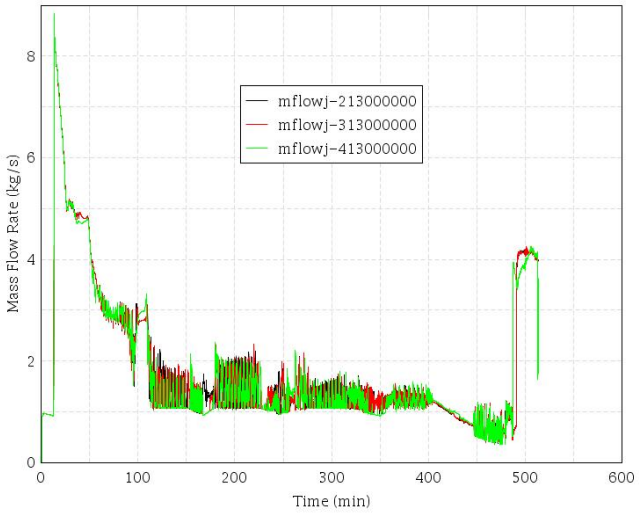

Figure 92. MCP Seal Leak Rate.

SBO: Sequence 2-16-45-no Core Damage

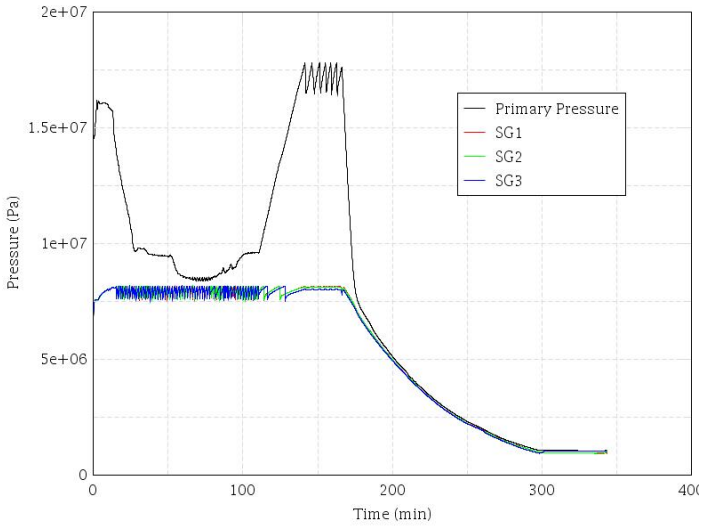

Figure 93. System Pressures.

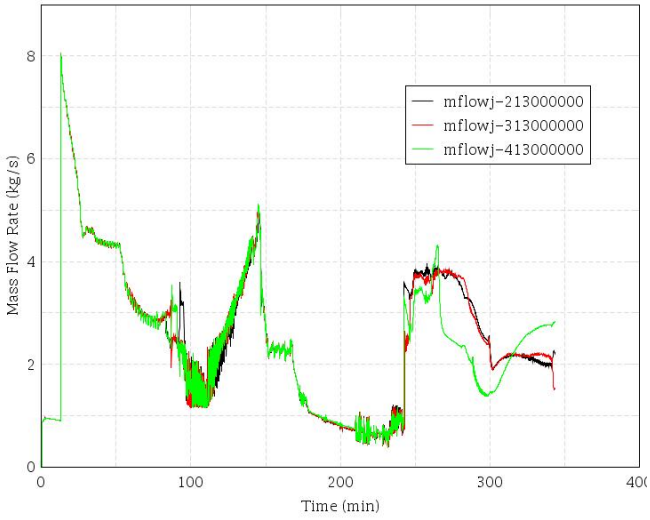

Figure 94. MCP Seal Leak Rate.

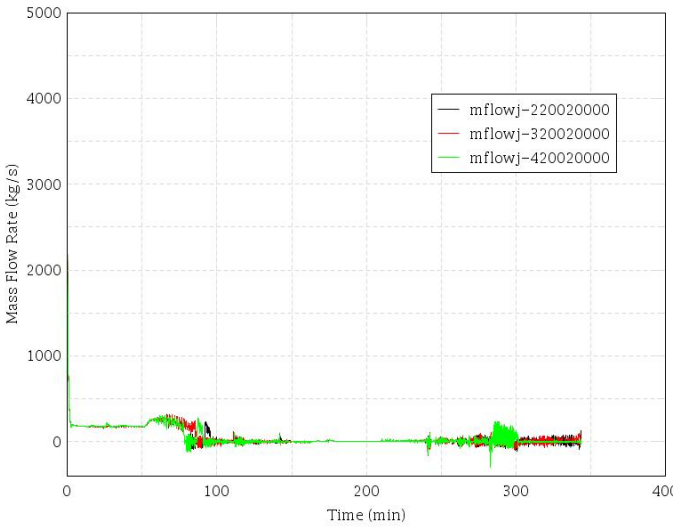

Figure 95. Main Circulation Circuit mass flow.

APPENDIX C – EXTERNAL EVENT ANIMATION SNAPSHOTS

A video was constructed to show the sequence of events from earthquake to piping failure, flooding, and thermal hydraulics simulations. Figures 62-65 show screen captures of this animation video.

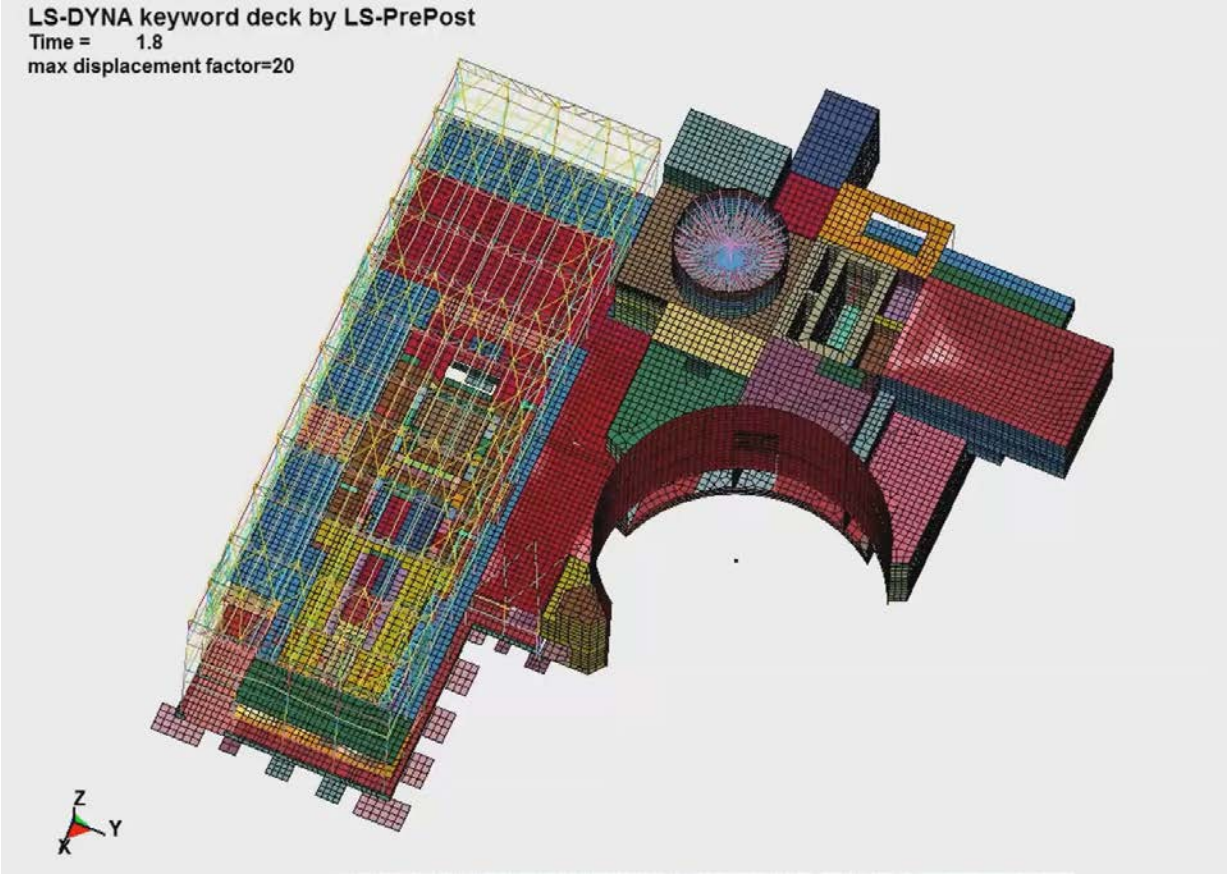

Figure 96. Snapshot of the video showing seismic simulation.

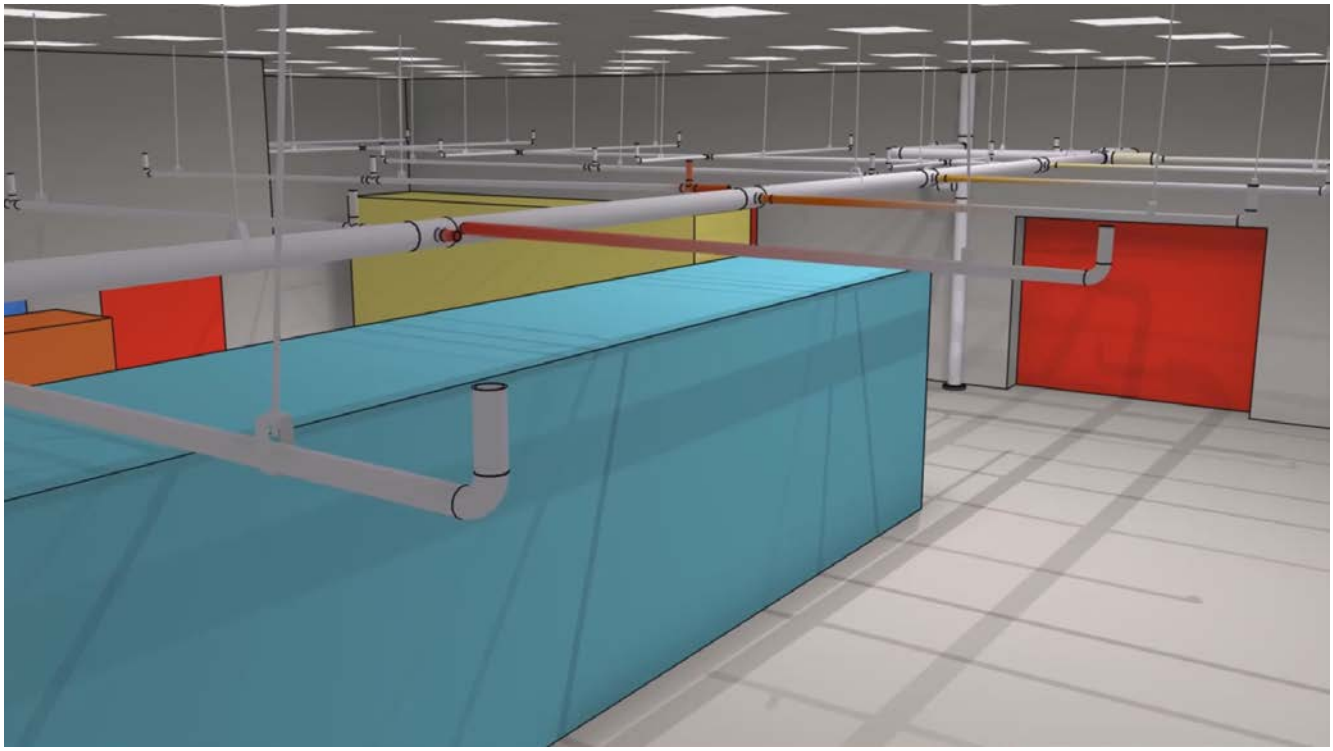

Figure 97. Snapshot of the video showing pipe sway and breaking.

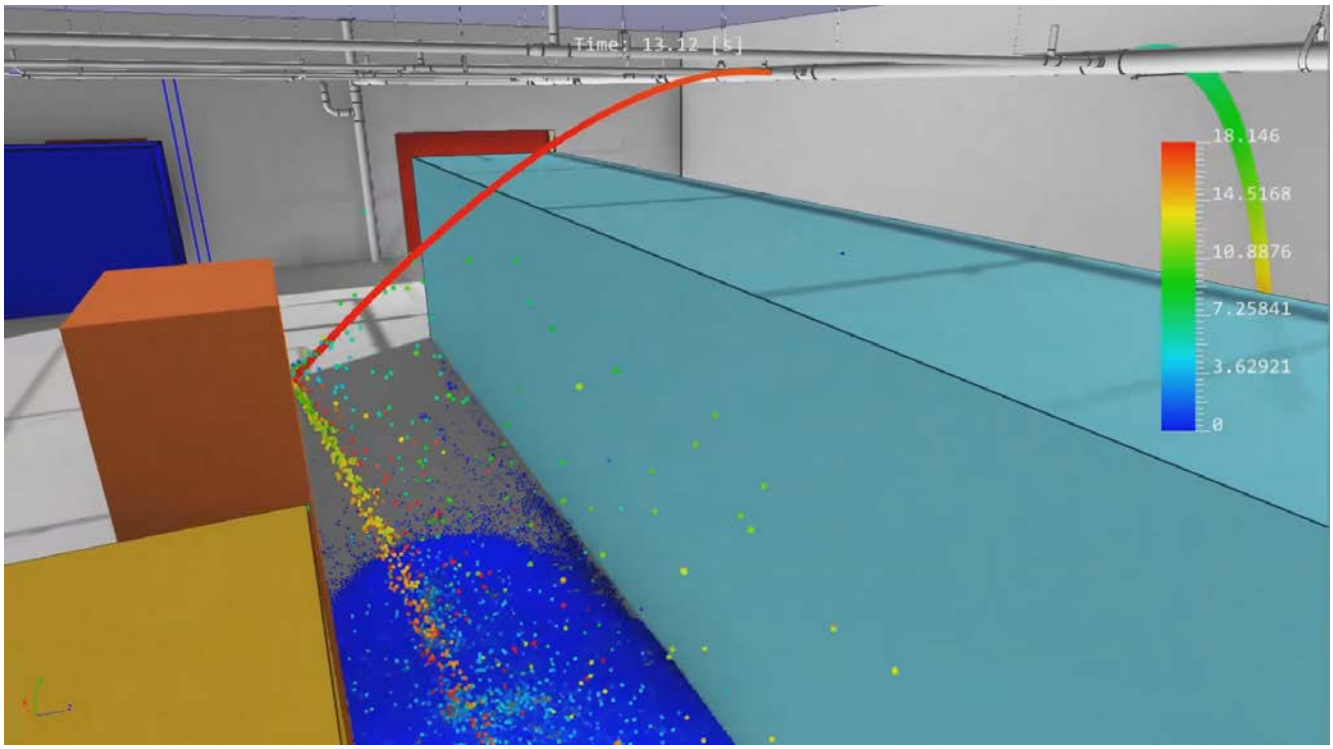

Figure 98. Snapshot of the video showing the fluid spray from the pipe breaks.

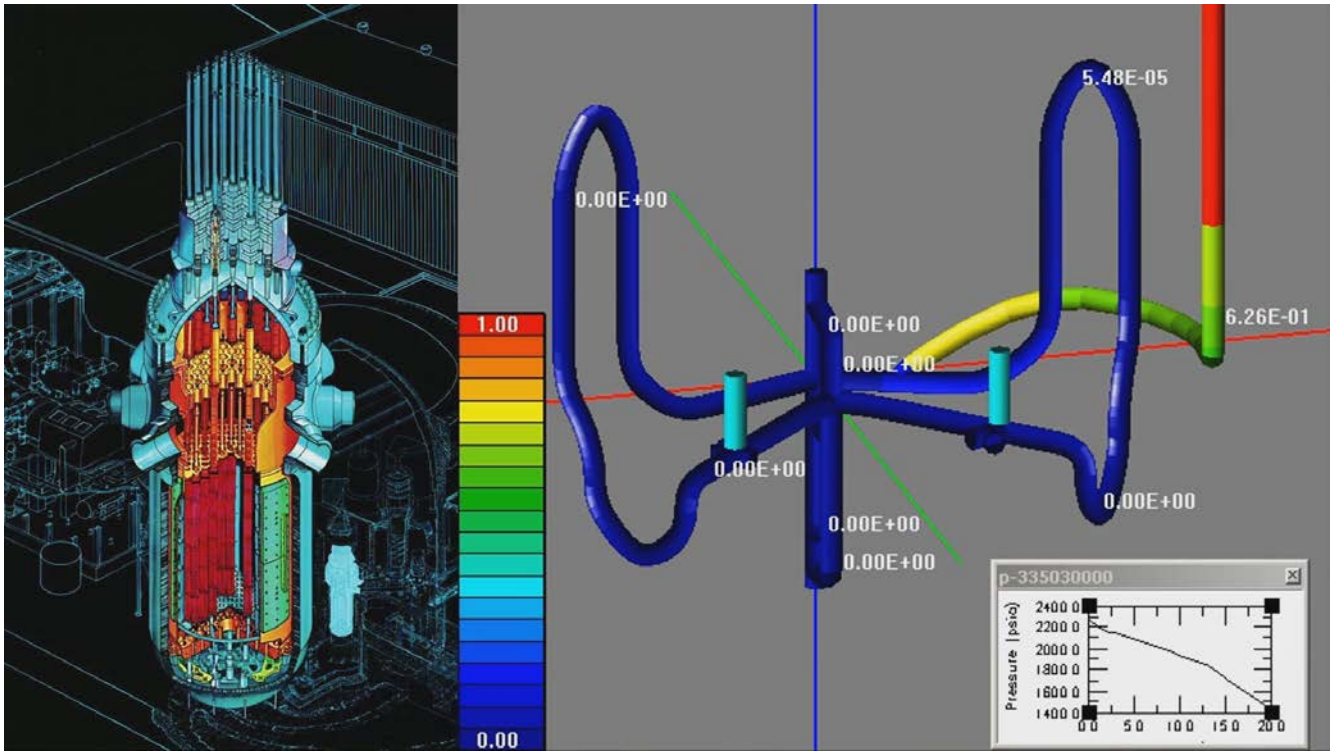

Figure 99. Snapshot of the video showing thermal hydraulics analysis of the core.